eLife

Reviewed Preprint
v1 • January 21, 2026
Not revised

Reviewed Preprint
v2 • August 3, 2026
Revised by authors

RAB14-dependent tubulovesicular recycling directs MET to invadopodia, promoting TNBC cell invasion

Amrita Khamari[1], Atreyee Guria[1], Kiran Tak[1], Rajiv Sharma[2], Yannis Kalaidzidis[3], Sunando Datta[1]

[1]Department of Biological Sciences, Indian Institute of Science Education and Research, Bhopal, Bhopal, India • [2]Indian Institute of Technology, New Delhi, India • [3]Max Planck Institute of Molecular Cell Biology and Genetics, Dresden, Germany

For correspondence: sunando@iiserb.ac.in

Competing interests: No competing interests declared

Funding: See page 40

Reviewing editor: Jonathan A Cooper, Fred Hutch Cancer Center, United States

eLife Assessment

This revised paper provides **solid** evidence for HGF-induced trafficking of the HGF receptor, MET, together with metalloprotease MT1-MMP into invadopodia and the role of this trafficking in triple-negative breast cancer (TNBC) cell invasion in vitro. The evidence could be improved with additional experimental controls and analysis, but the findings will be **valuable** for cancer cell biologists investigating TNBC.

https://doi.org/10.7554/eLife.109472.2.sa3

Abstract

Metastasis is one of the primary causes of cancer-related death in Triple-negative breast cancer patients. During metastatic dissemination, the cancer cells infiltrate in to surrounding tissue employing specialized membrane-protrusion with proteolytic activity called invadopodia. Cues from growth factors via the cognate receptor tyrosine kinases promote invadopodia formation and cancer cell invasion. We report the role of HGF and its cognate receptor MET in TNBC invasion. The results from our study demonstrate that the TNBC cells when stimulated with HGF promotes invadopodia formation and facilitates delivery of MT1-MMP to the invadopodia in a MET dependent manner. We also showed that MET resides at invadopodia and its localization at invadopodia increases upon HGF treatment due to enhanced surface delivery of the RTK. By employing a degradation defective mutant, we demonstrated the critical role of MET recycling in driving breast cancer invasion. Moreover, we observed that the RCP–RAB14 axis mediates the surface delivery of MET through tubulovesicular carriers, with KIF16B promoting the formation of vesicular tubules on RAB14-positive endosomes. Collectively, the study provides mechanistic insights on the growth factor-mediated recycling of RTK and the associated metalloprotease in invadopodia-dependent matrix degradation and cancer cell invasion.

Introduction

Triple-negative breast cancer (TNBC) is a highly aggressive subtype of breast cancer and is characterized by the lack of expression of three key receptors: estrogen receptor (ER), progesterone receptor (PR), and human epidermal growth factor receptor 2 (HER2), which are generally targeted in conventional breast cancer therapies (1). The absence of these hormonal receptors in TNBCs imposes challenges in the treatment. Since one of the receptor tyrosine kinases (RTK), EGFR is often amplified in TNBC patients, they are usually targeted for its treatment (2). However, often patients develop resistance to EGFR-targeted therapies due to overexpression of another RTK MET (3,4).

In addition to the therapeutic challenges, TNBC exhibit a greater tendency for tumor invasion and metastasis which is one of the leading causes of higher mortality in TNBC patients (5,6). Metastasis requires the tumor cells to breach the tissue barrier employing proteolytic activity that remodel

the extra cellular matrix (ECM), enabling the cancer cells to infiltrate in to the stroma (7). Subsequently the invasive cancer cells migrate to a distant organ through circulation and colonize to form a secondary tumor. Invadopodia, are actin-rich membrane protrusions decorated with proteases, that act as a tool for ECM and basement membrane degradation during cancer cell invasion (8). MT1-MMP is one of the invadopodia-associated metalloproteases and is overexpressed in TNBC cell lines. Perturbation in MT1-MMP delivery to invadopodia impairs ECM degradation and invasion (9,10). Studies suggest that the invasive cells in the leading front form invadopodia to create micro-tracks for the follower cells (11). Growth factors and their receptors, including EGF-EGFR and HGF-MET, can modulate the invadopodia-associated molecules, thereby promoting invadopodia-associated cancer invasion and metastasis (12–15).

Signaling cues from RTKs are essential for invadopodia formation and ECM remodelling (14,16). EGFR induces cortactin phosphorylation through SRC and Abl-related gene (ARG), which triggers the formation of invadopodia (12). However, MET-directed cortactin phosphorylation in invadopodia is SRC or ARG-independent, implicating for a distinct mode of function for MET in invadopodia formation (14). A chemically induced cytoplasmic variant of the RTK, TPR-MET disrupts the balance between intracellular signalling and regulatory mechanisms, promotes invadopodia associated ECM degradation (14,17,18).

At the cell surface, the RTKs bind to their respective ligands, leading to receptor dimerization and activation. Subsequently, they internalize rapidly and continue to signal from endosomes (19). The signalling of RTKs from the endosomes are tightly regulated by endocytic trafficking (20). From the early endosomes, the RTKS are sorted in to distinct pathways directing them either towards lysosomal degradation or recycling to deliver them back to the plasma membrane (19,21). The sorting of cargo from the early endosomes is a highly co-ordinated process, that is majorly facilitated by RAB GTPases (22,23). RAB GTPases act as molecular switches, that provide membrane identity by recruitment of downstream effectors. RABs recruit tethering complexes, molecular motors, adapters for cargo or motors, lipid modifying enzymes etc, together which promotes efficient cargo selection, segregation and sorting (24). Membrane tubulation is a key mechanism of cargo sorting on the endosomal membrane (25,26). The tubular membrane curvature are often initialled and stabilized by Sorting nexins (SNX) having a BAR domain (27). The pulling force exerted by the molecular motors further help to elongate the structure (28–30). RAB dependent recruitment of specific machinery ensure the enrichment of cargo at these microdomains. Upon fission these tubular structures becomes independent carrier for cargo trafficking (31).

RAB GTPases like RAB4, RAB11 along with their associated trafficking machinery are known to facilitate the recycling of MET to the plasma membrane driving cell migration (32,33). Additionally, SNARE-dependent delivery of EGFR to invadopodia promotes invadopodia-associated tumor invasion, highlighting the potential role of RTK trafficking in cancer cell invasion (13). Although cell migration and invasion are tightly coupled processes, the significance of MET trafficking in cancer cell invasion is still poorly understood.

Here, we investigated the role of HGF and its cognate receptor, MET, in invadopodia-associated cancer cell invasion in TNBC cell lines. Our study revealed that activated MET resides at invadopodia and its invadopodia-recruitment is enhanced upon HGF stimulation. Our findings emphasize the importance of the growth factor-mediated cell-surface transport of MET in invadopodia formation and MT1-MMP recruitment through physical interaction with the protease that leads to enhanced TNBC invasion upon HGF stimulation. We further delineated the involvement of the cellular recycling repertoire in the growth factor-stimulated recycling of MET.

Results

HGF-induced MET activity promotes TNBC breast cancer invasion through invadopodia-mediated ECM degradation

The upregulation of EGFR and MET promotes breast cancer invasion (34,35). We examined the MET expression in TNBC cell lines MDA-MB-231, BT-549, and the pre-invasive MCF10A DCIS by immunoblotting. We observed comparable MET expression in all 3 cell lines (Fig. S1A, S6).

MET-HGF signalling axis is reported to promote invasion in gastric cancer cells and melanoma cells (15,36). To inspect the effect of HGF on the invasive properties of breast cancer cell lines, we employed a spheroid invasion assay that closely resembles the physiological environment. Spheroids were formed using MDA-MB-231 or BT-549 cells and embedded in collagen I with or without HGF or in complete media. The spheroids were allowed to invade for 48 hours. The ratio of core area to invaded area was calculated, revealing that HGF-treated cells invaded more into collagen compared to untreated conditions (Fig. 1A, S1B, Movie 1).

To invade the stroma, tumor cells degrade the underlying basement membrane. To understand the effect of HGF on ECM remodelling, we carried out a fluorescent-labelled gelatin degradation assay. We seeded cells on Alexa568-labeled gelatin-coated coverslips in the presence or absence of HGF and allowed them to degrade gelatin for a minimum of three hours. The loss of fluorescence due to gelatin degradation, represented as the degradation index, was calculated as detailed in the methods section. Our results showed that HGF treatment significantly increased gelatin degradation activity in MDA-MB-231, BT-549, and MCF10A DCIS cell lines (Fig. 1B, S1C-E).

The ECM degradation activity of cancer cells is attributed to invadopodia formation (37,38). Therefore, we investigated the ability of HGF to induce invadopodia in these cell lines. Cells were seeded on gelatin in the presence or absence of HGF for 6h, fixed, and immunostained for known invadopodia markers, i.e., TKS5, cortactin, or Actin. Puncta positive for two invadopodia markers were considered as invadopodia. When stimulated with HGF, increased numbers of invadopodia were observed in MDA-MB-231, BT-549 and MCF10A DCIS cells (Fig. 1C, S1C, D, F). The percentage of cells forming invadopodia was also found to be increased upon HGF treatment in MDA-MB-231 cells (Fig. S1G). Additionally, the other most abundant RTK in TNBC cells, EGFR, when activated by EGF, resulted in a significant increase in invadopodia number in MDA-MB-231 (Fig. S1H) cells, corroborating previous studies (12).

To investigate, whether MET is important for HGF-governed invadopodia formation, we depleted MET using siRNA and TKS5-Actin positive structures were quantified. The invadopodia numbers were found to be decreased upon MET silencing (Fig. 1D, S1I, S6). Since MET is an RTK, we asked whether the activation of MET is essential for invadopodia formation. To address this question, we inhibited the kinase activity of MET using the drug PHA665752. Immunoblot analysis revealed that HGF stimulation increased MET pTyr1234-1235 (p-MET), which was abolished by the drug (Fig. S1J). Interestingly, the drug treatment also promoted degradation of MET (Fig. S1J, S6). MDA-MB-231 cells were analyzed for their ability to form invadopodia in the presence of 5 μM of the drug or vehicle, with or without HGF. Inhibition of MET kinase activity using PHA665752 abolished the HGF-induced invadopodia formation (Fig. 1E, E′).

Next, we silenced MET using shRNA and analyzed the the effect on gelatin degradation. Different clones of shRNA against MET were transfected, and the level of silencing was evaluated (Fig. S1K, S6). MDA-MB-231 cells were transfected with control SHC002 or MET shRNA C#3. After 36h, cells were seeded on labelled gelatin for 6h, fixed, and immunostained with phalloidin and an antibody against MET. Gelatin degradation and invadopodia formation was abrogated in the MET-depleted cells compared to the control (Fig. 1F, S1L).

Taken together, HGF activates RTK MET and promotes TNBC invasion by enhancing invadopodia formation and associated activity.

Enhanced MET recruitment to invadopodia upon HGF stimulation

Since MET activity was found to be important for invadopodia formation, we first asked if MET is localized at invadopodia. MDA-MB-231 cells were seeded on a gelatin-coated surface for 6 hours. Then, the cells were fixed and immunostained for MET and cortactin. A notable population of cortactin puncta was found to be localized with MET (Fig. 2A). Next, the colocalization of MET to GFP-TKS5 was examined using TIRF microscopy (TIRFM). Approximately 30% of the TKS5 population showed staining for MET (Fig. 2B, D). Confocal imaging of BT-549 cells immunostained for TKS5 and MET revealed that MET-TKS5 colocalization follows the same trend as MDA-MB-231 (Fig. S2A). Next, we asked whether MET is in its active form at invadopodia.

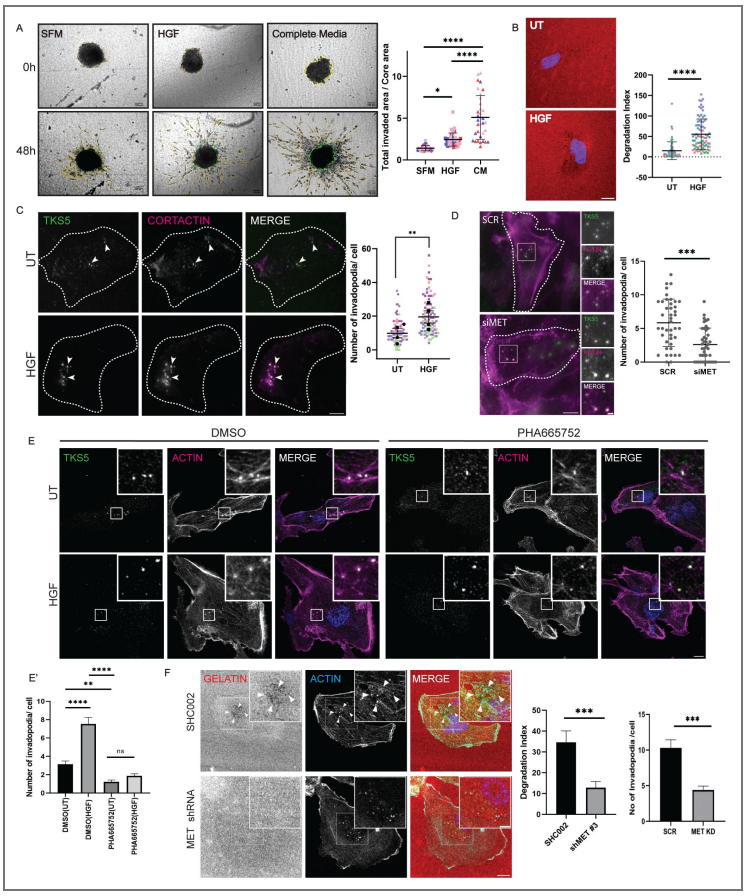

Figure 1. HGF-induced MET activity promotes TNBC breast cancer invasion through invadopodia-mediated ECM degradation

(A) Bright-field images of MDA-MB-231 spheroids embedded in the collagen matrix at 0h and 48h in the presence or absence of HGF or complete media. The ratio of the invaded area to the core area was quantified and plotted. The core has been outlined in green, and the invaded area has been outlined in yellow. Data points from individual biological replicates are distinctly color-coded. The error bar represents Mean ±SD, One-way ANOVA with multiple comparisons. **** P < 0.0001, * P < 0.05, Scale bar: 100µm. N=3, n=30. (B) MDA-MB-231 cells were seeded on Alexa568-labeled gelatin-coated coverslip with or without HGF for 3h. Cells were fixed and imaged with a confocal microscope. The degradation index was quantified and plotted. The arrowhead represents degradation spots. Data points from individual biological replicates are distinctly color-coded. The error bar represents Mean ±SD, Unpaired t-test, **** P < 0.0001. scale bar: 10µm. N=3, n=200. (C) MDA-MB-231 cells were seeded on a gelatin-coated glass-bottom dish and allowed to attach for 3 hours, followed by incubation with or without HGF for an additional 3 hours. Cells were fixed and immunostained for TKS5 and cortactin. Images were captured using a TIRF microscope. TKS5 puncta positive for cortactin were considered as invadopodia. Arrowheads indicate TKS5-cortactin positive puncta. Data points from individual biological replicates are distinctly color-coded. The error bar represents Mean ±SD, Paired t-test, ** P < 0.01. scale bar: 10µm. N = 4, n = 150. (D) MDA-MB-231 cells were transfected with control or MET siRNA. After 60 hours of transfection, cells were seeded on a gelatin-coated glass-bottom dishes for 6h. Cells were fixed and immunostained for TKS5, and F-actin. Images were captured using a Nikon TIRF microscope. TKS5 and Actin-positive structures were identified and plotted. The inset shows a magnified view of the region indicated by the box. The error bar represents Mean ±SEM, Unpaired t-test, *** P < 0.001. scale bar: 10µm. Inset: 2µm. N=3, n=60. (E, E') MDA-MB-231 cells were seeded on gelatin-coated coverslips for 3h, followed by incubation with vehicle or PHA665752 (5 µM) with or without HGF for an additional 3h. Cells were fixed, immunostained with anti-TKS5 antibody, Phalloidin to stain F-actin, and DAPI. Images were captured using a confocal microscope. TKS5 puncta positive for Actin were considered as invadopodia. The inset shows a magnified view of the region indicated by the box. scale bar: 10µm. Inset: 2µm. The error bar represents Mean ±SEM, One-way ANOVA with multiple comparisons. **** P < 0.0001, ** P < 0.01, ns P > 0.05, N=3, n=200. (F) MDA-MB-231 cells were transfected with control SHC002 or MET shRNA clone #3, and after 36h of transfection, cells were seeded on Alexa568-labeled gelatin-coated coverslip for 6h. The cells were fixed and immunostained with anti-MET antibody, Phalloidin, and DAPI. Degradation index and degradation spots immunostained for Actin were quantified. The inset shows a magnified view of the region indicated by the box. The Arrowheads indicate the degradation spots that were immunostained for Actin. scale bar: 10µm. Inset: 2µm. The error bar represents Mean ±SEM, Unpaired t-test. *** P < 0.001, N=3, n=200.

Cherry-TKS5 expressing cells were seeded on gelatin, fixed, and immunostained for phosphorylated MET. TIRF imaging revealed that 27% of TKS5 puncta are positive for p-MET, similar to that of MET localization to TKS5-positive invadopodia (Fig. 2C, D).

TKS5 is a critical component of invadopodia and its concentration gradually increases as the invadopodia matures (39). When we plotted the normalized steady-state fluorescence intensity of MET and TKS5 localized at invadopodia, the resulting plot showed two different populations of invadopodia. Invadopodia with TKS5 intensity less than 4 showed no correlation with MET intensity (R^2 = 0.03 for linear regression); however, invadopodia with TKS5 intensity more than 4 showed a negative correlation (R^2 = 0.3 for linear regression) (Fig. 2E). Further, we analyzed the frequency distribution of the MET to TKS5 fluorescence intensity ratio across invadopodia. It revealed that most invadopodia structures exhibited lower MET/TKS5 ratios (Fig. S2B). This observation prompted us to investigate the apparent absence of MET from mature invadopodia. To address this, the localization of MET at the invadopodia-mediated degradation spots was examined in the MDA-MB-231 cells plated on fluorescence-labelled gelatin. As implied above, the degradation spots did not show strong colocalization with MET (Fig. 2F).

As we have observed that HGF stimulates invadopodia formation via MET and the RTK is physically localized at the invadopodia site, we asked if HGF influences MET localization to the invadopodia. Cells were seeded on gelatin with or without HGF, fixed, and immunostained for MET and invadopodia markers. Intriguingly, upon treatment with HGF, we observed an increased MET-containing TKS5-positive invadopodia structure in both MDA-MB-231 and BT-549 (Fig. 2G-H, S2C- D). This observation led us to hypothesize that HGF may induce the surface delivery of MET to invadopodia.

Previously, it was reported that HGF stimulation leads to endocytosis of MET, followed by lysosomal degradation of the RTK (18,40). First, we analyzed the effect of HGF on receptor endocytosis and degradation of MET. To study the HGF-mediated receptor endocytosis, the colocalization of MET with RAB5 was quantified with or without HGF. The percent colocalization of MET with RAB5 was found to be increased from 12% to 43% in the presence of HGF stimulation (Fig. S2E). Next, cells were incubated with HGF for different time points, and the total MET levels were quantified using immunoblotting. After 3h of HGF stimulation, ~44% of MET was found to be degraded (Fig. S2F, S6).

Next, to validate our hypothesis that HGF can induce surface delivery of MET, GFP-MET-expressing cells were imaged with TIRFM with or without HGF, and MET tracks were quantified as explained in the method. In the presence of HGF, an increased number of MET tracks were found near the plasma membrane compared to the untreated cells (Fig. 2I, Movie 2). This suggests that HGF indeed increases the trafficking of MET to the cell surface. We also observed a similar effect of EGF on EGFR localization at invadopodia (Fig. S2G, H), consistent with an earlier study in MDA-MB-231 (13).

These observations convey that MET resides in the invadopodia structures and HGF treatment leads to enhanced surface delivery of MET and its recruitment to invadopodia.

HGF-mediated surface delivery of MET promotes invadopodia-associated ECM degradation and breast cancer cell invasion

As HGF promotes MET recycling and breast cancer invasion, we investigated whether MET recycling drives invadopodia-associated TNBC invasion. To address this, we employed the degradation-defective M1250T mutant and the endocytosis-defective LL/AA MET mutant as a negative control. An oncogenic mutation in MET at M1268T (M1250 in the MET constructs used in this study) is naturally found in papillary renal carcinoma, has a degradation defect leading to continuous endocytosis and recycling (33). The dileucine motif of MET is required for endocytosis of the receptor, which is mutated to AA in this study (41). First, we have characterized the mutants for endocytosis and degradation. We looked into the degradation kinetics of the mutants by immunoblotting. Unlike the wild-type (WT) MET, the M1250T MET mutant did not undergo degradation upon HGF stimulation (Fig. 3B, S6). Since the M1250T mutant has a slower

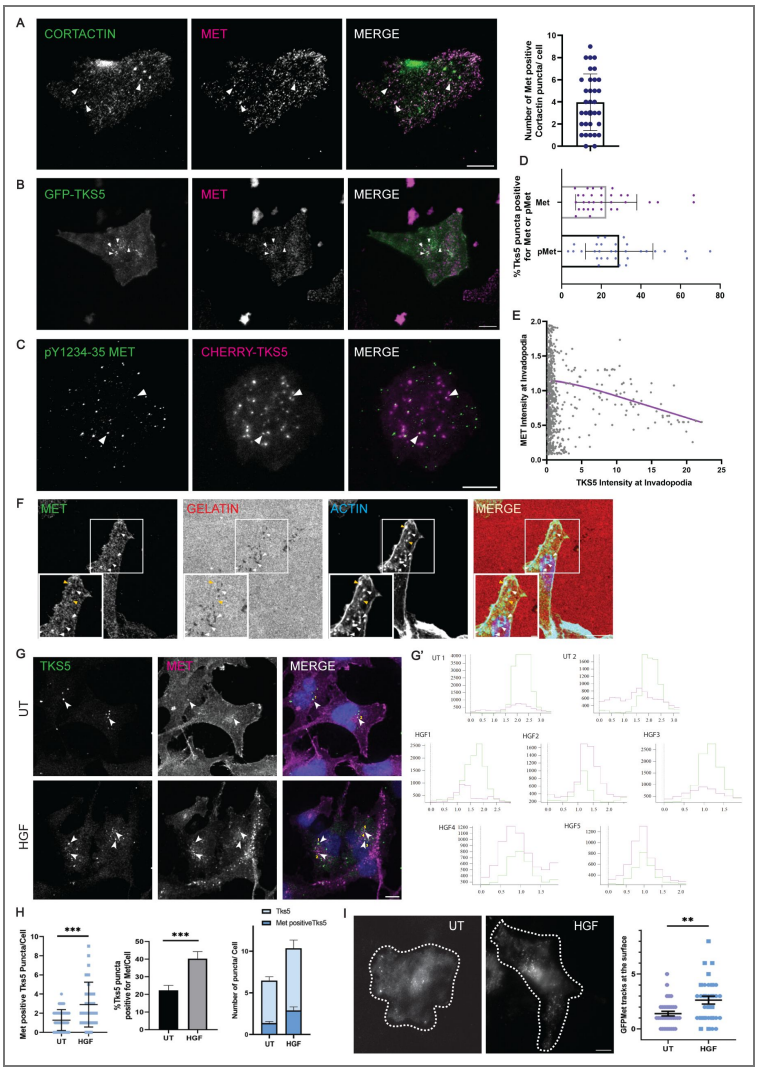

Figure 2. Enhanced MET recruitment to invadopodia upon HGF stimulation

(A) MDA-MB-231 cells were seeded on gelatin-coated imaging dishes for 6h. Cells were fixed and immunostained for cortactin and MET. Images were captured using a TIRF microscope. Colocalized cortactin-MET puncta were quantified and plotted. The arrowheads indicate the MET-positive cortactin puncta. The error bar represents Mean ±SD, scale bar: 10μm, n= 60. (B) GFP-TKS5-expressing MDA-MB-231 cells were seeded on gelatin-coated imaging dishes for 6h. Cells were fixed, immunostained for MET and imaged with TIRFM. The arrowhead indicates the MET-positive TKS5 puncta. scale bar: 10μm. (C) Cherry-TKS5-expressing MDA-MB-231 cells were seeded on gelatin-coated glass-bottom imaging dishes for 6h. Cells were fixed, immunostained with anti-p-MET antibody and imaged with TIRFM. The arrowhead indicates the p-MET-positive TKS5 puncta. scale bar: 10μm. (D) Colocalized TKS5-MET or p-MET puncta were quantified and plotted. The error bar represents Mean ±SD, N=3, n ≤ 50. (E) The fluorescence intensity of TKS5 and MET at individual invadopodium was quantified using Motiontracking and normalized with their respective mean intensities. The normalized fluorescence intensities of TKS5 (X-axis) and MET (Y-axis) were plotted. The points were fitted with a smoothing spline. n=800 (invadopodia). (F) MDA-MB-231 cells were seeded on Alexa568-labeled gelatin-coated coverslips for 12h. Cells were fixed and immunostained for F-actin and MET. The inset shows a magnified view of the region indicated by the box. The white Arrowhead represents Actin at the degradation spots, and the yellow arrowhead represents Actin-MET puncta without degradation. scale bar: 10μm. Inset: 2μm. (G) BT-549 cells were seeded on gelatin-coated coverslips for 3h followed by incubation with or without HGF for 3h. Cells were fixed, immunostained for TKS5, MET and Nucleus. Images were taken using the confocal microscope. scale bar: 10μm. (G') Using Motiontracking a line was drawn across indicated MET-TKS5 puncta and the intensities of both channels were plotted. (H) Colocalized TKS5-MET puncta were quantified using Motiontracking and plotted. The error bar represents Mean ±SEM/SD, Unpaired t-test, *** P < 0.001, N=3, n = 200. (I) BT-549 cells expressing GFP-MET were seeded on glass-bottom dishes. The cells were imaged using a TIRF microscope in the presence or absence of HGF. The GFP-MET vesicles moving in the TIRF field for a minimum of 4 consecutive frames were quantified and plotted as MET tracks. The error bar represents Mean ±SEM, Unpaired t-test. scale bar: 10μm. ** P < 0.01, N=3, n=30.

degradation rate, we asked whether the M1250T mutant is in its activated form. V5 tagged-MET WT or the mutant was overexpressed and pulled down using Ni-NTA beads through the His-tag present in the coding region. The pulled-down samples were analysed by immunoblotting using the p-MET antibody. M1250T MET was highly phosphorylated at the active site compared to the WT MET (Fig. 3C, S6). The observation was further confirmed by immunofluorescence. The normalized CTCF value of p-MET in M120T MET expressing cells was found to be higher compared to WT MET (Fig. S2I). Next, the effect of HGF on the endocytosis of WT or the mutant MET was investigated. Cells were transfected with WT V5-MET or the mutant constructs, and their percentage of localization with EEA1, an early endosomal marker, was quantified in the presence or absence of HGF. HGF stimulation leads to an increased MET population localizing with EEA1 in WT MET expressing cells, whereas M1250T mutant cells showed an increased colocalization with EEA1 irrespective of the HGF stimulation (Fig. 3D, D'). The endocytosis-defective LL/AA mutant did not show any increase in the EEA1 colocalization in response to HGF.

To understand the effect of intracellular trafficking of MET on breast cancer invasion, cells expressing the WT or mutant forms of MET were analyzed for their ECM degradation ability. WT or the mutant V5-MET expressing BT-549 cells were seeded on Alexa568-labeled gelatin-coated coverslip with or without HGF, fixed, and immunostained with anti-V5 antibody. Confocal image analysis showed that WT MET-expressing cells have enhanced ECM degradation ability when stimulated with HGF; however, neither mutant responded to HGF (Fig. 3E, E'). The mutant M1250T MET showed comparable gelatin degradation as the WT MET stimulated with HGF, whereas the LL/AA had decreased invasion ability. We repeated the experiment in MDA-MB-231 cells and observed similar trends for the mutants (Fig. S2J).

Since the ECM degradation ability of M1250T was higher, we asked whether it was because of increased invadopodia formation. M1250T MET-expressing cells showed increased invadopodia formation compared to WT MET-expressing cells (Fig. 3F, S2K, K'). However, cells expressing the LL/AA mutant did not show a significant difference compared to WT MET (Fig. S2K, K'). Also, the number of invadopodia positive for M1250T MET was higher compared to WT MET-positive invadopodia (Fig. 3F)

To further investigate the effect of the M1250T MET mutant on breast cancer invasion, we employed a spheroid invasion assay. We generated a doxycycline-inducible GFP-MET WT and M1250T cell line in BT-549. Spheroids were formed for WT and M1250T MET expressing cells and embedded in collagen for 24 hours to allow invasion. The M1250T GFP-MET expressing cell line invaded more into the collagen compared to the WT MET expressing spheroid (Fig. 3G), supporting our observations from gelatin degradation.

These observations demonstrated that MET recycling ensures a steady delivery of the RTK to the invadopodia structures, thereby promoting breast cancer invasion.

HGF promotes RAB4 & RAB14-mediated MET delivery to the plasma membrane

RAB GTPases are molecular switches, localized to distinct endosomal compartments, and orchestrate various endocytic, trans, and exocytic pathways (42). To investigate the RABs involved in MET recycling, we first inspected the colocalization of MET with endosomal markers that work in the recycling pathways, like RAB4, RAB22, RAB14 and RAB11. Cells were transfected with the different RAB constructs and incubated in the presence or in the absence of HGF before fixing and immunostaining for MET. The object-based percentage of colocalization was calculated using Motiontracking, for which vesicles for each molecule were identified, and the objects were considered to be colocalized if the overlap of their respective area was more than 35%. While the localization of MET with RAB4 and RAB14 was found to be increased in the HGF-stimulated cells (Fig. 4A-C, S3A-C), the colocalization with RAB22 and RAB11 remained unchanged, suggesting them to be associated with an HGF-independent trafficking pathway (S3D, E).

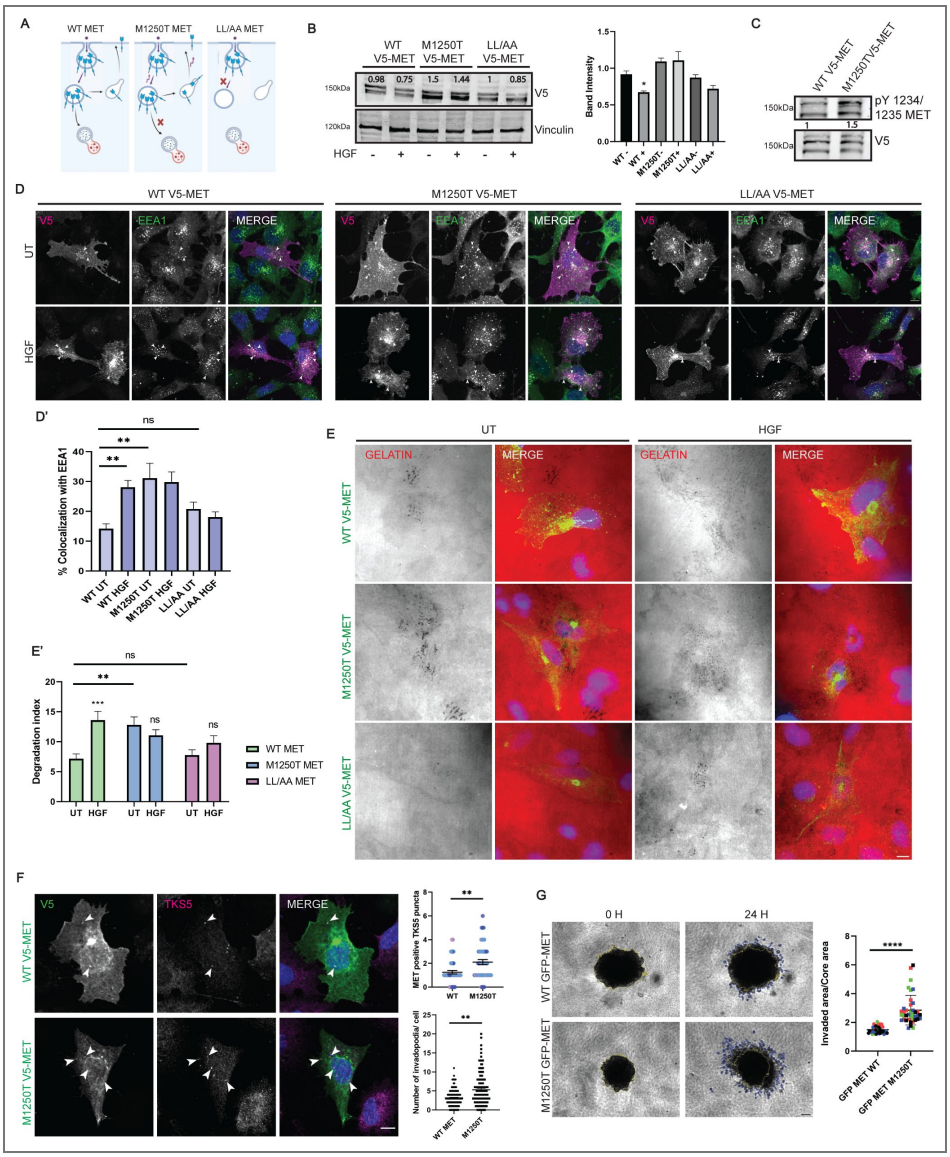

Figure 3. Intracellular trafficking of MET promotes invadopodia-associated ECM degradation and breast cancer cell invasion

(A) Graphical representation of WT MET and mutants' endocytosis and degradation. (B) BT-549 cells expressing WT or the mutants of V5-MET were treated with or without HGF for 2 hours, followed by cell lysis. The lysates were subjected to immunoblotting with anti-V5 and anti-vinculin antibodies. The V5 signal intensity was quantified and normalized with Vinculin. Error bar represents Mean ±SEM. Unpaired t-test. * $P < 0.05$. (C) BT-549 cells expressing WT or M1250T V5-MET were lysed and incubated with Ni-NTA beads. The pulled-down samples were separated by SDS PAGE and processed for immunoblotting with anti-V5 and anti-p-MET antibody. (D, D') WT or mutant V5-MET expressing BT-549 cells were seeded on glass coverslips with or without HGF. Cells were fixed, immunostained for V5 and EEA1. Images were captured with a confocal microscope. V5-MET puncta localizing with EEA1 were quantified and plotted. scale bar: 10μm. The error bar represents Mean ±SEM. ** $P < 0.01$. ns $P > 0.05$ N=3, n=60. (E, E') BT-549 cells expressing V5-MET WT or mutants were seeded on Alexa568-labeled gelatin-coated coverslips with or without HGF for 6h. Cells were fixed, then immunostained for V5 and the Nucleus and imaged with the confocal microscope. Gelatin degradation by the V5-MET overexpressing cells was calculated and plotted. scale bar: 10μm. The error bar represents Mean ±SEM, Unpaired t-test. ** $P < 0.01$, ns $P > 0.05$, N=3, n=120. (F) V5-MET WT or M1250T mutant expressing BT-549 cells were seeded on a gelatin-coated coverslip for 6h and fixed. Cells were immunostained for V5, TKS5, and images were captured with the confocal microscope. The error bar represents Mean ±SEM, Unpaired t-test. scale bar: 10μm. ** $P < 0.01$, N=3, n=120 (G) Bright-field images of GFP-MET WT or M1250T expressing BT-549 spheroids embedded in the collagen matrix at 0h and 24h. The ratio of the invaded area to the core area was quantified and plotted. Data points from individual biological replicates are distinctly color-coded. The error bar represents Mean ±SD, Unpaired t-test. scale bar: 100μm. **** $P < 0.0001$, N=3, n=40.

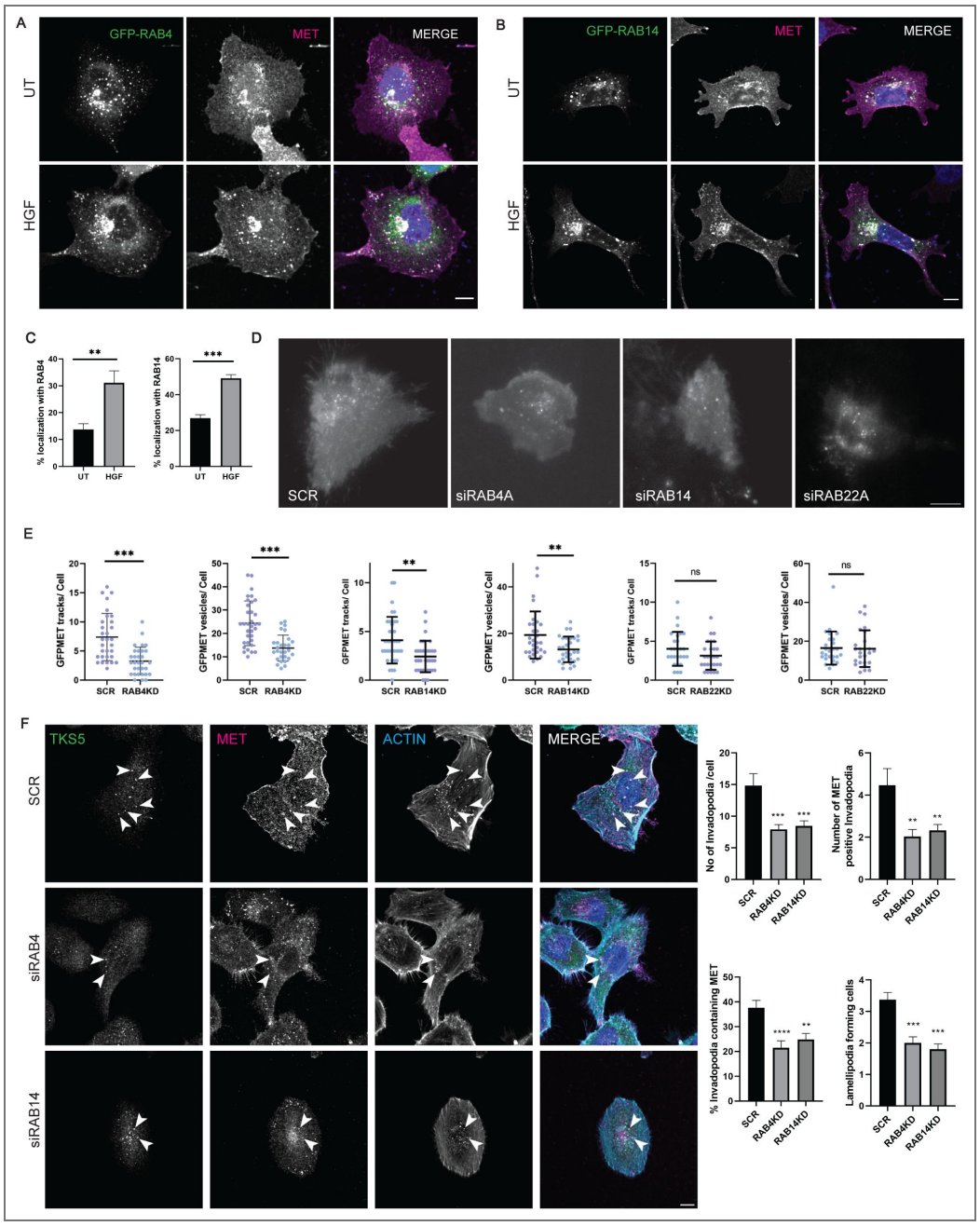

Figure 4. HGF promotes RAB4 & RAB14 mediated MET delivery to the plasma membrane

BT549 cells, seeded on glass coverslips, were transfected with (A) GFP-RAB4 or (B) GFP-RAB14. After 14h of transfection, cells were incubated for 2h with or without HGF, then fixed and immunostained for MET. Images were captured using a confocal microscope. scale bar: 10μm. (C) Graph showing the percent colocalization of MET with GFP-RAB4 and GFP-RAB14 in the presence of absence of HGF treatment. The error bar represents Mean ±SD, Unpaired t-test. ** P< 0.01. N=3, n=90 (D) BT-549 cells were transfected with siRNA against RAB4, RAB14, RAB22, or control siRNA. After 60 hours, cells were transfected with GFP-MET and seeded on the gelatin-coated glass-bottom dish. The GFP-MET-transfected cells were imaged in the presence of HGF using a TIRF microscope for 30 frames without an interval. scale bar: 10μm (E) The GFP-MET vesicles forming the track were identified as mentioned in the Method section. The numbers of GFP-MET tracks moving for at least 4 consecutive frames were quantified for each condition and plotted. In addition, the total number of GFP-MET vesicles was quantified. The error bars represent Mean±SD. Unpaired t-test. *** P< 0.001, ** P< 0.01, ns P > 0.05, N=3, n = 30. (F) BT-549 cells were depleted with RAB4 or RAB14, and after 60h, cells were seeded on gelatin-coated coverslips for 6h with 3h of HGF stimulation. Cells were fixed and immunostained for MET, TKS5, and F-actin. Images were captured in a confocal microscope. MET colocalizing with invadopodia was quantified and plotted. The number of cells forming lamellipodia was quantified. scale bar: 10μm. The error bar represents Mean ±SEM, One-way ANOVA, *** P< 0.001, ** P< 0.01. N=3, n=200.

Next, to identify the RABs that are involved in the HGF-dependent MET surface delivery, live cell TIRF imaging was performed in RAB4, RAB14, and RAB22-depleted cells. As the role of RAB4 in MET recycling has been established before, it was included as a positive control (32). The RABs were silenced using SMARTpool siRNA, and knockdown efficiency was quantified (Fig. S3F). GFP-MET was overexpressed in the control and the RABs-depleted cells and imaged using a TIRF microscope in the presence of HGF. The total number of MET vesicles, including MET tracks at the surface, was found to be reduced when RAB4 or RAB14 was deleted compared to the control cells (Fig. 4D-E, Movie 3).

When the recycling is impaired, a significant population of the RTKs is subjected to degradation (33,43). Next, to study the fate of MET in the RABs-depleted cells, we performed immunoblotting to quantify the total population of cellular MET. Cells depleted of the RABs mentioned above were treated with HGF. Cells were lysed and subjected to immunoblotting. The RAB4 and RAB14-depleted cells were observed to have a decreased total MET level compared to the control (Fig. S3G, S6).

Since the retromer is known to drive the recycling of various cargoes to the plasma membrane, we checked the role of retromer depletion on MET recycling (44). The co-localization of MET with VPS35, a retromer subunit, was comparable with or without HGF (Fig. S3M). Further to analyze whether retromer is essential for MET trafficking, MDA-MB-231 cells were depleted for the VPS26A retromer subunit, and the MET localization to Actin at fan-shaped membrane protrusions in response to HGF stimulation was quantified. The membrane pool of MET localizing with actin-rich structures was unchanged in the retromer-depleted condition (Fig. S3N). The total MET in the retromer-silenced cells also remained unaffected (Fig. S3K).

As HGF stimulation leads to increased recruitment of MET to invadopodia, we asked whether RAB4 & RAB14-mediated MET recycling plays a role in invadopodia formation and MET colocalization at the invadopodia. Cells depleted with RAB4 or RAB14 were analyzed for their ability to form invadopodia and the MET localization to the structure. As expected, invadopodia numbers were reduced in RAB4 and RAB14-depleted cells. Further, MET localization to invadopodia was also found to be reduced (Fig. 4F). In line with previous findings, the number of lamellipodia-forming cells was also drastically reduced in the RAB4 and RAB14-silenced cells (Fig. 4F) (32,43,45).

We examined the colocalization of RAB14 with EEA1, and 60% of the RAB14 was found to be colocalized with EEA1 (Fig. S3H). However, a small population of MET-containing RAB14 vesicles (~10%) was not EEA1 positive and present away from the nucleus. Next, we analyze the distribution of MET to RAB4 and RAB14 vesicles using super-resolution microscopy. The GFP-RAB4 and Cherry-RAB14 expressing cells were stimulated with HGF, then fixed and immunostained for MET. The peripheral vesicles containing MET were positive for RAB4 or RAB14, with RAB14-positive MET endosomes showing minimal or no RAB4 presence, whereas the RAB4-positive MET endosomes are devoid of RAB14 (Fig. S3I).

A study from Wang et.al. suggests that RAB14 vesicles can also be budded out from the Golgi (46). We analyzed the localization with a Golgi marker to understand the biogenesis of these RAB14-MET vesicles. Cherry-RAB14 expressing cells were fixed and immunostained with anti-MET and anti-Golgin97 antibody. A small fraction (4%) of RAB14-positive MET puncta localized with the Golgi (Fig. S3L).

When we analyzed the effect of HGF on RAB14 vesicular characteristics. GFP-RAB14 expressing cells were treated with or without HGF, fixed, and imaged with a confocal microscope. The integral intensity and area of RAB14 vesicles were quantified. The area of GFP-RAB14 vesicles was found to be increased in the HGF-treated cells, whereas the integral intensity was unaffected (Fig. S3J). This indicates that the effect of HGF on the trafficking pathway is not mediated solely by RAB14, but also that additional players are involved in the RAB14-mediated trafficking.

The above results suggest that a fraction of the MET recycles back to the surface via the RAB4 or RAB14-mediated recycling pathway, which is crucial for the recruitment of MET to invadopodia.

RCP-RAB14-KIF16B axis regulates MET trafficking

The mechanism behind HGF-mediated MET recycling through RAB4 has been demonstrated earlier (32,43). So, we set out to study the RAB14-dependent trafficking of MET. Rab coupling protein (RCP) is known to be an interacting partner of RAB14, and a study in the H1299 cell line reported it to interact with MET (47,48). RCP is also reported to be overexpressed in several cancer type and associated with metastatic property (49,50). To explore the alterations of RCP in breast cancer, we analyzed 32 publicly available breast cancer datasets consisting of a total of 15404 patients in cBioportal and found that RCP is amplified in these datasets, supporting Zhang et al (Fig. S4A) (49).

First, we analyzed the colocalization of MET and GFP-RCP with EEA1. Cells transfected with GFP-RCP were treated with HGF and then fixed, followed by immunostaining for MET and EEA1. In colocalization analysis, we found that 37 % of MET-positive RCP vesicles colocalize with EEA1 (Fig. S4B). To study whether RCP has any role in the RAB14-mediated MET recycling, we examined its subcellular localization on RAB14-MET vesicles in the presence or absence of HGF. Due to the unavailability of a validated antibody for immunocytochemistry for RAB14 and RCP, overexpression constructs were used. The anti-RCP antibody used for immunoblotting was not applicable for immunofluorescence. GFP-RCP and Cherry-RAB14 co-expressing cells were fixed and immunostained for MET. Images were captured using a confocal microscope, and the colocalization of MET-RAB14 with RCP was analyzed. In agreement with Gundry et.al, we observed an increased localization of RCP with RAB14 (35% to 51%) in the presence of HGF stimulation (48). Further, the colocalization of RCP with MET (32% to 48%) and MET-RAB14 (22% to 37%) was found to be increased upon HGF stimulation (Fig. 5A).

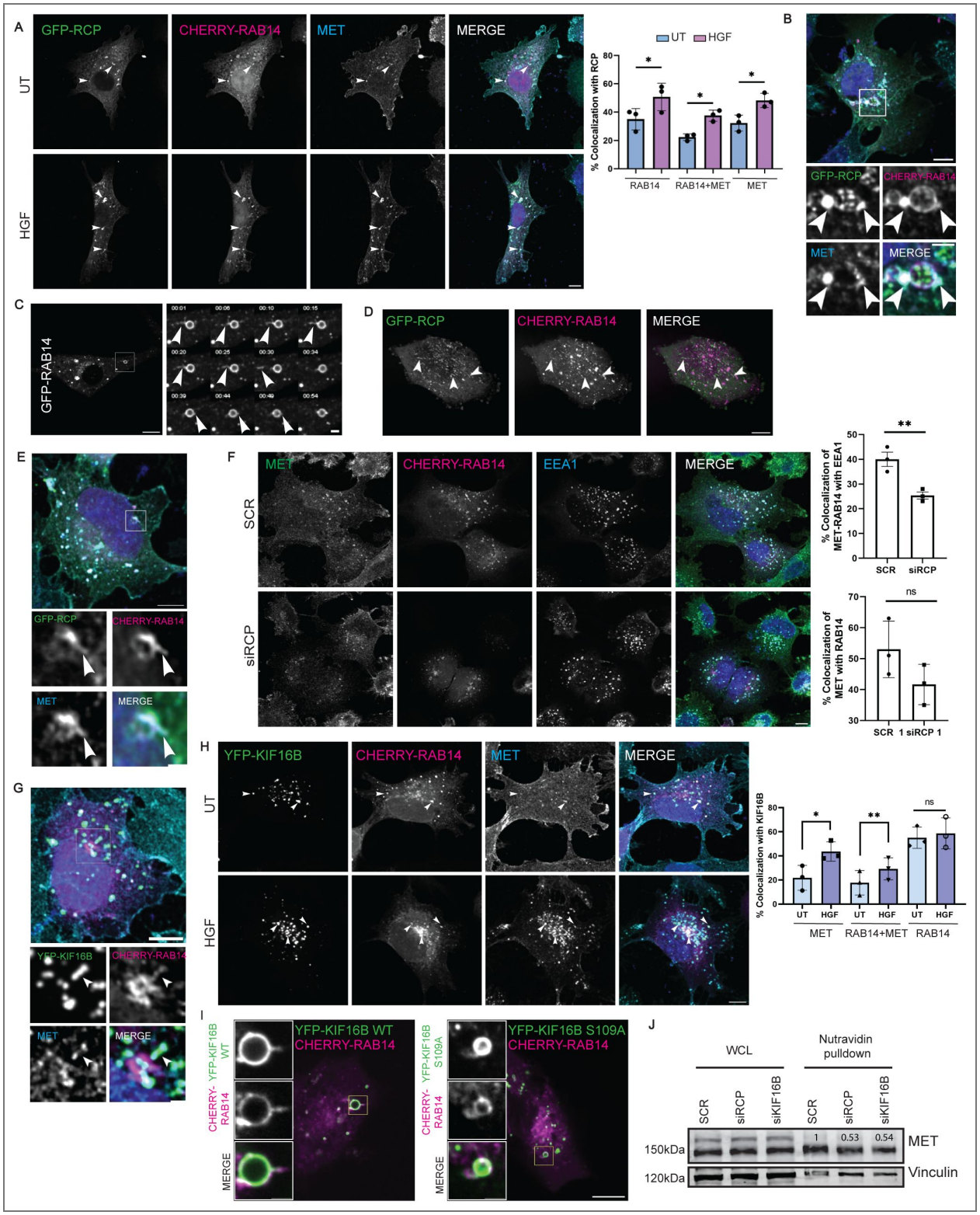

Figure 5. RCP-RAB14-KIF16B trafficking axis regulates MET recycling

(A) BT-549 cells seeded on glass coverslips were transfected with GFP-RCP and Cherry-RAB14. After 14h of transfection, cells were incubated for 2h with or without HGF, then fixed and immunostained for MET. Images were captured using a confocal microscope. scale bar: 10μm. The percent colocalization of GFP-RCP with RAB14 or RAB14-MET in the presence or absence of HGF treatment was calculated and plotted. scale bar: 10μm. The error bar represents Mean ±SD. Paired t-test. * P< 0.05, N=3, n=200. (B) BT-549 cells seeded on glass coverslips were

transfected with GFP-RCP and Cherry-RAB14. After 14h of transfection, cells were incubated for 2h with HGF stimulation, then fixed and immunostained for MET. Images were captured using a confocal microscope. The inset shows a magnified view of the region indicated by the box. scale bar: 10μm. Inset: 2μm. (C) BT-549 cells were transfected with GFP-RAB14 and seeded on a glass-bottom imaging dish. Time-lapse images were captured using a confocal microscope. The inset shows the events over time, where the tubule is formed and, upon fission, dissociates from the vesicular body. Scalebar: 10μm, Inset: 2μm (D) BT-549 cells co-transfected with GFP-RCP and Cherry-RAB14 were seeded on a glass-bottom imaging. Time-lapse movies were captured using a confocal microscope. Arrowheads indicate the endosomal tubules containing RCP and RAB14. Scalebar: 10μm. (E) BT-549 cells seeded on glass coverslips were transfected with GFP-RCP and Cherry-RAB14. After 14h of transfection, cells were incubated for 2h with HGF stimulation, then fixed and immunostained for MET. Images were captured using a confocal microscope. The inset shows a magnified view of the region indicated by the box. scale bar: 10μm, Inset: 2μm. (F) BT-549 cells were treated with control or SMARTpool siRNA against RCP. 60h after transfection, cells were transfected with Cherry-RAB14. After providing 2 hours of HGF stimulation, cells were fixed and immunostained for MET and EEA1. Images were captured using a confocal microscope. The percentage colocalization of RAB14 endosomes containing MET with EEA1 was calculated. scale bar: 10μm. The error bar represents Mean ±SD. Paired t-test. ** P< 0.001, ns P > 0.05, N=3, n=200. (G) BT-549 cells seeded on glass coverslips were transfected with YFP-KIF16B and Cherry-RAB14. After 14h of transfection, cells were incubated for 2h with HGF stimulation, then fixed and immunostained for MET. Images were captured using a confocal microscope. The inset shows a magnified view of the region indicated by the box. scale bar: 10μm, inset: 2μm. (H) BT-549 cells seeded on glass coverslips were transfected with YFP-KIF16B and Cherry-RAB14. After 14h of transfection, cells were incubated for 2h with or without HGF, then fixed and immunostained for MET. Images were captured using a confocal microscope. scale bar: 10μm. The percent colocalization of YFP-KIF16B with RAB14 or RAB14-MET in the presence or absence of HGF treatment was calculated and plotted. scale bar: 10μm. The error bar represents Mean ±SD. Unpaired t-test. ** P< 0.01, * P< 0.05, ns P > 0.05, N=3, n=200. (I) BT-549 cells co-transfected with YFP-KIF16B WT or S109A mutant and Cherry-RAB14 were seeded on a glass-bottom imaging dish. Time-lapse images were captured using a confocal microscope. The inset shows a magnified view of the region indicated by the box. scale bar: 10μm, Inset: 2μm. N=3, n=20. (J) RCP or KIF16B were silenced using SMARTpool siRNA in MDA-MB-231 cells. After 72h of transfection of siRNA, cells were treated with HGF for 30 minutes and proceeded for surface biotinylation. The cells were incubated with biotin at 4°C for 45 minutes. Washes were given to remove excess biotin; subsequently, biotin was quenched, and cells were lysed. The lysate was allowed to bind with Neutravidin beads and the biotinylated proteins were precipitated. The samples were separated by SDS-PAGE and processed for immunoblotting. The number indicates the MET signal normalized with MET signal intensity of the respective WCL and further normalized with vinculin signal intensity.

Gundry et al demonstrated that HGF stimulation induces phosphorylation of RCP at Ser435, which enhances its complex formation with RAB14. We analyzed the distribution of MET and RAB14 in the presence or absence of HGF stimulation with the RCP S435A mutant. An increased colocalization of RCP S435A with MET (38% to 58%) and MET-RAB14 (28% to 48%) vesicles was observed upon HGF stimulation (Fig. S4C). However, the colocalization of RCP S435A with RAB14 did not increase with HGF treatment.

Interestingly, we observed that MET and RCP are enriched at the vesicular buds on RAB14 vesicles (Fig. 5B), which are critical for cargo sorting and recycling. Live cell imaging of GFP-RAB14 revealed that these buds elongate and undergo fission to form tubulovesicular structures (Fig. 5C, Movie 4). Live-cell confocal imaging of cells expressing GFP-RCP and Cherry-RAB14 revealed the presence of RCP in the RAB14 tubules (Fig. 5D, Movie 5). Subsequently, fixed cell confocal imaging highlighted that MET is present in these tubular elongations emanating from endosomes along with RCP and RAB14 (Fig. 5E). Further, the MET-containing GFP-RCP vesicles were positive for WASH staining, which promotes actin polymerization at endosomes (Fig. S4D) (30).

To investigate whether RAB14 plays a role in RCP recruitment to MET-endosomes, we overexpressed GFP-RCP in RAB14-depleted cells, then fixed and immunostained them with the anti-MET antibody. Confocal imaging revealed that the percentage of colocalization of MET with RCP was unaltered in the RAB14-silenced cells (Fig. S4E). Next, we examined the role of RCP in RAB14 and MET endosomal association. RCP was depleted with siRNA and validated with qRT-PCR

and immunoblotting (Fig. S4F, G). The cells were transfected with Cherry-RAB14, treated with HGF, and fixed. Subsequently, the cells were immunostained with antibodies against MET and EEA1. Images were captured with a confocal microscope, and colocalization was quantified. A 15% decrease in colocalization of MET to RAB14 endosomes that was present with EEA1 was observed in the RCP-silenced cells compared to the control (Fig. 5F). Further, upon RCP depletion, the colocalization of MET to RAB14 was found to be reduced by 10%, but was statistically non-significant (Fig. 5F). The pool of MET or RAB14 vesicles that do not colocalize with EEA1 as observed in (Fig S3H) was unperturbed upon RCP silencing (Fig. S4I).

Molecular motors are one of the effectors of RAB GTPase, which cause membrane tubulation, thereby promoting protein sorting and trafficking. KIF16B is one of the motor proteins known to work with RAB14 (51). Hence, we analysed the colocalization of MET-containing RAB14 vesicles with KIF16B. Cells expressing YFP-KIF16B and Cherry-RAB14 were fixed and immunostained for MET. Confocal imaging revealed that KIF16B also resides in the endosomal tubules along with RAB14 and MET (Fig. 5G). Next, we analyzed the colocalization of RAB14-MET endosomes with KIF16B in the presence or absence of HGF. YFP-KIF16B and Cherry-RAB14 co-expressing cells were fixed and immunostained for MET. Images were captured using a confocal microscope, and percentage colocalization was quantified using Motiontracking. An increased colocalization of MET (21% to 43%) and MET-RAB14 (17% to 29%) vesicles with KIF16B was observed in the presence of HGF (Fig. 5H). However, RAB14 colocalization to KIF16B remained unaltered upon HGF treatment (Fig. 5H). Since KIF16B is an effector of RAB14, upon silencing of the GTPase, the colocalization of KIF16B with MET was found to be reduced, as expected (Fig. S4J) (51).

KIF16B is known to promote tubulation in the early endosomes (52). So, to investigate the potential role of KIF16B in RAB14 endosomal tubulations, we overexpressed WT or the dominant negative form of the motor with an Ala substitution at the S109 position of KIF16B. BT-549 cells co-expressing Cherry-RAB14 with WT KIF16B or the S109A mutant were subjected to live cell imaging. In 40% of the WT KIF16B expressing cells, RAB14 tubules were observed, whereas it was only 15% in the case of the S109A mutant expressing cells (Fig. 5I, Movie 6). This result suggests a potential role for KIF16B in endosomal tubule formation.

Next, to investigate the role of RCP or KIF16B in the surface delivery of MET, we quantified total MET pool at the surface employing surface biotinylation. We performed the surface biotinylation in MDA-MB-231, since a substantial loss of cells was observed in BT-549 during the experimental procedures resulting in insufficient cell lysate for downstream analysis. The RCP or KIF16B silenced cells were treated with HGF for 30 minutes and proceeded for surface biotinylation. Vinculin is taken as a loading control as it is reported to also present in the membrane fraction (53). The MET population at the cell surface was found to be reduced upon RCP or KIF16B silencing, indicating their role in the delivery of MET to the plasma membrane (Fig 5J, S6). Depletion of RCP or KIF16B did not alter the MET total protein expression (Fig. S4H, S6).

Next, we performed gelatin degradation assay to investigate the role of RAB14, RCP or KIF16B in TNBC invasion. MDA-MB-231 or BT-549 cells were transfected with SMARTpool siRNA targeting the respective genes or control siRNA, subsequently seeded on labelled gelatin and the degradation index was analyzed. We observed a significant reduction in the gelatin degradation in MDA-MB-231 as well as BT-549 cells upon silencing of RAB14, RCP or KIF16B compared to control (Fig S4K-L). To validate this observation, we used single oligoes targeting RAB14 and RCP and performed gelatin degradation assays. Consistent with the SMARTpool siRNA data, silencing of RAB14 or RCP using individual oligoes also showed a reduction in the gelatin degradation activity (Fig S4L).

Together, these observations suggest that RAB14-RCP-KIF16B axis facilitates the MET surface delivery through tubulovesicular carriers.

HGF-MET facilitates ECM degradation by recycling MT1-MMP to the surface

MT1-MMP is one of the invadopodia-associated surface proteases with a wide range of substrate specificity for diverse ECM components (54). Perturbed MT1-MMP recycling impedes ECM degradation and cancer invasion (9,55). HGF is known to increase the expression and activity of invadopodia-associated metalloproteases MMP2 &MMP9 (56). We asked if HGF-stimulated invadopodia activity is mediated by MT1-MMP. We began by studying the expression of MT1-MMP in HGF-treated conditions. 3h of HGF stimulation did not alter the expression or degradation of MT1-MMP (Fig. S5A, A', S6).

Next, we investigated whether HGF treatment leads to enhanced recycling of the protease. We performed an antibody uptake assay, where cells were incubated with MT1-MMP antibody at 4°C, followed by internalization at 37°C. Antibodies available at the surface were removed, and cells were incubated with HGF to allow recycling at 37°C. The percent of recycling was calculated as described in the methods. Antibody uptake assay revealed that HGF stimulation induced 30% recycling of antibody-bound MT1-MMP, whereas, in the untreated condition, the recycling of MT1-MMP was 10% (Fig. 6A).

To support our observation from the antibody uptake assay, we employed TIRFM-based imaging to capture MT1-MMP exocytosis in real time. We overexpressed a pH-sensitive GFP, pHluorin-tagged MT1-MMP in MDA-MB-231, and quantified the number of exocytic events using TIRFM. We could see an increased surface delivery of pHluorin MT1-MMP when stimulated with HGF (Fig. 6B, Movie 7A, B).

The observation was further validated using surface biotinylation. For biotinylation, untreated or HGF-treated cells were incubated with uncleavable biotin, EZ-linked Sulfo-NHS biotin at 4°C. The cells were lysed, and the biotinylated pool was captured with streptavidin beads. Immunoblot analysis revealed that the HGF-treated cells have a higher surface MT1-MMP pool than the untreated cells (Fig. S5B). CIMPR has been taken as control, whose surface level did not alter with HGF treatment (Fig. S5B').

Next, we asked whether HGF also promotes the endocytosis of MT1-MMP. To address this, an antibody uptake assay was performed in the presence or absence of HGF. Cells grown on coverslips were incubated with MT1-MMP antibody at 4°C for 1h. The cells are allowed to internalize the antibody in the presence or absence of HGF. Cells were fixed, imaged with a confocal microscope, and the integral intensity of the internalized MT1-MMP antibody was quantified. HGF stimulation did not show any effect on the endocytosis of MT1-MMP (Fig. S5C).

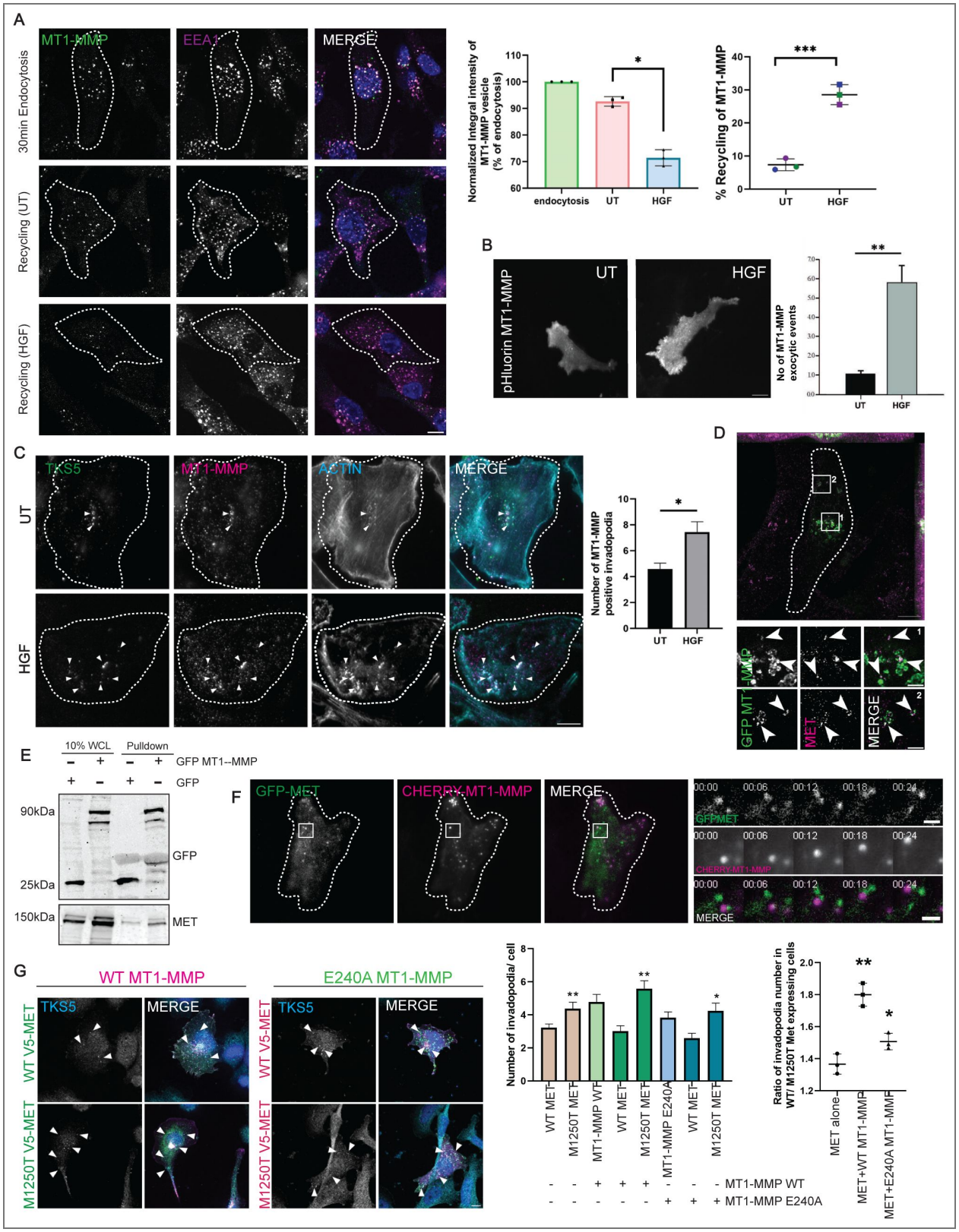

Figure 6. HGF/MET facilitates ECM degradation by recycling MT1-MMP to the surface

(A) MDA-MB-231 cells seeded on coverslips, surface labeled with MT1-MMP antibody at 4°C for 1 h Complete media was added, and cells were shifted to 37°C for 30 minutes to allow endocytosis. To remove surface-bound antibodies, an acid wash was given. After washing with PBS, serum-free media was added with or without HGF, and the cells

were shifted to 37°C for 10 minutes to allow recycling from the endocytosed pool. Cells were fixed and immunostained for EEA1. The integral intensity of the MT1-MMP and the percentage of MT1-MMP antibody recycling were calculated. N = 3, n= 300; scale bars = 10 μm. The error bar represents means ± SD. Paired t-test, *** P< 0.001, Unpaired t-test, * P < 0.05. (B) MDA-MB-231 cells transfected with pHluorin MT1-MMP were seeded on gelatin-coated glass-bottom dishes. Time-lapse imaging was performed in the presence or absence of HGF stimulation using a Nikon TIRF microscope without any intervals for 300 frames. The flashes of pHluorin MT1-MMP, which represent exocytic events, were calculated using Motiontracking. scale bars = 10 μm. The error bar represents Means ± SEM. Unpaired t-test, ** P < 0.001. N = 4, n= 35. (C) MDA-MB-231 cells were seeded on gelatin-coated glass-bottom dishes and allowed to attach for 3h, followed by incubation with or without HGF for another 3h. Cells were fixed and immunostained for TKS5, MT1-MMP, and F-actin. Images were captured using a Nikon TIRF microscope. TKS5, MT1-MMP, and Actin-positive structures were identified using Motiontracking. The error bar represents Mean ±SEM, Unpaired t-test, * P < 0.01. scale bar: 10μm. N=3, n=120. (D) GFP-MT1-MMP expressing MDA-MB-231 cells were fixed and immunostained for MET. Images were captured using an LSM900 Airyscan super-resolution microscope. Images were processed using the Airyscan Joint deconvolution (jDCV) method. The image was converted to Maximum Intensity projection for representation. The inset shows a magnified view of the region indicated by the box. Scale bar: 10 μm, inset: 2 μm. (E) GFP or GFP-MT1-MMP expressing BT-549 cells were lysed and incubated with GST agarose beads bound to 25μg of GFP binding protein (GBP). Next washes were given to remove unbound proteins and proceeded for immunoblotting with GFP and MET. WCL: whole-cell lysates (F) BT-549 cells co-expressing GFP-MET and Cherry MT1-MMP were subjected to live-cell TIRF imaging. The inset represents an event at different time points. Scale bar: 10 μm, Inset: 2 μm. (G) BT-549 cells expressing MT1-MMP WT or a catalytic mutant alone or with V5-MET WT or M1250T mutant were seeded on gelatin-coated coverlips for 6h and fixed. Cells were immunostained for V5 and TKS5. Images were captured with the confocal microscope. The number of TKS5 puncta in the MT1-MMP and/or MET expressing cells was calculated and plotted. The error bar represents Mean ±SD, Unpaired t-test. scale bar: 10μm. ** P<0.01, * P < 0.05, N=3, n=150.

MT1-MMP is recruited to invadopodia for efficient ECM remodelling. Since we saw an increased MT1-MMP recycling to the surface, we investigated the MT1-MMP recruitment to invadopodia in the presence or absence of HGF. MDA-MB-231 was seeded on gelatin with or without HGF. After 6h, cells were fixed and immunostained for invadopodia markers. TIRF imaging revealed that, indeed, HGF treatment leads to more MT1-MMP-containing invadopodia compared to the untreated condition (Fig. 6C). Further, to understand whether the receptor MET is also involved in the MT1-MMP recruitment to invadopodia, MET was silenced using siRNA, and the MT1-MMP population at invadopodia was quantified. Upon depletion of MET, the number of MT1-MMP-containing invadopodia was reduced (Fig. S5D). However, MET depletion did not alter MT1-MMP expression (Fig. S1I).

Next, to gain insight into the possible role of MET in MT1-MMP recruitment to invadopodia, we examined the localization of MT1-MMP with MET. The percentage of colocalization was increased from 12% to 45% when the cells were stimulated with HGF (Fig. S5F). Super-resolution microscopy revealed that in GFP-MT1-MMP expressing cells, MET localizes to the same endosomal microdomain as MT1-MMP (Fig. 6D). Interestingly, a protein-protein interaction prediction database PSOPIA anticipated the interaction between MT1-MMP and MET (57). To establish the physical interaction between MET and MT1-MMP, we employed a GFP nanobody pulldown approach. Lysates of GFP or GFP-MT1-MMP expressing cells were incubated with GST bead-bound GFP binding protein. The interaction was analyzed by immunoblotting. An increased binding of MET to GFP-MT1-MMP compared to GFP was observed (Fig. 6E, S6). The interaction was supported by performing GFP nanobody pulldown in HeLa and MCF10A DCIS (Fig. S5F). Next, to validate the interaction, we performed a reverse pull-down. We overexpressed GFP or GFP-MT1-MMP with V5-MET. V5-MET was trapped using Ni-NTA beads. Immunoblotting of the pulldown sample revealed that V5-MET exclusively interacts with GFP-MT1-MMP (Fig. S5G, S6). However, immunoprecipitation with endogenous MET we observed a weak interaction of MT1-MMP with MET (Fig S5H, S6).

MT1-MMP is known to cleave and shed the ectodomain of LDL receptor, apo-A1, ApoE, p-selectin, MMP2, MMP13, and αV integrin (58–61). As MT1-MMP and MET interact, we asked whether MT1-MMP can also activate MET by shedding its pro-domain. We quantified the mature MET population of 140 kDa in MT1-MMP-silenced cells by immunoblotting. The total matured MET population remains unchanged in the protease-depleted cells, whereas GFP-MMP2 which act as a substrate for MT1-MMP showed increase in the protein level (Fig. S5I, S6). Further, to comprehend the relevance of the interaction between the RTK and MT1-MMP, we hypothesize that their physical association plays a crucial role in their simultaneous enrichment at invadopodia, potentially via co-trafficking. To test this hypothesis, cells were transfected with GFP-MET and Cherry-MT1-MMP and imaged under a TIRF microscope. In live-cell TIRFM, GFP-MET and Cherry-MT1-MMP were found to be co-transported at the cell surface (Fig. 6F, Movie 8). These data suggest that HGF promotes MT1-MMP surface delivery and the receptor MET via physical interaction with MT1-MMP, ensuring a directed delivery to invadopodia.

A study by Ferrari et.al. suggests that MT1-MMP is not only required for invadopodia maturation but also can affect invadopodia formation (62). To explore the role of MT1-MMP on invadopodia formation, the protease was overexpressed, and the number of invadopodia formed was quantified. The overexpression of MT1-MMP WT or a catalytically inactive mutant E240A MT1-MMP increases the invadopodia number; however, no significant change was observed between the E240A MT1-MMP and WT MT1-MMP (Fig. S5L, L′). Next, we analyzed the number of invadopodia in the MT1-MMP knocked-out cells. Interestingly, the invadopodia formation was drastically reduced in the MT1-MMP-deleted cells compared to the control, highlighting the significance of MT1-MMP in invadopodia formation (Fig. S5M).

Interestingly, when we co-expressed MT1-MMP and MET together, we observed an increased invadopodia formation. The co-expression of MET WT or M1250T with WT MT1-MMP leads to a 1.8-fold increase in the difference observed in the number of invadopodia formed between the WT and M1250T MET compared to the 1.35-fold increase in overexpression of MET WT and M1250T alone (Fig. 6G). However, E240A MT1-MMP could enhance invadopodia formation up to 1.5-fold in M120T MET expressing cells (Fig. 6G). This highlights the potential influence of MT1-MMP on invadopodia formation. When we analyzed the MT1-MMP recruitment to invadopodia in the presence of the M1250T mutant, we observed an increased colocalization of MT1-MMP to invadopodia compared to the WT MET (Fig. S5K).

Further, to understand whether the increased invadopodia number in the M1250T MET and MT1-MMP (Fig. 6G) was due to the higher affinity of the MET mutant for MT1-MMP, we employed a pulldown approach. Cell lysates from V5/His-MET WT or M1250T and GFP or GFP-MT1-MMP were incubated with Ni-NTA beads. The pulldown samples were analyzed by immunoblotting. We did not observe a preferential binding of MT1-MMP to M1250T (Fig. S5N, S6), nor was the MT1-MMP expression altered in the mutant expressing cells (Fig. S5J, S6), inferring the increased invadopodia formation of M1250T MET in the presence of MT1-MMP is not because of physical interaction.

Taken together, our observations suggest that the HGF-MET axis directs MT1-MMP to invadopodia. The physical association between MT1-MMP and RTK MET ensures their co-trafficking to the surface, thereby promoting invadopodia formation.

Discussion

The current study elucidates how intracellular trafficking of MET could promote invadopodia-driven breast cancer invasion in TNBC cells. The results highlight- (i) HGF stimulation promotes MET and MT1-MMP recycling to invadopodia, (ii) MET and MT1-MMP physically interact, which we believe to be crucial for their co-trafficking to the cell surface, (iii) RAB4 and RAB14 facilitates the MET delivery to invadopodia, (iv) The RTK colocalizes with RCP on RAB14 endosomal tubules, (v) the formation of which is promoted by KIF16B for efficient MET trafficking.

RTK signalling was shown to play a critical role in invadopodia formation by coordinating activation of key invadopodia associated proteins and subsequent actin remodelling (63). In the current study we have demonstrated that MET or EGFR signalling facilitate invadopodia formation with the RTKs getting enriched at invadopodia in a ligand dependent manner (Fig. 1A-F, 2A-G, S2H). This enhanced recruitment of RTKs to invadopodia is potentially due to targeted delivery of RTKs through increased recycling upon growth factor stimulation. Consistent with our observation, a previous study have reported that SNARE-mediated delivery of EGFR to invadopodia facilitates invasive activity (13). Together, this suggests that growth factor-mediated recruitment of RTKs to invadopodia may be a generalized mechanism applicable to RTKs that are known to promote invadopodia-associated activities.

Further, our study reveals that MET localizes only to a sub-set of TKS5-positive invadopodia. The mature degradation-positive structures largely devoid of the RTK, suggesting a temporal association of MET with invadopodia at an early stage of the biogenesis (Fig. 2D, F). TKS5 is one of the crucial scaffold proteins required during invadopodia formation and maturation. Kreider-Letterman et al have shown that accumulation of TKS5 gradually increases as invadopodia mature (39). We observed an inverse correlation between MET and TKS5 levels at the TKS5 enriched invadopodia (Fig. 2E). Analysis of the MET/TKS5 fluorescence intensity ratio demonstrated that the majority of invadopodia exhibited a low ratio (Fig. S2B). Together, these observations suggest that MET is preferentially associated with nascent structure and may function during the early stages of invadopodia biogenesis prior to maturation, which is marked by progressive TKS5 recruitment (64). Further investigation of MET localization to invadopodia using live cell time-lapsed microscopy would enable us to analyze the temporal dynamics of MET recruitment to invadopodia and establish its temporal role during the biogenesis process.

It is well established that HGF treatment leads to endocytosis of the RTK leading to its degradation in lysosomal compartments (65). In the current study we also observed a pool of RTK that is recycled to invadopodia upon HGF stimulation (Fig 2). Our results further suggested that recycling of the RTK is associated with invadopodia mediated ECM degradation (Fig 3, S2). These observations corroborated well with enhanced invasive phenotype exhibited by the TNBC cells that overexpressed degradation defective mutant of MET which possess enhanced recycling ability (Fig. 3E) (33). However, the endocytosis defective mutant failed to promote invasive behaviour to a similar extend, suggesting that receptor internalization with subsequent surface recycling is critical to drive the invasive activity. Previous reports demonstrated that in response to HGF stimulation, GGA3 and CLIP170 regulate RAB4-mediated recycling of MET driving cancer cell migration (66,67). Here, we identified a previously unknown, RAB14-mediated recycling pathway of MET, that promotes invadopodia formation and TNBC invasion. Moreover, the MET localized to distinct endosomes positive for RAB4 or for RAB14 near the cell cortex, implicating for discrete recycling pathways regulated by these RABs (Fig. S3I). RAB14 is associated with the recycling of cargoes like MT1-MMP, which is one of the most well-studied invadopodia-associated metalloproteases (68). Perturbation in the delivery of MT1-MMP to invadopodia impairs ECM degradation and invasion (9,10). Our observations suggest that the HGF-MET axis promotes co-trafficking of MT1-MMP and the RTK to invadopodia, potentially facilitated by their physical interaction as demonstrated by immunoprecipitation assay (Fig. 6).

The role of MT1-MMP during invadopodia maturation is well established (69,70). The protease facilitates cell invasion via its degradative activity on ECM components. Interestingly, recent literature reported an emerging role for the protease during the initial stage of invadopodia formation (62,71). In agreement with these reports, overexpression or depletion of MT1-MMP altered invadopodia formation (Fig. S5L-M). Additionally, when MT1-MMP was co-expressed with the WT or the M1250T MET, the mutant expressing cells showed enhanced invadopodia formation compared to WT MET (Fig. 6G, S5L). The effect of MT1-MMP co-expression on invadopodia formation was also exhibited by the catalytically inactive mutant. Collectively, these findings highlight the role of MT1-MMP in invadopodia formation that is independent of its

catalytic function. We speculate that the increased recycling ability of the MET mutant may promote the targeted delivery of MT1-MMP to invadopodia through their physical association during the initial stages of invadopodia biogenesis.

Regulation of MET trafficking through RCP-RAB14-KIF16B axis

RAB GTPases orchestrate cargo trafficking by recruiting diverse sets downstream molecules that operate on the sorting and the delivery of the cargo to destined membrane (24). Adapter proteins represent a class of the RAB-effectors that helps in efficient cargo trafficking by bridging the cargo and the trafficking machinery (72). Among these, RAB11 family-interacting proteins (RAB11FIPs) are RAB11 binding proteins that engage endocytic vesicles with motors (72). RCP, a member of the RAB11FIP family, interacts with multiple RAB GTPases, including RAB11, RAB4, and RAB14, as well as cargos such as MET (47,73,74). Gundry et al have established that RAB14 along with RCP co-ordinates HGF dependent trafficking of Epinephrin receptor2 (EphA2) (48). This study further demonstrated that the HGF mediated phosphorylation of RCP at S435 strengthens its binding with RAB14. We showed unaltered colocalization of RAB14 with RCP S435A in response to HGF, which substantiate the findings of Gundry et al (Fig S4C). However, our colocalization analysis showed that HGF stimulation enhances the association of MET with both WT and phosphodeficient RCP mutant, suggesting this HGF-induced RCP phosphorylation is not crucial for its association with MET (Fig S4C). Notably, the reduced colocalization of MET and RAB14 at the EEA1 compartment upon silencing of RCP indicate that RCP may function as a bridging molecule between RAB14 and MET facilitating efficient MET recycling (Fig. 5F) (47,48).

RAB14-positive endosomes are known to generate bud-like microdomains that function as specialized hubs for selective cargo sorting (46). These bud like specialized microdomains serve as a platform for cargo segregation through recruitment of specific trafficking machineries that direct proteins towards recycling pathway (75). In our study, we observed that these RAB14 buds elongate to tubular structures containing both MET and RCP (Fig. 5B-E, Movie 5). Moreover, KIF16B was also found to be present on these tubular vesicles (Fig 5G). KIF16B is an established downstream effector of RAB14 that facilitates the vesicle movement containing cargo like MT1-MMP and FGFR (51,68). Our findings further showed that KIF16B promotes the surface delivery of MET by promoting RAB14-positive tubulovesicular structures (Fig. J, Movie 6). Previous studies have demonstrated that molecular motors play important roles not only in vesicular transport but also in endosomal tubule generation, with KIF16B promotes the endosomal tubulation in early endosomes, while KIF13A promotes tubulation in RAB11 recycling endosomes (52,76). Collectively, these studies together with our findings demonstrate the crucial role of molecular motors in regulating membrane tubulation and driving distinct trafficking pathways.

Together our study provides a mechanistic understanding of the HGF-MET-mediated invadopodia formation and MT1-MMP recycling (Fig. 7). We present evidence demonstrating MET localization to invadopodia is regulated by RAB4 and RAB14-dependent recycling in response to HGF stimulation. We speculate that RCP forms a trafficking-assembly with MET and RAB14 on the sorting endosomes. This trafficking-assembly localizes to the endosomal buds, which in turn elongates due to the activity of KIF16B forming tubular carriers. Thus, the RCP co-ordinated association of MET with RAB14-KIF16B may be a possible mechanism underlying the sorting of the RTK from the endosomal subdomains directing its trafficking to the cell surface. In addition, functional interaction between MET and MT1-MMP facilitates their co-transport to invadopodia, driving ECM degradation during TNBC invasion.

Material and Methods

Plasmids, antibodies, and reagents

The following antibodies were purchased commercially: rabbit anti-FISH (TKS5) (SantaCruz, sc-30122), 1:500 (IF), mouse anti-cortactin (Millipore, 05–180), 1:300 (IF); (SantaCruz, sc-55579) 1:500 (IF), rabbit anti-MET (CST, D1C2 XP) 1:400 (IF), 1:1000 (IB), mouse anti-MET (CST, L6E7) 1:500 (IF), 1:1000 (IB), rabbit anti-Phospho-Met (Tyr1234/1235) (CST, D26 XP) 1:800 (IF), 1:1000 (IB), mouse

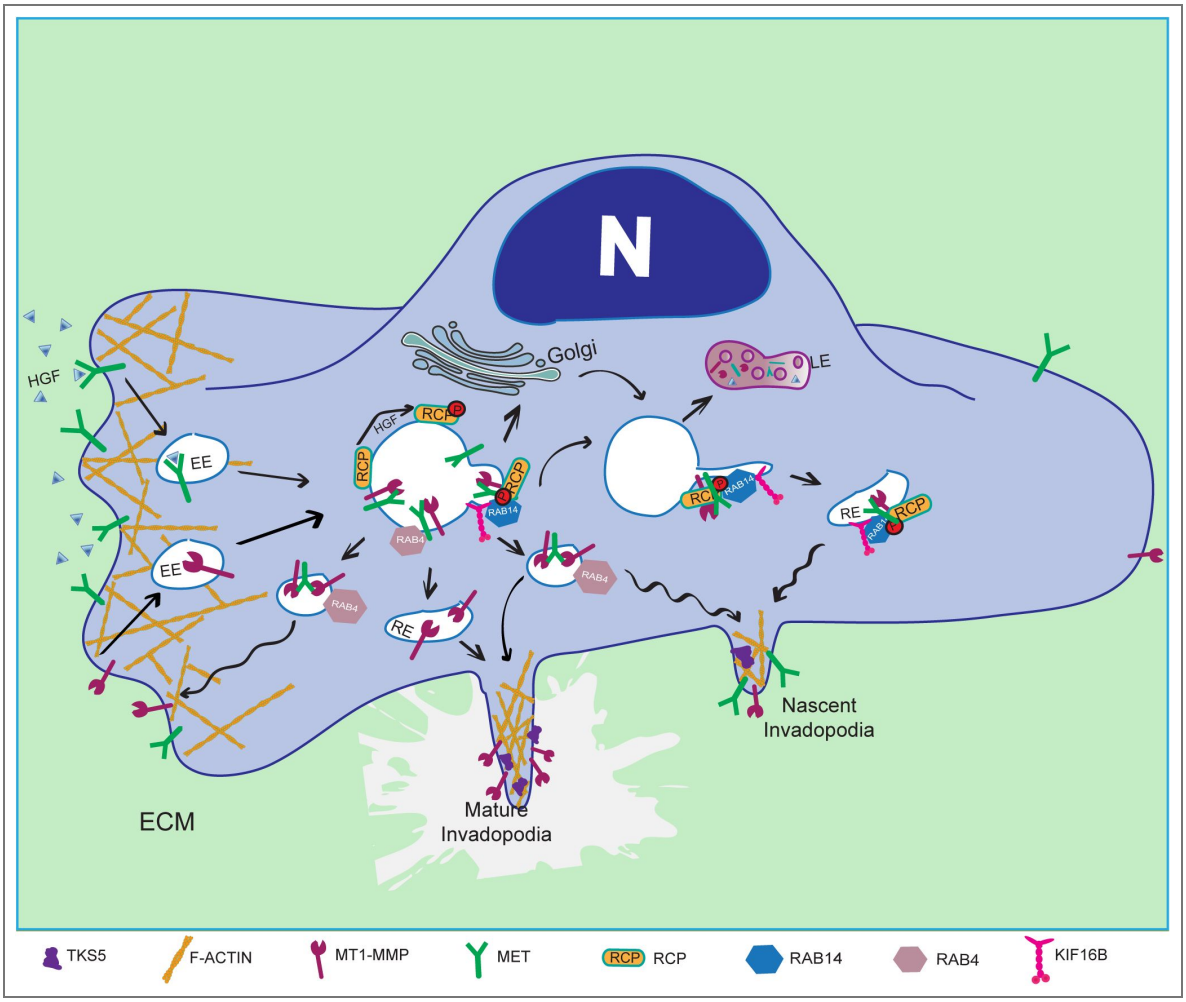

Figure 7. Proposed model showing RAB14-mediated MET trafficking to invadopodia along with MT1-MMP in the presence of HGF stimulation.

HGF stimulation triggers invadopodia formation and ECM degradation by promoting invadopodia formation and MT1-MMP recycling. HGF also increases the recruitment of MET to invadopodia by stimulating the trafficking of the RTK in a RAB4 or RAB14-dependent trafficking pathway. HGF stimulation increases the phosphorylation (34) and colocalization of RCP with MET-containing RAB14 vesicles. RCP and MET are present on the endosomal budding site of RAB14, which further elongate and form tubules. KIF16B gets recruited to these endosomes through RAB14 and drives the endosomal tubulation for efficient cargo trafficking. MT1-MMP interacts with MET, presumably promoting their co-trafficking to invadopodia.

anti-V5 (Sigma, SV5-Pk1) 1:400 (IF), 1:1000 (IB), rabbit anti-Rab11Fip1 (Protein technology, 16778-1-AP) 1:1000 (IB), rabbit anti-mouse MT1-MMP (Millipore, MAB3328), 1:1,000 (IB) and 1:400 (IF); mouse anti-MT1-MMP (R&D Systems, MAB9181-SP), 1:200 (IF), mouse anti-Vps35(SantaCruz, sc-374372) 1:300 (IF); rabbit anti-Vps26 (Abcam, ab23892) 1:1000 (IB), rabbit anti-EGFR (CST, D38B1), rabbit anti-Golgin97 (CST, D8P2K) 1: 200 (IF); mouse anti-vinculin (Sigma, V9131), 1:1,000 (IB); rabbit anti-actin (Sigma, A2066), 1:1,000 (IB); mouse anti-γ-tubulin (Sigma, T6557), 1:3000 (IB), mouse anti-GFP (Roche, 11814460001), 1:2000 (IB); mouse anti-Rab5 (BD Biosciences, 610724), 1:300 (IF); mouse anti-His (ThermoFischer Scientific), 1:1,000 (IB), Rabbit anti-MMP2 antibody (Proteintech, 10373-2-AP), 1:1000 (IB). The anti-rabbit EEA1 antibody was a kind gift from Professor Marino Zerial (Max Planck Institute of Molecular Cell Biology and Genetics, Dresden, Germany) and was used at 1:1000 (IF). Rabbit anti-WASH antibody was kindly shared by Professor Alexis Gautreau, used at 1:300 (IF).

pLenti MET-GFP (37560) and pCDNA3.1 MET-V5/His (201982) were purchased from Addgene. MET was amplified from pLenti MET-GFP using PCR and cloned into pEGFPN1 vectors using the XhoI and HindIII sites. M1250T and LL/AA mutants were generated in pCDNA3.1 MET-V5/His using site-directed mutagenesis. Primer details are provided in the Table 1. pLVX Tre3G MET-GFP WT was constructed by Mutagenex. pLVX TRE3G MET-GFP M1250T was generated by BIOBOX.

Cell culture

MDA-MB-231 (HTB-26), BT-549 (HTB-122) and HeLa (CCL-2) cell lines were purchased from ATCC and verified to be free of contaminants. All the cell lines were cultured for maximum of 20 passages and then discarded. MDA-MB-231 cells were maintained in L-15 (Invitrogen) media with 10% FBS, 100 µg ml^{-1} penicillin, and 100 µg ml^{-1} streptomycin at 37°C in CO_2-free conditions. BT-549 cells were maintained in RPMI (Invitrogen) supplemented with 0.023U/ml of Insulin, 10% FBS, 100 µg/ml penicillin, 100 µg/ml streptomycin, at 37°C with 5% CO2. Professor Phillipe Chavrier from the Centre National de la Recherche Scientifique in Paris, France, kindly shared the MCF10A DCIS cell line, which was maintained at 37°C with 5% CO2 in Advanced DMEM-F12 media supplemented with 2 mM glutamine and 5% horse serum (Invitrogen), 100 µg ml^{-1} penicillin, and 100 µg ml^{-1} streptomycin. HeLa cells were cultured using Dulbecco's modified Eagle's medium (DMEM) supplemented with 10% FBS, 100 µg/ml penicillin, 100 µg/ml streptomycin, and 2 mM glutamine, at 37°C with 5% CO2.

Transient transfection and Generation of stable cell lines

50,000 cells per well were seeded on coverslips in 24-well plates one day before the experiment to transfect expression plasmids transiently. Cells were transfected with 0.5 µg of plasmid DNA using LTX/Plus transfection reagent (Life Technologies) for MDA-MB-231 cells and Lipofectamine 3000 for BT-549 cells. HeLa cells were transfected with polyethylenimine (PEI-1mg/ml), 5µl of PEI /1µg of DNA.

To generate a stable cell line, 2×10^6 cells per ml were seeded in a 35 mm dish and, after 24 h, were transfected with pLVX TRE3G GFP-MET WT or M1250T with pLVX-pEF1a-Tet3G in a 4:1 ratio. Transfected cells were selected using complete media containing 800 µg/ml G418 and 1µg/ml puromycin. The media was changed every third day. Cells that survived antibiotic stress proliferated and formed colonies, were collected, and grown. Each clone was detected for GFP expression by performing immunoblotting and immunofluorescence. After antibiotic selection, cells were maintained in media containing 500 µg/ml G418 and 1µg/ml puromycin. For gene expression, 50-100 ng/ml of Doxycycline was used.

siRNA and shRNA transfection

OntargetPlus siRNA SMARTpool targeting the gene of interest was purchased from Dharmacon. All siRNAs were used at the working concentration of 10–20 nM. Cells were seeded 24 h before performing siRNA transfection. The manufacturer's protocol was used for transfection using Dharmafect as the transfection reagent. The sequences of SMARTpool siRNAs are provided in the Table 2.

All shRNA clones were part of the MISSION shRNA product line from Sigma-Aldrich. The TRC1.5 pLKO.1-puro non-mammalian shRNA Control Plasmid DNA (SHC002) is a negative control containing a sequence that should not target any known mammalian genes but engage with RISC. Cells were seeded 24 h before performing shRNA transfection. Cells were transfected at 50–60% confluency with 0.5 µg of shRNA plasmid DNA using LTX/Plus transfection reagent (Life Technologies). The sequences for MISSION plasmid shRNAs are provided in the Table 3.

RNA extraction and quantitative real-time PCR

Total RNA was extracted from the cells using RNAeasy kit (QIAGEN, Cat# 74104), and cDNA was prepared using the High-Capacity RNA-to-cDNA kit (Life Technologies, Cat# 4387406). Real-time qPCR reactions were performed using the SYBR Green Kit and corresponding primers on Applied Biosystems 7300 Real-Time PCR System or Thermo Quant Studio 3.0. The primer details are provided in the Table. 1.

Immunofluorescence and confocal imaging

Immunofluorescence was performed as described earlier by Parveen et al (55). Cells were fixed in 4% paraformaldehyde (PFA) for 15 min at room temperature followed by permeabilized with 0.1% Triton X-100 for 10 min at room temperature. The cells were blocked with 5% FBS in 1× PBS and were immunostained with the primary antibodies, followed by Alexa-labeled secondary antibodies. The coverslips were mounted using Mowiol (Calbiochem, Cat. 475904) on glass slides and imaged using an LSM780 or FV3000 confocal microscope. Data from three independent experiments were subjected to analysis by Motiontracking.

Object-based colocalization analysis

Colocalization of objects were quantified using Motiontracking as described by Parveen et al (55). The objects were identified as vesicles in each channel depending on their size, fluorescence intensity, elongation, etc by Motiontracking. Objects identified in two different channels were considered to be colocalized if the relative overlap of respective areas was >35%. The colocalization value is the ratio of the integral intensities of colocalized objects to the integral intensities of all objects in the base channel. The values can range from 0.0 to 1.0. The random colocalization was estimated by random permutation of object localization in different channels, and the apparent colocalization was corrected for random colocalization. Similar way, the Motiontracking defines multicolor objects as those objects with a colocalization value greater than 0.35.

CTCF calculation using ImageJ

To calculate Corrected Total cell fluorescence (CTCT) in ImageJ, a cell boundary was drawn. The area, integrated density, and mean gray value of the ROI were calculated by using the “measure” function under “Analyze”. To correct the background fluorescence, an ROI of similar size was drawn in the background where no cell is present, and the mean gray value was calculated. The corrected total cell fluorescence (CTCF) was then calculated using the following formula:

CTCF = Integrated density – (Area of the selected cell× Mean fluorescence of the background reading)

Live-cell imaging

Cells were transfected with GFP- and/or mCherry-fused proteins alone or together for 12 h. Cells were trypsinized and seeded on glass-bottom dishes. Cells in complete medium were allowed to get attached at 37°C and further imaged with an Olympus IXplore spinSR microscope with a 100× Plan Apo N objective (oil, 1.42 NA) on an inverted stage equipped with a Tokai Hit onstage incubation system. Images were acquired and analyzed using Motiontracking.

TIRF microscopy and analysis

Live-cell TIRF-M

To specifically capture events occurring near the cell surface, imaging was performed using a Nikon Eclipse Ti2-E inverted microscope equipped with an H-TIRF module and an Okolab on-stage incubation system for temperature and CO_2 regulation. Cells expressing GFP and/or mCherry fusion proteins were seeded on gelatin-coated, glass-bottom dishes containing complete medium. Dual-color imaging was carried out simultaneously using an Apo-TIRF 60× oil DIC N2 objective lens (NA 1.49) and a Nikon LU-N4 laser combiner, with two Orca-Flash4.0 V3 sCMOS cameras (Hamamatsu Photonics). Images were acquired using NIS-Elements AR software version 5.11.00. GFP-tagged proteins were excited using a 488 nm laser, and mCherry-tagged proteins were excited using a 561nm laser.

Calculation of MT1-MMP exocytosis

The movies were imported into the MotionTracking software and processed as described by Goto-Silva et.al. (77). Briefly, to distinguish endosomes from background fluorescence, we applied the Bayesian Foreground/Background Discrimination (BFBD) filter, as implemented in the MotionTracking software (*https://Motiontracking.mpi-cbg.de*). The BFBD algorithm separates the image intensity into a fast-changing foreground and a slowly changing background, corresponding to moving vesicles and cytoplasmic fluorescence, respectively. This procedure efficiently suppresses the Poisson noise of fluorescence. Since the BFBD attributed the signal from non-moving objects to the background, we sum the previously found foreground and background. Then, a new background estimation was performed as described in Kalaizidis et al (78) with a window size of 1μm and subtracted from the de-noised images. The images were thresholded by signal-to-noise ratio (SNR) = 2.0, where the amplitude was estimated as signal uncertainty predicted by the BFBD algorithm. The resulting images were segmented by the watershed algorithm. Detected endosomes were associated with the tracks by a dynamic programming algorithm that performs local-in-time/global-in-space optimization as described in Rink et al (79). The exocytosis events were preceded by a docking event, which corresponds to immobilization of the endosome and a fast increase of intensity (flash) due to the physics of TIRF microscopy, with consequent total disappearance of the signal. We filtered events with a duration of flash < 4 sec.

Track identification and quantification

MotionTracking was used to identify and analyze vesicles near the cell surface. In the time-lapse movie, fluorescent objects (vesicles) were detected in each frame. Each object was assigned an x-y position, and its fluorescence intensity and size were calculated. Next, objects were linked across consecutive frames to generate tracks, representing the trajectories of individual vesicles over time. Each track was characterized by parameters such as speed, direction, displacement, intensity, and area. To adjust the track break thresholds, the following parameters were considered: total score, area score, intensity score, and integral intensity score. These thresholds were critical for maintaining track accuracy. After optimization of the parameter, the tracks were generated per movie. Each track was considered to represent a vesicle positioned near the plasma membrane.

Fixed-cell TIRF-M

Fixed-cell TIRF-M was performed by plating cells over a gelatin-coated glass-bottom dish, followed by fixation using 4% PFA, and then proceeded for immunostaining. While imaging with a TIRF microscope, the cells were kept in 1×PBS. *Z*-stack images of the fixed samples were acquired with a *z*-step of 0.02 μm. Acquired images were analyzed as maximum intensity projection (MIP) and searched for multicolor objects (as described above) using the automated image analysis program Motiontracking.

Super-resolution microscopy sample preparation

BT549 or MDA-MB-231 cells expressing the protein of interest were fixed in 4% PFA for 15 min at room temperature and then proceeded for indirect immunofluorescence as mentioned above. Image was captured using Zeiss LSM 900 Airyscan or Olympus IXplore spinSR microscope sequentially with laser wavelengths 488 nm and 561 nm. *Z*-stack images of the fixed samples were acquired with a *z*-step of 0.02 µm.

For Airyscan image processing, the Airyscan Joint deconvolution (jDCV) method was used, which uses the Richardson-Lucy algorithm to achieve a resolution up to 90nm.

Gelatin degradation assay

Gelatin degradation assay was performed as described by Sharma et.al. (9). MDA-MB-231, BT549 and MCF10DCIS cells were trypsinized and 50,000 cells were plated on Alexa Fluor 568-labeled gelatin for 3-12h. Cells were then fixed and immunostained with DAPI. Images were captured using a Zeiss LSM780 confocal laser scanning microscope with a 40×1.4 NA oil immersion objective or an Olympus FV3000 microscope. Images were processed in the Motiontracking software, where the degradation spots were identified as objects, and the degradation index was calculated using the formula

$$\{[\,(\text{Mean background Intensity} - \text{mean Intensity of the degradation spots}) \div \text{Mean background intensity}\,] \times \sum \text{Area of the degradation spots}\} \div \text{Number of cells perframe}$$

Generation of multicellular spheroids

Spheroids were formed as described previously in Nazari et al with minor modifications (80). Briefly, non-adherent agarose microwells were generated by pipetting 50μl of pre-warmed 2% w/v agarose solution, made in PBS, into each well of a 96-well plate and allowed to solidify. MDA-MB-231 or BT549 cells were trypsinized, resuspended and 2000 cells were seeded into each well. Plates were centrifuged for 5 min at 100 ×g, 25°C to initiate aggregation of cells within each well. Plates were incubated at 37°C for 2 days to allow cells to grow and form more compact aggregates. For MDA-MB-231, on day 2, 100μl of media was taken out and 100μl of 10% Matrigel (v/v) (Corning, Cat#354277) was added into each well, making the final Matrigel concentration 5%. After brief centrifugation, plates were returned to the incubator and allowed to form compact spheroids for an additional 2 days.

Spheroid invasion into collagen and quantification

The multicellular spheroids were harvested from the microwells and added in the media. Cooled rat tail collagen type I (ThermoFischer Scientific, Cat#A1048301) was neutralized following the manufacturer's protocol to make collagen hydrogels. The spheroids were mixed with the collagen solution for ~ 5 spheroids/ 70μl in a final collagen concentration of 2mg/mL. Next, the solution was added to a 96-well plate and allowed to gel for 30 min at 37°C. 200ul of complete media or Serum serum-free media or serum-free media containing 100ng/ml HGF was added into each well. The spheroids were allowed to invade for 48 hours, and images were captured at Day 0 and after 48 hours using a Nikon Eclipse Ti inverted microscope using the 4× objective at bright field mode. For BT549 GFP-MET WT or M1250T Mutant spheroids, doxycycline was added to complete media to make a final concentration of 50ng/ml, respectively. Spheroid images were immediately captured at Day 0 with a Nikon Eclipse Ti inverted microscope using a 4× objective at bright field mode. The spheroids were transferred to the incubator and imaged after 24 hours.

The spheroid invasion area was calculated by ImageJ. By color threshold and the wand tracing tool, the core area and the invaded area were identified, the boundary was drawn, and the area was measured. Spheroid invasion was calculated as the ratio of the invaded area to the core area and was plotted. Experiments were performed in triplicate with a minimum of 30 spheroids per condition.

MT1-MMP antibody uptake assay

MDA-MB-231 cells were trypsinized and counted, and 50,000 cells per well were seeded on the gelatin-coated coverslips for 24 h. After the cells had properly adhered and regained their morphology, antibody uptake was performed using anti-MT1-MMP antibody (R&D Systems, MAB9181-SP). Cells were incubated at 4°C with 10 µg ml^{-1} anti-MT1-MMP antibody diluted in serum-free L-15 medium for 1 h. The unbound antibody was removed by washing with 1× PBS. L-15 complete medium was added, and cells were shifted to 37°C to allow internalization of the surface-bound antibody for 30 minutes. Next, an acid wash (0.2 M Acetic acid and 0.5 M NaCl) was given for 4 minutes to remove the surface-bound antibody. Again, the cells were washed with 1× PBS, and complete media was added with or without HGF to allow recycling of the internalized pool. At the required time point, cells were fixed by adding 4% PFA, followed by staining with anti-EEA1 and DAPI.

The % MT1-MMP recycling was calculated using the formula:

$$[(\text{Integal intensity of MT1 - MMP at } T_0 \text{ - Integral intensity of MT1} - MMP \text{ at } T_{10}) \div \text{ Integal intensity of } MT1 - MMP \text{ at } T_0] \times 100$$

Western blotting

Cells were harvested and lysed in lysis buffer (50 mM Tris-HCl, pH 7.4, 150 mM NaCl, 2 mM DTT, 1% NP40, and 1 mM EDTA) supplemented with 10 µg ml^{-1} protease inhibitor cocktail (PIC, Sigma). Cell debris was removed by centrifuging at 19,000 ×g for 15 min at 4°C. Protein concentration was estimated using the Bradford assay. Samples were prepared by adding 1× SDS loading dye and boiling at 95°C. Proteins were separated by running on SDS-PAGE, then transferred to a nitrocellulose membrane (0.45 µm; GE Healthcare, Cat. 10600002). The membrane was blocked with 5% BSA, then incubated for 1 h at room temperature or overnight at 4°C with the respective primary antibody. To detect the bound antibody signal, the membrane was incubated with fluorescently labelled secondary antibody, and protein bands were detected using the Li-Cor Odyssey Infrared Scanning System.

Blot quantification using ImageJ

Densitometric analysis of blot images was performed using ImageJ software. Blot images were saved as 8-bit grayscale files. Using the rectangular selection tool, equal-sized boxes were drawn around each band, and the Gel Analysis function was used to generate intensity profiles. The area under each peak, corresponding to band intensity, was measured after manually defining baselines and subtracting the background signal obtained from a non-band region of the blot. Band intensities were normalized to the corresponding loading control, and relative expression levels were calculated. Quantification was performed on at least three independent experiments, and results are presented as mean ± SD.

MT1-MMP surface biotinylation

Surface Biotinylation was performed as described by Parveen et.al. (55). To measure the surface population, MDA-MB-231 cells were grown in a 35-mm plate. After 24h, the cells were treated with or without HGF for 10 minutes at 37°C. Then the culture medium was removed and the cells were washed with 1× PBS (6.7 mM $NaHPO_4$, 3.3 mM $NaH2PO_4$, and 140 mM NaCl, pH 7.2) and incubated with EZ-link Sulfo-NHS-Biotin (Invitrogen, Cat. 21217) at 4°C for 45 min. Next, to quench free biotin, cells were treated with 50 mM Tris-HCl, pH 8.0. After quenching, cells were washed with 1×

PBS and lysed. The lysate was clarified and incubated with Neutravidin beads (Pierce, Cat. 29200) for 30 min at room temperature. Biotin-labelled proteins were eluted from the beads and subjected to immunoblotting. The intensity of the biotinylated MT1-MMP was quantified for HGF-treated or untreated samples using ImageJ software.

Co-immunoprecipitation

20µl of the protein A/G beads agarose beads were washed and incubated with 2µg of IgG or anti-MET antibody for 1h at 4°C with gentle rotation. The unbound antibodies were washed off. Subsequently the MDA-MB-231 lysate was added and further incubated for 2h at 4°C. To remove unbound proteins washes were given. The beads-antibody-protein complex containing 1× SDS sample loading buffer was boiled at 95°C. The samples were separated by SDS-PAGE and subjected to immunoblotting.

GFP-trap pulldown

The GBP clone was purchased from Addgene and subcloned into the pGEX-6P1 vector to express GST-tagged GBP. GFP vector or GFP fusion proteins were overexpressed in the 6-well format. After 16 h of transfection, cells were lysed in 50 mM Tris-HCl, pH 7.4, 150 mM NaCl, 2 mM DTT, 1 mM EDTA, and 1% NP-40, and cleared by centrifuging at 19,000 ×*g* at 4°C for 20 min. The cell lysates were mixed with 25 µg of purified GST–GBP bound to the glutathione Sepharose beads. The beads bound with GBP–GFP protein complexes were then washed three times with PBS, followed by elution using 1× SDS sample loading buffer. Samples were then separated on an 8% SDS-PAGE gel, followed by Western blotting.

His-Pulldown

His pulldown was performed as mentioned by Sharma et.al. (9). Cells expressing proteins of interest were harvested after 16 hours of transient transfection. Cells were lysed and cleared by centrifuging at 19,000 ×*g* at 4°C for 20 min. Prepared lysates were incubated with Ni-NTA agarose beads. The beads bound with His tagged protein complexes were then washed with 1× PBS and eluted. The samples were further processed for Western blotting.

Protein turnover experiment

The protein turnover was estimated as described by Sharma et.al. (9). 50,000 cells were seeded for 24 h before the experiment. The next day, cells were treated with or without HGF with cycloheximide at a working concentration of 10 µg ml^{-1}. At different time points, cells were lysed and clarified. The cell lysates were then subjected to Western blotting.

PHA665752 or Pervanadate treatment

To inhibit the Tyr phosphatases, Pervanadate was added to the cells as described by Parveen et.al. (55). Briefly, 6mM of pervanadate solution was prepared by mixing 1 ml of a 20 mM sodium orthovanadate with 330 µl of 30% H_2O_2 and incubating for 5 min at room temperature. These cells were treated with 40 µM of pervanadate solution diluted in serum-free L-15 medium. As pervanadate/H_2O_2 is unstable, a fresh solution was prepared each time. Cells were treated with pervanadate for 30 min at 37°C. Cells were harvested and lysed, were analyzed by anti-phospho-MET immunoblotting (55).

Statistical analysis

For the statistical evaluation of the datasets from quantitative image analysis, paired or unpaired Student's *t*-test or one-way ANOVA with a Dunnett's multiple comparisons test was performed using GraphPad Prism 6 and 8 software version 6.01 and 8.0.2, respectively. Datasets are presented as Mean±SD or Mean± SEM. For the data that are displayed using SuperPlots, each biological replicate is distinctly color-coded and each dot represents the number of identified multicolor objects in a field of view (frame). One frame comprises 1–3 cells, contributing to a total number of cells (*n*) across the total number of frames acquired. The frame-wise values were separately

pooled for each biological replicate to calculate the mean in the SuperPlots, and the SD represents the deviation of the data from these three means (81). The significance is as follows: $P>0.05$, ns (non-significant), $*P\leq0.05$, $**P\leq0.01$, $***P\leq0.001$, and $****P\leq0.0001$. The number of samples, images, and experiments used for quantification is mentioned in the respective figure legends or in figures. In all figures, n= number of cells and N= number of experiments.

Data availability

RAB14-dependent tubulovesicular recycling directs MET to invadopodia, promoting TNBC cell invasion

Supplemental figures

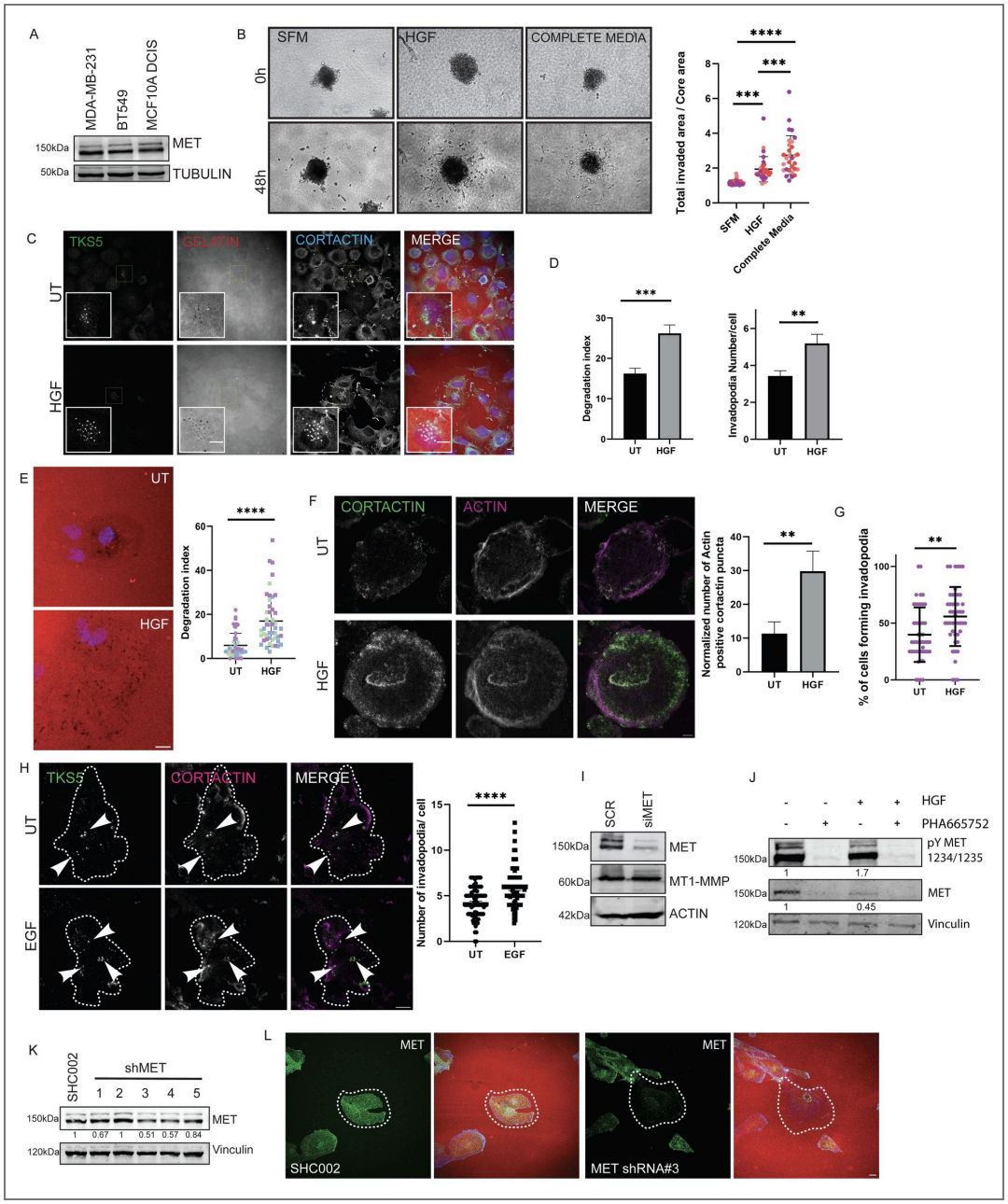

Figure S1. HGF-induced MET activity promotes TNBC breast cancer invasion through invadopodia-mediated ECM degradation. (A) Lysates of MDA-MB-231, BT-549 and MCF10A DCIS were separated by SDS-PAGE and analyzed by Western blot. Membranes were probed with anti-MET and anti-Vinculin antibody. (B) Bright-field

images of BT-549 spheroids embedded in the collagen matrix at 0h and 48h in the presence or absence of HGF or complete media. The ratio of the invaded area to the core area was quantified and plotted. Data points from individual biological replicates are distinctly color-coded. The error bar represents Mean ±SD, One-way ANOVA with multiple comparisons. scale bar: 100μm. **** P < 0.0001, *** P < 0.001 N=3, n=30. (C, D) BT-549 cells were seeded on Alexa568-labeled gelatin-coated coverslip for 3h, followed by incubation with or without HGF for an additional 3h. Cells were fixed, immunostained for TKS5, cortactin, and imaged with a confocal microscope. The degradation index and number of colocalized TKS5-cortactin puncta were quantified and plotted. The inset shows a magnified view of the region indicated by the box. The error bar represents Mean ±SEM, Unpaired t-test. scale bar: 10μm. Inset: 2μm, *** P < 0.001, ** P < 0.01, N=3, n=200. (E) MCF10A DCIS cells were seeded on Alexa568-labeled gelatin-coated coverslip with or without HGF for 6h. Degradation Index was quantified and plotted. The Arrowhead represents degradation spots. Data points from individual biological replicates are distinctly color-coded. The error bar represents Mean ±SD, Unpaired t-test. scale bar: 10μm. **** P < 0.0001, N=3, n=200. (F) MCF10A DCIS cells were seeded on a gelatin-coated glass-bottom dish for 3h, followed by incubation with or without HGF for 3h. Cells were fixed and immunostained for cortactin and F-actin. Images were captured using a TIRF microscope. Actin-positive cortactin puncta were quantified and plotted. The error bar represents Mean ±SEM, Unpaired t-test. scale bar: 10μm. ** P < 0.01, N=3, n=100. (G) MDA-MB-231 cells were seeded on a gelatin-coated glass-bottom dish for 3h, followed by incubation with or without HGF for 3h. Cells were fixed and immunostained for cortactin and TKS5. Images were captured using a TIRF microscope. Percentage of cells showing invadopodia formation per frame were calculated and plotted. The error bar represents Mean ±SD, Unpaired t-test. ** P < 0.01, N=3, n=90. (H) MDA-MB-231 cells were seeded on a gelatin-coated glass bottom dish for 3h, followed by incubation with or without EGF stimulation for an additional 3h. Cells were fixed and immunostained for TKS5 and cortactin. Images were captured using a TIRF microscope. TKS5 puncta positive for cortactin were considered as invadopodia. The error bar represents Mean ±SD, Unpaired t-test. scale bar: 10μm. **** P < 0.0001, N=3, n=90 (I) MDA-MB-231 cells were treated with control or MET siRNA. The efficiency of gene silencing was estimated by immunoblotting. To analyze total MT1-MMP levels in MET-depleted cells, the membrane was probed for MT1-MMP. Actin was used as a loading control. (J) MDA-MB-231 cell treated with or without HGF in the presence of vehicle or PHA665752 for 3h, lysed and separated by SDS-PAGE. The membrane was probed for pY1234-35 MET or MET and vinculin. The numbers indicates the normalized MET of p-MET intensities. To calculate p-MET intensity, the signal intensity of p-MET was normalized with MET and further with loading control. (K) MDA-MB-231 cells were transfected with SHC002 control shRNA or 5 shRNA clones against MET. After 48 hours, cells were lysed and subjected to immunoblotting with anti-MET antibody. The numbers indicate the normalized signal intensity of MET. (L) MDA-MB-231 cells were transfected with control SHC002 or MET shRNA clone #3, and after 36h of transfection, cells were seeded on Alexa568-labeled gelatin-coated coverslip for 6h. The cells were fixed and immunostained with anti-MET antibody, Phalloidin, and DAPI.

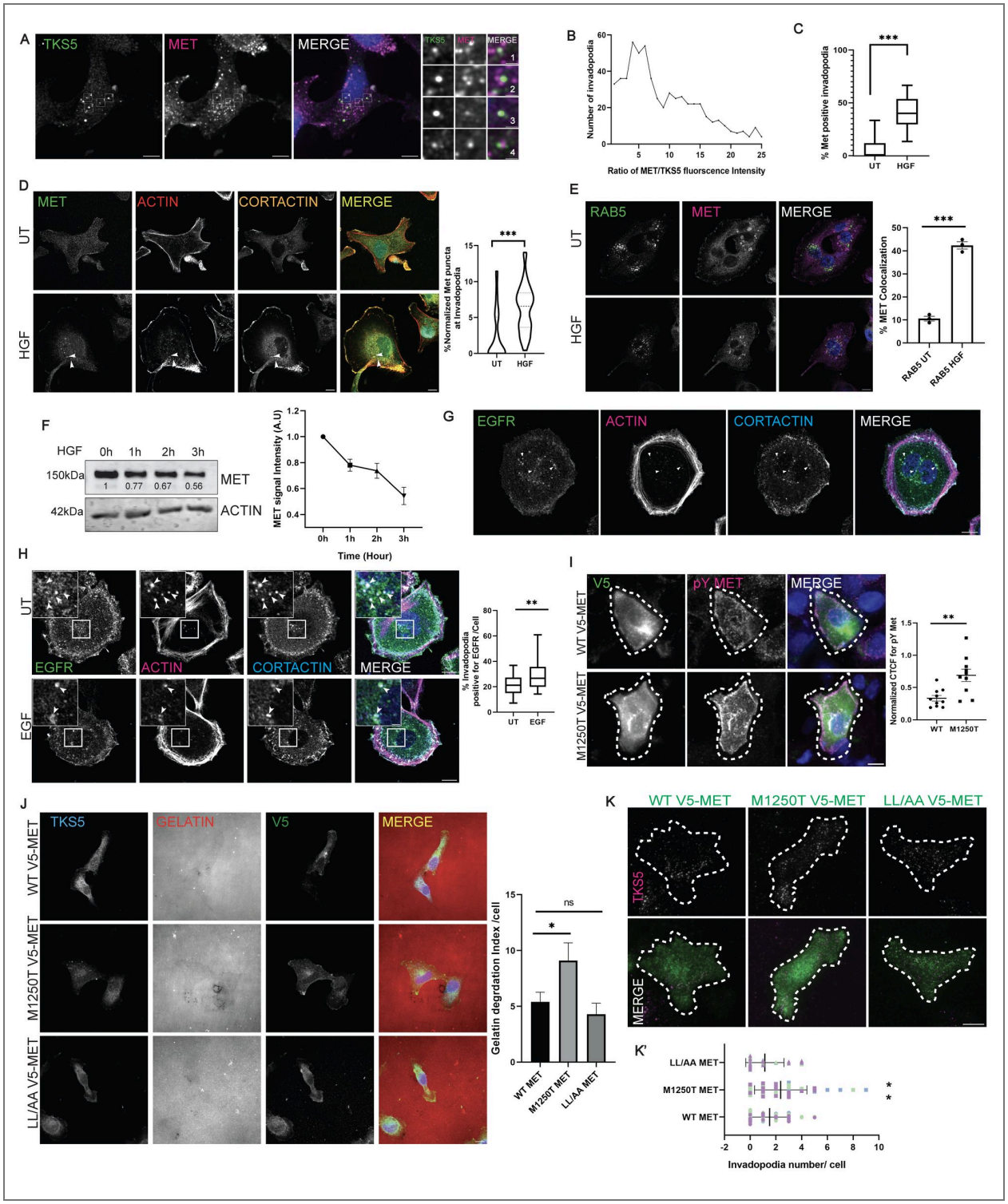

Figure S2. HGF promotes MET recycling that drives breast cancer invasion.

(A) BT-549 cells were seeded on gelatin-coated coverslips and allowed to adhere for 3h, followed by 3 hours with HGF stimulation. Cells were fixed, immunostained for TKS5, MET, and the Nucleus. Images were captured using the confocal microscope. The inset shows a magnified view of the region indicated by the box. Scale bar: 10µm. Inset: 2µm. (B) The ratio of the integral intensity of MET to TKS5 was calculated, and the frequency distribution was plotted. n= 800 invadopodium. (C) GFP-TKS5 transfected MDA-MB-231 cells were seeded on gelatin-coated glass-bottom dishes in the presence or absence of HGF, after 6h, fixed, and immunostained for MET. The cells were imaged using a TIRF microscope. The percentage of TKS5 puncta positive for MET was quantified and plotted. scale bar: 10µm.

Unpaired t-test. *** P < 0.001, N=3, n=120. (D) MDA-MB-231 cells were seeded on gelatin-coated glass coverslips for 3h, followed by incubation with or without HGF for an additional 3h. The cells were fixed and immunostained with anti-MET, anti-cortactin antibody, and Phalloidin. The cells were imaged using a confocal microscope. Numbers of Actin-cortactin puncta positive for MET were quantified and plotted. Scale bar: 10μm. Unpaired t-test. *** P < 0.001, N=3, n=200. (E) MDA-MB-231 cells seeded on glass coverslips were stimulated with or without HGF for 2h. Cells were fixed and immunostained for MET and RAB5. The percent colocalization of MET with RAB5 was calculated. scale bar: 10μm. The error bar represents Mean ±SEM. N=3, n=200. (F) MDA-MB-231 cells were treated with HGF for a period of 0-3h in the presence of cycloheximide, lysed at the indicated time points, and subjected to immunoblotting. The numbers represent the relative MET expression at the mentioned time point. The relative MET intensity was calculated for 3 replicates and plotted. (G) BT-549 cells were seeded on gelatin-coated coverslips for 6h and fixed. Cells were immunostained for EGFR, F-actin, and cortactin. Images were captured with the confocal microscope. scale bar: 10μm. (H) BT-549 cells were seeded on gelatin-coated coverslips for 6h with or without EGF stimulation and fixed. Cells were immunostained for EGFR, F-actin, and cortactin. Images were captured with the confocal microscope. The percentage of Actin-cortactin puncta that immunostained for EGFR was quantified and plotted. The inset shows a magnified view of the region indicated by the box. scale bar: 10μm. Inset: 2μm. Unpaired t-test. ** P < 0.01, N=3, n=100. (I) WT or M1250T V5-MET expressing BT-549 cells were seeded on glass coverslips cells fixed, and immunostained for V5 and p-MET. Images were acquired with a confocal microscope. Corrected total cell fluorescence (CTCF) for V5 and p-MET was calculated using ImageJ. The CTCF of p-MET was normalized with that of V5 and plotted. scale bar: 10μm. The error bar represents Mean ±SEM, Unpaired t-test. ** P < 0.01. N=3, n=10. (J) MDA-MB-231 cells expressing V5-MET WT or mutants were seeded on Alexa568-labeled gelatin-coated coverslips for 12h. Cells were fixed, then immunostained for V5, TKS5, and the Nucleus. Cells were imaged with the confocal microscope. Gelatin degradation by the V5-MET overexpressing cells was calculated. The error bar represents Mean ±SEM, Unpaired t-test. * P < 0.05 ns P > 0.05 scale bar: 10μm. N=3, n=120 (K, K') V5-MET WT or M1250T or LL/AA mutant expressing MDA-MB-231 cells were seeded on a gelatin-coated glass-bottom dish for 6h and fixed. Cells were immunostained for TKS5, and images were captured with the TIRF microscope. Data points from individual biological replicates are distinctly color-coded. The error bar represents Mean ±SD, Unpaired t-test. Scale. ** P < 0.01, ns P > 0.05 bar: 10μm. N=3, n=60.

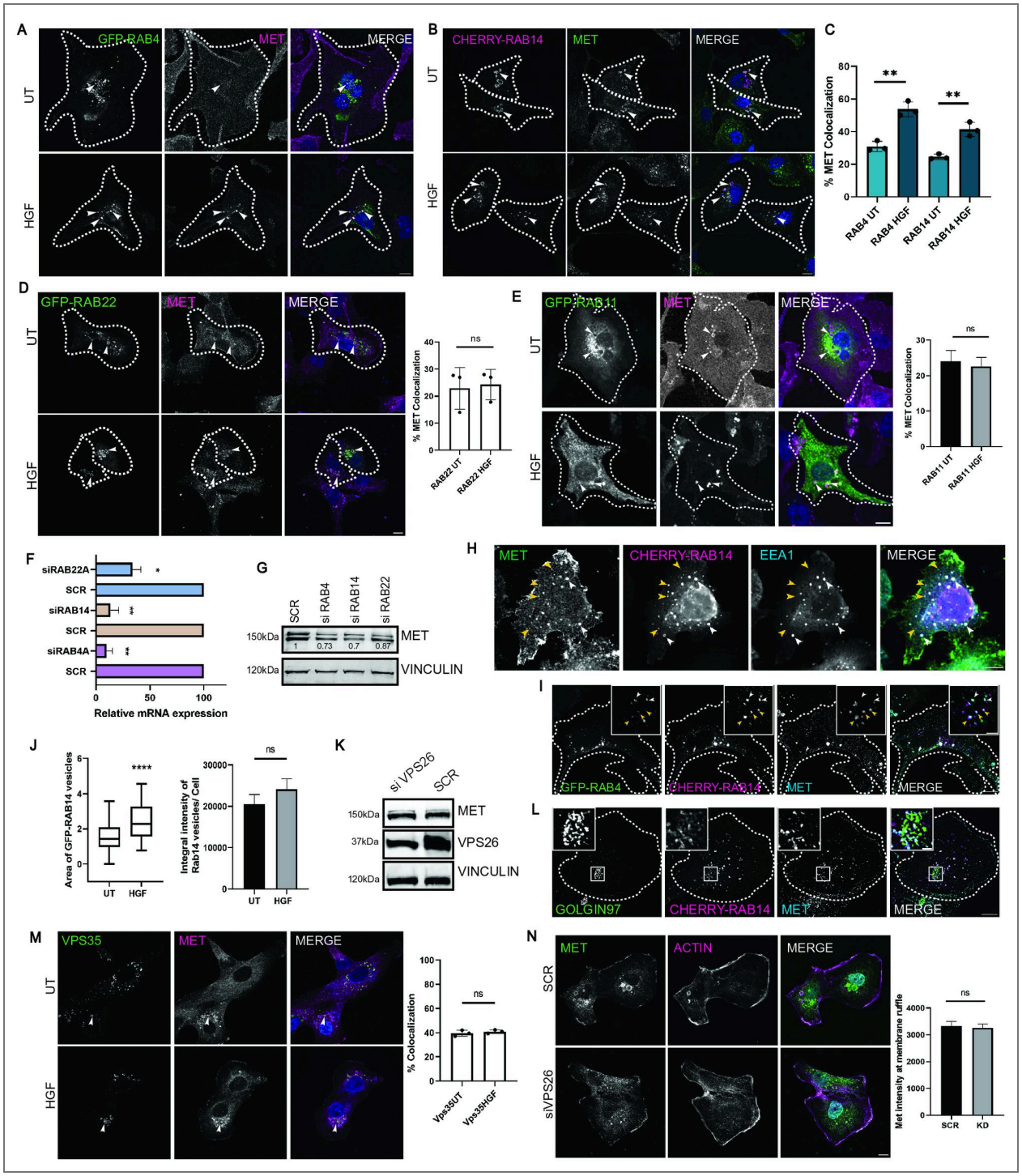

Figure S3. HGF promotes RAB4 and RAB14-mediated MET delivery to the plasma membrane.

MDA-MB-231 cells, seeded on glass coverslips, were transfected with (A) GFP-RAB4 or (B) Cherry-RAB14. After 14h of transfection, cells were incubated for 2h with or without HGF, then fixed and immunostained for MET. Images were captured using a confocal microscope. scale bar: 10μm. (C) Graph showing the percent colocalization of MET with GFP-RAB4 and Cherry-RAB14 in the presence of absence of HGF treatment. The error bar represents Mean ±SD, One-way ANOVA. ** P< 0.01. N=3, n=200. (D, E) MDA-MB-231 cells seeded on glass coverslips were transfected with (D) GFP-RAB22 or (E) GFP-RAB11. After 14h of transfection, cells were incubated for 2h with or without HGF, then fixed and immunostained for MET. Images were captured using a confocal microscope. The percent colocalization of MET with GFP-RAB22 or GFP-RAB11 in the presence or absence of HGF treatment was calculated and plotted. Scale bar:

10μm. The error bar represents Mean ±SD. Unpaired t-test. ns P > 0.05 N=3, n=200. (F) The KD efficiency of RAB4, RAB14, and RAB22 was confirmed by quantitative RT-PCR. N = 3. Values in the graph represent means ± SEM. Paired t-test, ** P < 0.01, * P < 0.05. (G) MDA-MB-231 cells were transfected with control or RAB4, RAB14, or RAB22 siRNA. After 60 hours, cells were harvested and processed for immunoblotting to analyse total MET levels. The relative MET levels were quantified. The numbers indicate the normalized MET signal intensity. (H) BT549 cells grown on coverslips were transfected with Cherry-RAB14. Cells were treated with HGF for 2h and fixed, followed by immunostaining with antibodies against MET and EEA1. Images were captured using a confocal microscope. The white arrowhead indicate the MET-RAB14-EEA1 positive puncta, yellow arrowhead indicates the MET-RAB14 endosomes devoid of EEA1. scale bar: 10μm. (I) BT-549 cells co-expressing GFP-RAB4 and Cherry-RAB14 were fixed, immunostained for MET and imaged with the super-resolution microscope. The inset shows a magnified view of the region indicated by the box. The white arrowhead represents RAB4-MET vesicles, and the yellow arrowhead represents RAB14-MET vesicles. scale bar: 10μm, Inset: 2μm. (J) MDA-MB-231 cells transfected with GFP-RAB14 and incubated with or without HGF. Cells were fixed, immunostained for MET, and then imaged using a confocal microscope. The mean Integral intensity and area of GFP-RAB14 vesicles were calculated and plotted. The error bar represents Mean ±SEM. Unpaired t-test. **** P< 0.0001, ns P>0.05, N=3, n=200. (K) MDA-MB-231 cells were transfected with control or VPS26A siRNA. After 60 hours of transfection, cells were harvested and processed for immunoblotting to analyse total MET levels. (L) BT-549 cells expressing Cherry-RAB14 were fixed, then immunostained with anti-MET and anti-GOLGIN 97 antibodies. Images were captured using the Olympus SpinSR super-resolution microscope. The inset shows a magnified view of the region indicated by the box. scale bar: 10μm, Inset: 2μm. (M) MDA-MB-231 cells seeded on glass coverslips were incubated for 2h with or without HGF. Cells were fixed and immunostained for MET and VPS35. The percent colocalization of MET with VPS35 was calculated. scale bar: 10μm. The error bar represents Mean ±SEM. Unpaired t-test. ns P> 0.05. N = 3, n = 200. (N) MDA-MB-231 cells were transfected with control or VPS26A siRNA. After 60 hours of transfection, cells were given a pulse of HGF for 5 min, and excess HGF was washed off. The cells were incubated at 37°C for 30 min and fixed. The cells were immunostained for MET and F-actin. Images were captured in a confocal microscope, and MET localized to Actin at the cell periphery was quantified. scale bar: 10μm. The error bar represents Mean ±SD. Unpaired t-test. ns P>0.05. N=3, n=200

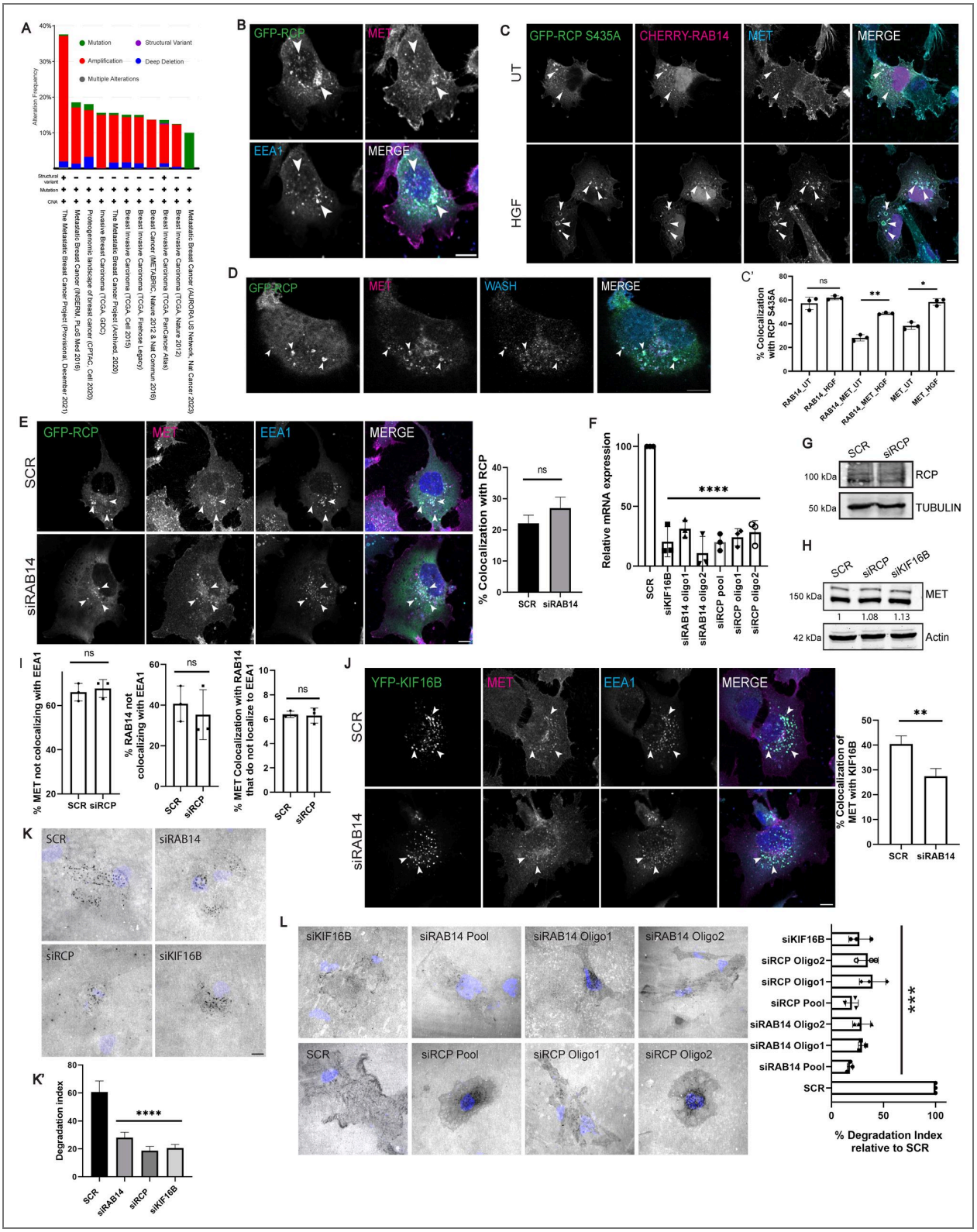

Figure S4. RCP-RAB14-KIF16B trafficking axis regulates MET recycling.

(A) The frequency of alteration of MET in 27 breast cancer datasets was analyzed using the publicly available database cBioportal. The graph shows the frequency of alterations for different breast tumor cohorts. (B) BT-549 cells seeded on glass coverslips were transfected with GFP-RCP. After 14h of transfection, cells were incubated for 2h with HGF stimulation, then fixed and immunostained for MET and EEA1. Images were captured using a confocal

microscope. scale bar: 10μm. (C, C') BT-549 cells seeded on glass coverslips were transfected with GFP-RCP S435A and Cherry-RAB14. After 14h of transfection, cells were incubated for 2h with or without HGF, then fixed and immunostained for MET. Images were captured using a confocal microscope. The percent colocalization of GFP-RCP S435A with RAB14 or RAB14-MET in the presence or absence of HGF treatment was calculated and plotted. scale bar: 10μm. The error bar represents Mean ±SD. Unpaired t-test. ** P< 0.01, ns P > 0.05 N=3, n=200. (D) BT-549 cells seeded on glass coverslips were transfected with GFP-RCP. After 14h of transfection, cells were incubated for 2h with HGF stimulation, then fixed and immunostained for MET and WASH. Images were captured using a confocal microscope. scale bar: 10μm. (E) BT-549 cells depleted with RAB14 or control siRNA-treated cells were transfected with GFP-RCP for 14 hours, followed by 2 hours of HGF stimulation. Cells were fixed and immunostained for MET and EEA1. Images were captured using a confocal microscope, and the percentage colocalization of RCP with MET was quantified and plotted. The graph represents Mean ±SD. Unpaired t-test. ns P > 0.05, N=3, n=200. (F) BT-549 cells were treated with control or siRNA against KIF16B, RCP or RAB14. The efficiency of gene silencing was estimated by qRT-PCR. (G) BT-549 cells were treated with control or RCP siRNA. The efficiency of gene silencing was estimated by immunoblotting. (H) MDA-MB-231 cells were transfected with RCP or KIF16B siRNA. After 72h cells were lysed and subjected to immunoblotting with anti-MET and anti-Actin antibody. (I) BT-549 cells were treated with control or SMARTpool siRNA against RCP. 60h after transfection, cells were transfected with Cherry-RAB14. After providing 2 hours of HGF stimulation, cells were fixed and immunostained for MET and EEA1. Images were captured using a confocal microscope. The percentage colocalization of RAB14 or MET endosomes that do not EEA1 was calculated. scale bar: 10μm. The error bar represents Mean ±SD. Paired t-test, ns P > 0.05, N=3, n=200. (J) BT-549 cells depleted of RAB14 or control siRNA-treated cells were transfected with YFP-KIF16B. After 14 hours of transfection, cells were treated with HGF, followed by fixing and immunostaining for MET and EEA1. Images were captured using a confocal microscope, and the percentage colocalization of KIF16B with MET was quantified and plotted. The graph represents Mean ±SD. Unpaired t-test. * P < 0.05 N=3, n=200. (K, K') MDA-MB-231 cells depleted of RAB14, RCP or KIF16B were seeded on Gelatin-568 for 12h. Fixed and imaged with a confocal microscope. The degradation index was calculated and plotted. scale bar: 10μm. The error bar represents Mean ±SEM. One-way ANOVA with multiple comparison, **** P < 0.0001, N=3, n=200. (L) BT-549 cells were transfected with SMARTpool or 2 individual oligoes targeting RAB14, RCP or KIF16B. After 60h of transfection, cells were seeded on Gelatin-568 for 12h. Fixed and imaged with a confocal microscope. The degradation index was calculated and plotted. scale bar: 10μm. The error bar represents Mean ±SEM. One-way ANOVA with multiple comparison, *** P < 0.001, N=3, n=200.

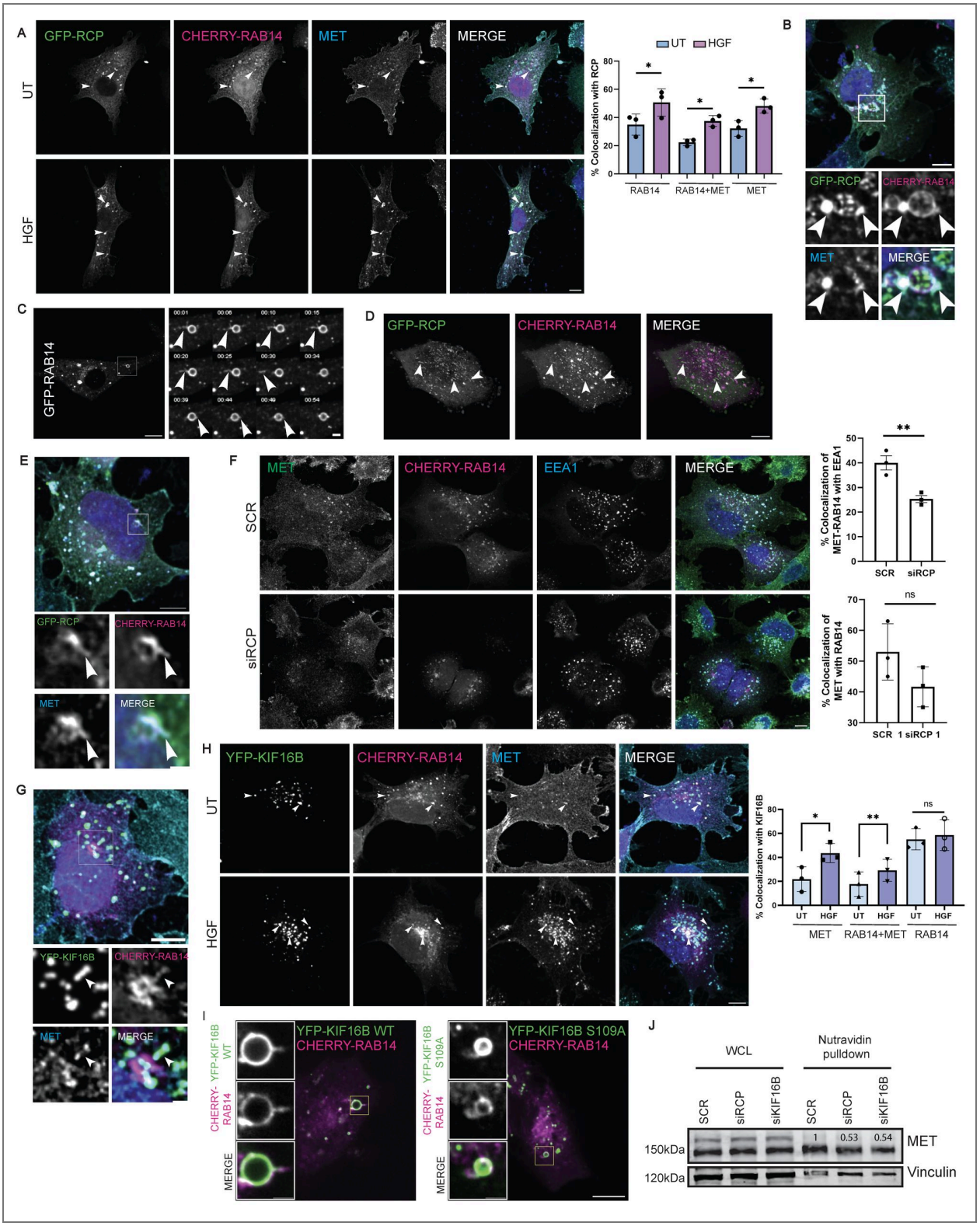

Figure S5. HGF/MET facilitates ECM degradation by recycling MT1-MMP to the surface.

(A) MDA-MB-231 cells treated with or without 100ng/ml of HGF were lysed and subjected to immunoblotting with anti-MT1-MMP antibody. Vinculin was taken as a loading control. The number indicates the normalized MT1-MMP intensity. (A') MDA-MB-231 cells treated with 10 µg/ml of cycloheximide, either in the presence or absence of HGF, were lysed and subjected to immunoblotting with an anti-MT1-MMP antibody. Tubulin was taken as a loading control. The number indicates the normalized MT1-MMP intensity. (B, B') Untreated or HGF-treated MDA-MB-231

cells were subjected to surface biotinylation. HGF stimulation was given for 10 minutes, followed by biotin labeling at 4°C for 45 minutes. Washes were given to remove excess biotin; subsequently, biotin was quenched, and cells were lysed. The lysate was allowed to bind with Neutravidin beads, followed by immunoblotting. The numbers indicate the Normalized signal intensity of MT1-MMP with that of WCL. In (B'), the MT1-MMP signal intensity has been normalized with CIMPR. Scale bar: The error bar represents Mean ±SD, Paired t-test, * $P < 0.05$. N=4. (C) MDA-MB-231 cells seeded on coverslips were incubated with MT1-MMP antibody at 4° C. After PBS washes, cells were shifted to 37° C to allow endocytosis in the presence or absence of HGF. The cells were fixed and immunostained with anti-EEA1 antibody. Images were captured using Zeiss LSM780. The integral intensity of the MT1-MMP antibody was calculated and plotted. Scale bar: 10μm. The error bar represents Mean ±SEM, ns $P > 0.05$, N=3, n = 200. (D) MDA-MB-231 cells were transfected with control or MET siRNA. After 60 hours of transfection, cells were seeded on a gelatin-coated glass-bottom dish and allowed to attach for 3h, followed by incubation with or without HGF for another 3h. Cells were fixed and immunostained for TKS5, MT1-MMP, and F-actin. Images were captured using a Nikon TIRF microscope. TKS5, MT1-MMP, and Actin-positive structures were identified and plotted. The inset shows a magnified view of the region indicated by the box. The error bar represents Mean ±SEM, Unpaired t-test, *** $P < 0.001$. scale bar: 10μm. Inset: 2μm. N=3, n=120. (E) MDA-MB-231 cells seeded on glass coverslips were incubated with or without HGF. Cells were fixed and immunostained for MT1-MMP and MET. The percentage colocalization was quantified using Motiontracking. Scale bar: 10μm. The error bar represents Mean ±SD, Unpaired t-test. **** $P<0.0001$. N=3, n=200. (F) Quantification of GBP pulldown assay of GFP-MT1-MMP in 3 different cell lines. The value represents the signal intensity of trapped MET normalized by pulled-down GFP or GFP-MT1-MMP per assay. GFP and GFP-MT1-MMP bars are represented by distinct colors. (G) GFP or GFP-MT1-MMP and V5/H6-MET co-expressing HeLa cell lysates were incubated with Ni-NTA beads. Washes were given, and the pull-down samples were processed for immunoblotting with anti-GFP and anti-V5 antibodies. WCL: whole-cell lysates. (H) MDA-MB-231 cell lysate was immunoprecipitated using anti-MET antibody. Immunoprecipitated proteins were separated by SDS-PAGE and analyzed by Western blot. Membranes were probed for MT1-MMP and MET. (I) BT-549 cells were treated with control or MT1-MMP siRNA. After 60h of transfection, cells were transfected with GFP-MMP2. After 14h cells were lysed and analyzed by immunoblotting. The membrane was probed with MET, MMP2, GFP, MT1-MMP and vinculin antibody. The total level of the mature form of MET with a molecular weight of 140 kDa was analyzed in control and MT1-MMP-depleted conditions. GFP-MMP2 with a molecular weight of 100kDa has been taken as appositive control and Vinculin as a loading control. The numbers indicate the normalized signal intensities. (J) BT-549 cells expressing V5-MET WT or M1250T were lysed and subjected to immunoblotting with V5, MT1-MMP, and Actin. (K) BT-549 cells co-expressing pHluorin MT1-MMP with V5-MET WT or M1250T mutant were seeded on gelatin-coated coverslips for 6h and fixed. Cells were immunostained for V5 and TKS5. Images were captured with the confocal microscope. The number of MT1-MMP puncta localizing with TKS5 was calculated and plotted. The inset shows a magnified view of the region indicated by the box. The error bar represents Mean ±SD, Unpaired t-test. scale bar: 10μm. Inset: 2μm. ** $P<0.01$, * $P < 0.05$, N=3, n=100 (L, L') BT-549 cells expressing WT or catalytically inactive (E240A) MT1-MMP were seeded on the gelatin-coated glass-bottom dish for 6h, then fixed and immunostained for TKS5. Images were captured using a confocal microscope. The number of TKS5 puncta in MT1-MMP-expressing cells was quantified and plotted. The error bar represents Mean ±SEM, One-way ANOVA, ** $P < 0.01$, * $P < 0.05$. scale bar: 10μm. N=3, n=150. (M) SCR and MT1-MMP knock-out MDA-MB-231 cells were seeded on gelatin-coated glass-bottom dishes for 6 hours. Cells were fixed and immunostained for TKS5 and F-actin. Images were acquired using a TIRF microscope. The number of Actin-TKS5 puncta was quantified and plotted. Scale bar: 10μm. The error bar represents Mean±SD, Unpaired t-test. **** $P<0.0001$. N=3, n=60. (N) BT-549 cells co-expressing V5-MET WT or M1250T with GFP or GFP-MT1-MMP were lysed and incubated with Ni-NTA beads. Washes were given to remove unbound proteins. The pulled-down samples were processed for immunoblotting with antibodies against V5 and GFP.

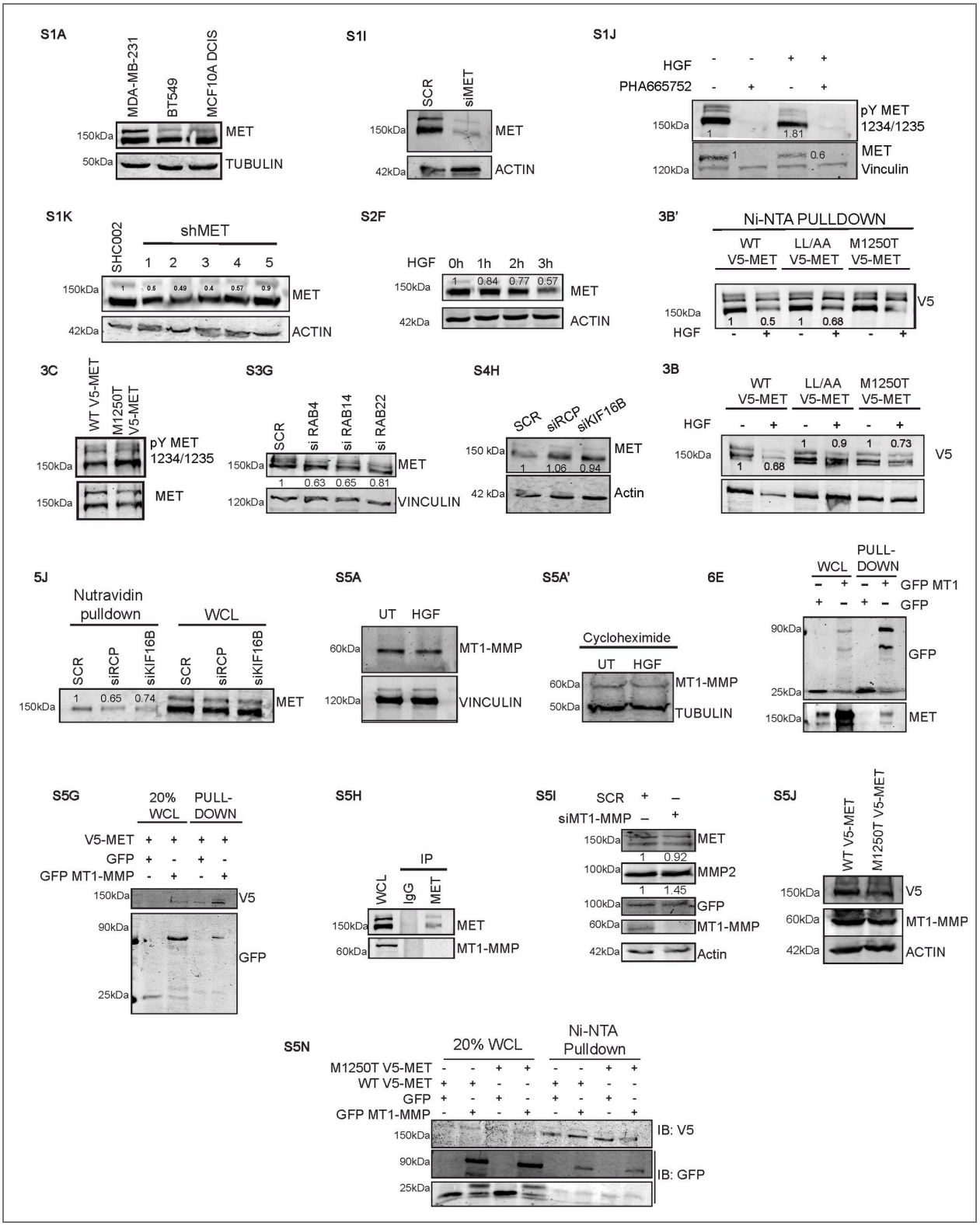

Figure S6. Additional blots.

(S1A) Lysates of MDA-MB-231, BT-549 and MCF10A DCIS were separated by SDS-PAGE and analyzed by Western blot. Membranes were probed with anti-MET and anti-Vinculin antibody. (S1I) MDA-MB-231 cells were treated with control or MET siRNA. The efficiency of gene silencing was estimated by immunoblotting. To analyze total MT1-MMP levels in MET-depleted cells, the membrane was probed for MT1-MMP. Actin was used as a loading control. (S1J) MDA-MB-231 cell treated with or without HGF in the presence of vehicle or PHA665752 for 3h, lysed and separated by SDS-PAGE.

The membrane was probed for pY1234-35 MET or MET and vinculin. The numbers indicates the normalized MET of p-MET intensities. To calculate p-MET intensity, the signal intensity of p-MET was normalized with MET and further with loading control. (S1K) MDA-MB-231 cells were transfected with SHC002 control shRNA or 5 shRNA clones against MET. After 48 hours, cells were lysed and subjected to immunoblotting with anti-MET antibody. The numbers indicate the normalized signal intensity of MET. (S2F) MDA-MB-231 cells were treated with HGF for a period of 0-3h in the presence of cycloheximide, lysed at the indicated time points, and subjected to immunoblotting. The numbers represent the relative MET expression at the mentioned time point. The relative MET intensity was calculated for 3 replicates and plotted. (3B') BT-549 cells expressing WT or M1250T or LL/AA V5-MET stimulated with or without HGF were lysed and incubated with Ni-NTA beads. The pulled-down samples were separated by SDS PAGE and processed for immunoblotting with anti-V5 antibody. (3B) BT-549 cells expressing WT or the mutants of V5-MET were treated with or without HGF for 2 hours, followed by cell lysis. The lysates were subjected to immunoblotting with anti-V5 and anti-vinculin antibodies. The V5 signal intensity was quantified and normalized with Vinculin. Error bar represents Mean ±SEM. Unpaired t-test. * $P < 0.05$. (3C) BT-549 cells expressing WT or M1250T V5-MET were lysed and incubated with Ni-NTA beads. The pulled-down samples were separated by SDS PAGE and processed for immunoblotting with anti-V5 and anti-p-MET antibody. (S3G) MDA-MB-231 cells were transfected with control or RAB4, RAB14, or RAB22 siRNA. After 60 hours, cells were harvested and processed for immunoblotting to analyse total MET levels. The relative MET levels were quantified. The numbers indicate the normalized MET signal intensity. (S4H) MDA-MB-231 cells were transfected with RCP or KIF16B siRNA. After 72h cells were lysed and subjected to immunoblotting with anti-MET and anti-Actin antibody. (5J) RCP or KIF16B were silenced using SMARTpool siRNA in MDA-MB-231 cells. After 72h of transfection of siRNA, cells were treated with HGF for 30 minutes and proceeded for surface biotinylation. The cells were incubated with biotin at 4°C for 45 minutes. Washes were given to remove excess biotin; subsequently, biotin was quenched, and cells were lysed. The lysate was allowed to bind with Neutravidin beads and the biotinylated proteins were precipitated. The samples were separated by SDS-PAGE and processed for immunoblotting. The number indicates the MET signal normalized with MET signal intensity of the respective WCL. (S5A) MDA-MB-231 cells treated with or without 100ng/ml of HGF were lysed and subjected to immunoblotting with anti-MT1-MMP antibody. Vinculin was taken as a loading control. The number indicates the normalized MT1-MMP intensity. (S5A') MDA-MB-231 cells treated with 10 µg/ml of cycloheximide, either in the presence or absence of HGF, were lysed and subjected to immunoblotting with an anti-MT1-MMP antibody. Tubulin was taken as a loading control. The number indicates the normalized MT1-MMP intensity. (6E) GFP or GFP-MT1-MMP expressing BT-549 cells were lysed and incubated with GST agarose beads bound to 25µg of GFP binding protein (GBP). Next washes were given to remove unbound proteins and proceeded for immunoblotting with GFP and MET. WCL: whole-cell lysates. (S5H) MDA-MB-231 cell lysate was immunoprecipitated using anti-MET antibody. Immunoprecipitated proteins were separated by SDS-PAGE and analyzed by Western blot. Membranes were probed for MT1-MMP and MET. (S5I) BT-549 cells were treated with control or MT1-MMP siRNA. After 60h of transfection, cells were transfected with GFP-MMP2. After 14h cells were lysed and analyzed by immunoblotting. The membrane was probed with MET, MMP2, GFP, MT1-MMP and vinculin antibody. The total level of the mature form of MET with a molecular weight of 140 kDa was analyzed in control and MT1-MMP-depleted conditions. GFP-MMP2 with a molecular weight of 100kDa has been taken as appositive control and Vinculin as a loading control. The numbers indicate the normalized signal intensities. (S5J) BT-549 cells expressing V5-MET WT or M1250T were lysed and subjected to immunoblotting with V5, MT1-MMP, and Actin. (S5N) BT-549 cells co-expressing V5-MET WT or M1250T with GFP or GFP-MT1-MMP were lysed and incubated with Ni-NTA beads. Washes were given to remove unbound proteins. The pulled-down samples were processed for immunoblotting with antibodies against V5 and GFP.

Acknowledgements

We thank Professor Philippe Chavrier [CNRS, Paris, France] for sharing the pCDNA3.1 MT1-MMP pHluorin construct and the *MCF10DCIS.com* line; Dr. Marc Coppolino for pEGFPN1 Mt1-MMP construct, Professor Marino Zerial (Max Planck Institute, Dresden, Germany) for sharing EEA1 antibody, pEGFP-C1 RAB4 and pEYFP C1 KIF16B construct, Prof. Subba Rao Gangi Setty (IISc, India) for GFPC1 and mCherryC1 RAB14 constructs, Professor Jim.C. Norman (University of Glasgow, UK) and Elizabeth Manning (Vanderbilt University) for pmCherry RCP, pEGFPC2 RCP; Professor Sara Courtneidge for the GFP-TKS5 construct. (Oregon Health & Science University, USA); Professor Luis S. Mayorga (IHEM-CONICET), Mendoza, Argentina, for the GFP-RAB22 construct. We acknowledge Dr. Sameena Parveen for her kind help in generating the MT1-MMP Knock-out cell line, Tanishka and Shaili for helping out with plasmid isolation. We are thankful to the Central Instrumentation Facility at IISER Bhopal, which was used to perform confocal, super-resolution and TIRF microscopy-based experiments. We also acknowledge the FIST facility at IISER Bhopal, supported by the DST, for providing the infrastructure to conduct live-cell imaging-based experiments.

Additional information

Author contribution

This work was funded by the Science and Engineering Research Board (CRG/2023/000563). Author contributions: A. Khamari: Conceptualization, data curation, investigation, methodology, visualization, analysis, manuscript writing and editing; A. Guria: investigation, methodology, visualization, analysis; K. Tak: investigation, methodology, analysis; R. Sharma: investigation, methodology, analysis; Y. Kalaidzidis: Motiontracking analysis. S. Datta: Conceptualization, data curation, analysis, funding acquisition, investigation, methodology, project administration, resources, supervision, validation, visualization, and manuscript.

Funding

Funder	Grant reference number	Author
Department of Science and Technology, Ministry of Science and Technology, India (DST)	CRG/2023/000563	Amrita Khamari Sunando Datta

Author ORCID iDs

Sunando Datta: https://orcid.org/0000-0002-1417-0276

Additional files

Movie 1. HGF promotes spheroid invasion. Spheroids were formed using MDA-MB-231 cells and embedded in collagen for 24h. Bright field images of the Spheroids invading into the collagen matrix in the presence or absence of HGF stimulation (Fig. 1A). 1 frame/15mins for 24 hours. Scale bar: 100µm.

Movie 2. HGF promotes the surface delivery of MET. BT-549 cells transfected with GFP-MET were seeded on the gelatin-coated glass-bottom dish and imaged using a TIRF microscope for 30s without intervals (Fig. 2H). Scale bar: 10µm, Exposure time (488): 900ms.

Movie 3. RAB4 and RAB14 facilitate MET trafficking to the surface. RAB4, RAB14, or RAB22 and control siRNA-treated BT-549 cells were transfected with GFP-MET. The cells were seeded on the gelatin-coated glass-bottom dish and imaged using a TIRF microscope for 30s without intervals. (Fig. 3D-E). Scale bar: 10µm, Exposure time (488): 900ms,

Movie 4. GFP-RAB14 endosomes make tubular protrusions. BT-549 cells expressing GFP-RAB14 were seeded on a glass-bottom dish and imaged using a confocal microscope (Fig. 5C). Scale bar: 10μm, Inset: 2μm. Exposure time: 80ms, 1frame/ 0.4s for 1 min

Movie 5. RCP and RAB14 localize to the endosomal tubules BT-549 cells co-expressing GFP-RCP and Cherry-RAB14 were seeded on a glass-bottom dish and imaged using a confocal microscope (Fig. 5D). Scale bar: 10μm, Exposure time: 80ms, 1frame/ 0.4s for 1 min

Movie 6. KIF16B promotes RAB14 endosomal tubulation. BT-549 cells co-expressing Cherry-RAB14 with YFP-KIF16B WT or YFP-KIF16B S109A were seeded on a glass-bottom dish and imaged using a confocal microscope (Fig. 5I). Scale bar: 10μm, Exposure time: 80ms, 1frame/ 2.25s for 90sec.

Movie 7A. HGF promotes MT1-MMP surface delivery. MDA-MB-231 cells expressing pH-MT1-MMP were seeded on the gelatin-coated glass-bottom dishes in the presence (7B) or absence of HGF (7A). Time-lapse images were captured using a TIRF microscope without an interval for 300 frames. Scale bar: 10μm, Exposure time: 500ms,

Movie 7B. HGF promotes MT1-MMP surface delivery. MDA-MB-231 cells expressing pH-MT1-MMP were seeded on the gelatin-coated glass-bottom dishes in the presence (7B) or absence of HGF (7A). Time-lapse images were captured using a TIRF microscope without an interval for 300 frames. Scale bar: 10μm, Exposure time: 500ms,

Movie 8. MET and MT1-MMP co-traffic at the cell surface. MDA-MB-231 cells co-expressing GFP-MET and Cherry-MT1-MMP were seeded on the gelatin-coated glass-bottom dishes. Time-lapse imaging was done using a TIRF microscope

Supplemental Tables

References

1. **Yin L,** Duan JJ, Bian XW, Yu S cang (2020) Triple-negative breast cancer molecular subtyping and treatment progress. *Breast Cancer Research* **22**:61 https://doi.org/10.1186/s13058-020-01296-5 | PubMed
2. **Burness ML,** Grushko TA, Olopade OI (2010) Epidermal Growth Factor Receptor in Triple-Negative and Basal-Like Breast Cancer. *The Cancer Journal* **16**:23-32 https://doi.org/10.1097/PPO.0b013e3181d24fc1 | PubMed
3. **Breen L,** Gaule PB, Canonici A, Walsh N, Collins DM, Cremona M, et al. (2020) Targeting c-Met in triple negative breast cancer: preclinical studies using the c-Met inhibitor, Cpd A. *Invest New Drugs* **38**:1365-1372 https://doi.org/10.1007/s10637-020-00937-y | PubMed
4. **Bardelli A,** Corso S, Bertotti A, Hobor S, Valtorta E, Siravegna G, et al. (2013) Amplification of the *MET* Receptor Drives Resistance to Anti-EGFR Therapies in Colorectal Cancer. *Cancer Discov* **3**:658-73 https://doi.org/10.1158/2159-8290.CD-12-0558 | PubMed
5. **Hanahan D** (2022) Hallmarks of Cancer: New Dimensions. *Cancer Discov* **12**:31-46 https://doi.org/10.1158/2159-8290.CD-21-1059 | PubMed
6. **Akshata Desai KA** (2012) Triple Negative Breast Cancer – An Overview. *Hereditary Genetics* https://doi.org/10.4172/2161-1041.S2-001
7. **Valastyan S,** Weinberg RA (2011) Tumor Metastasis: Molecular Insights and Evolving Paradigms. *Cell* **147**:275-92 https://doi.org/10.1016/j.cell.2011.09.024 | PubMed
8. **Eddy RJ,** Weidmann MD, Sharma VP, Condeelis JS (2017) Tumor Cell Invadopodia: Invasive Protrusions that Orchestrate Metastasis. *Trends Cell Biol* **27**:595-607 https://doi.org/10.1016/j.tcb.2017.03.003 | PubMed
9. **Sharma P,** Parveen S, Vinod Shah L, Mukherjee M, Kalaidzidis Y, Joseph Kozielski A, et al. (2020) SNX27-retromer assembly directs MT1-MMP trafficking to invadopodia and promotes breast cancer metastasis. *J Cell Biol* **219**:e201812098 https://doi.org/10.1083/jcb.201812098 | PubMed

10. **Frittoli E,** Palamidessi A, Marighetti P, Confalonieri S, Bianchi F, Malinverno C, et al. (2014) A RAB5/RAB4 recycling circuitry induces a proteolytic invasive program and promotes tumor dissemination. *Journal of Cell Biology* **206**:307-28 https://doi.org/10.1083/jcb.201403127 | PubMed
11. **Perrin L,** Belova E, Bayarmagnai B, Tüzel E, Gligorijevic B (2022) Invadopodia enable cooperative invasion and metastasis of breast cancer cells. *Commun Biol* **5**:758 https://doi.org/10.1038/s42003-022-03642-z | PubMed
12. **Mader CC,** Oser M, Magalhaes MAO, Bravo-Cordero JJ, Condeelis J, Koleske AJ, et al. (2011) Molecular and Cellular Pathobiology An EGFR-Src-Arg-Cortactin Pathway Mediates Functional Maturation of Invadopodia and Breast Cancer Cell Invasion. *Cancer research* **71**:1730-41 https://doi.org/10.1158/0008-5472.CAN-10-1432 | PubMed
13. **Williams KC,** Coppolino MG (2014) SNARE-dependent interaction of Src, EGFR and ß1 integrin regulates invadopodia formation and tumor cell invasion. *J Cell Sci.* **127** https://doi.org/10.1242/jcs.134734 | PubMed
14. **Rajadurai C V,** Havrylov S, Zaoui K, Vaillancourt R, Stuible M, Naujokas M, et al. (2012) Met receptor tyrosine kinase signals through a cortactin-Gab1 scaffold complex, to mediate invadopodia. *J Cell Sci* **125**:2940-53 https://doi.org/10.1242/jcs.100834 | PubMed
15. **Makowiecka A,** Simiczyjew A, Nowak D, Mazur AJ (2016) Varying effects of EGF, HGF and TGFβ on formation of invadopodia and invasiveness of melanoma cell lines of different origin. *Eur J Histochem* **60**:2728 https://doi.org/10.4081/ejh.2016.2728 | PubMed
16. **Hoshino D,** Branch KM, Weaver AM (2013) Signaling inputs to invadopodia and podosomes. *J Cell Sci* **126**:2979-89 https://doi.org/10.1242/jcs.079475 | PubMed
17. **Gonzatti-Haces M,** Seth A, Park M, Copeland T, Oroszlan S, Vande Woude GF (1988) Characterization of the TPR-MET oncogene p65 and the MET protooncogene p140 protein-tyrosine kinases. *Proceedings of the National Academy of Sciences* **85**:21-5 https://doi.org/10.1073/pnas.85.1.21 | PubMed
18. **Peschard P,** Fournier TM, Lamorte L, Naujokas MA, Band H, Langdon WY, et al. (2001) Mutation of the c-Cbl TKB Domain Binding Site on the Met Receptor Tyrosine Kinase Converts It into a Transforming Protein. *Mol Cell* **8**:995-1004 https://doi.org/10.1016/S1097-2765(01)00378-1 | PubMed
19. **Mukherjee S,** Tessema M, Wandinger-Ness A (2006) Vesicular Trafficking of Tyrosine Kinase Receptors and Associated Proteins in the Regulation of Signaling and Vascular Function. *Circ Res* **98**:743-56 https://doi.org/10.1161/01.RES.0000214545.99387.e3 | PubMed
20. **Wiley HS,** Burke PM (2001) Regulation of Receptor Tyrosine Kinase Signaling by Endocytic Trafficking. *Traffic* **2**:12-8 https://doi.org/10.1034/j.1600-0854.2001.020103.x | PubMed
21. **Goh LK,** Sorkin A (2013) Endocytosis of Receptor Tyrosine Kinases. *Cold Spring Harb Perspect Biol* **5**:a017459-a017459 https://doi.org/10.1101/cshperspect.a017459 | PubMed
22. **Stenmark H** (2009) Rab GTPases as coordinators of vesicle traffic. *Nat Rev Mol Cell Biol* **10**:513-25 https://doi.org/10.1038/nrm2728 | PubMed
23. **Jin H,** Tang Y, Yang L, Peng X, Li B, Fan Q, et al. (2021) Rab GTPases: Central Coordinators of Membrane Trafficking in Cancer. *Front Cell Dev Biol* **9** https://doi.org/10.3389/fcell.2021.648384 | PubMed
24. **Grosshans BL,** Ortiz D, Novick P (2006) Rabs and their effectors: Achieving specificity in membrane traffic. *Proceedings of the National Academy of Sciences* **103**:11821-7 https://doi.org/10.1073/pnas.0601617103 | PubMed
25. **Polishchuk RS,** Capestrano M, Polishchuk E V (2009) Shaping tubular carriers for intracellular membrane transport. *FEBS Lett* **583**:3847-56 https://doi.org/10.1016/j.febslet.2009.10.031 | PubMed
26. **Wandinger-Ness A,** Zerial M (2014) Rab Proteins and the Compartmentalization of the Endosomal System. *Cold Spring Harb Perspect Biol* **6**:a022616-a022616 https://doi.org/10.1101/cshperspect.a022616 | PubMed
27. **van Weering JRT,** Verkade P, Cullen PJ (2012) SNX–BAR-Mediated Endosome Tubulation is Co-ordinated with Endosome Maturation. *Traffic* **13**:94-107 https://doi.org/10.1111/j.1600-0854.2011.01297.x | PubMed

28. **Chibalina M V,** Seaman MNJ, Miller CC, Kendrick-Jones J, Buss F (2007) Myosin VI and its interacting protein LMTK2 regulate tubule formation and transport to the endocytic recycling compartment. *J Cell Sci* **120**:4278-88 https://doi.org/10.1242/jcs.014217 | PubMed

29. **McIntosh BB,** Pyrpassopoulos S, Holzbaur ELF, Ostap EM (2018) Opposing Kinesin and Myosin-I Motors Drive Membrane Deformation and Tubulation along Engineered Cytoskeletal Networks. *Current Biology* **28**:236-248.e5 https://doi.org/10.1016/j.cub.2017.12.007 | PubMed

30. **Simonetti B,** Cullen PJ (2019) Actin-dependent endosomal receptor recycling. *Current Opinion in Cell Biology* 22-33 https://doi.org/10.1016/j.ceb.2018.08.006 | PubMed

31. **Gopaldass N,** Chen KE, Collins B, Mayer A (2024) Assembly and fission of tubular carriers mediating protein sorting in endosomes. *Nat Rev Mol Cell Biol* **25**:765-83 https://doi.org/10.1038/s41580-024-00746-8 | PubMed

32. **Zaoui K,** Duhamel S, Parachoniak CA, Park M (2019) CLIP-170 spatially modulates receptor tyrosine kinase recycling to coordinate cell migration. *Traffic* **20**:187-201 https://doi.org/10.1111/tra.12629 | PubMed

33. **Joffre C,** Barrow R, Ménard L, Calleja V, Hart IR, Kermorgant S (2011) A direct role for Met endocytosis in tumorigenesis. *Nat Cell Biol* **13**:827-37 https://doi.org/10.1038/ncb2257 | PubMed

34. **Masuda H,** Zhang D, Bartholomeusz C, Doihara H, Hortobagyi GN, Ueno NT (2012) Role of epidermal growth factor receptor in breast cancer. *Breast Cancer Res Treat* **136**:331-45 https://doi.org/10.1007/s10549-012-2289-9 | PubMed

35. **Ho-Yen CM,** Louise Jones J, Kermorgant S (2015) The clinical and functional significance of c-Met in breast cancer: a review. *Breast cancer research : BCR* https://doi.org/10.1186/s13058-015-0547-6 | PubMed

36. **Ding X,** Ji J, Jiang J, Cai Q, Wang C, Shi M, et al. (2018) HGF-mediated crosstalk between cancer-associated fibroblasts and MET-unamplified gastric cancer cells activates coordinated tumorigenesis and metastasis. *Cell Death Dis* **9** https://doi.org/10.1038/s41419-018-0922-1 | PubMed

37. **Augoff K,** Hryniewicz-Jankowska A, Tabola R (2020) Invadopodia: clearing the way for cancer cell invasion. *Ann Transl Med* **8** https://doi.org/10.21037/atm.2020.02.157 | PubMed

38. **Linder S,** Cervero P, Eddy R, Condeelis J (2023) Mechanisms and roles of podosomes and invadopodia. *Nat Rev Mol Cell Biol* **24**:86-106 https://doi.org/10.1038/s41580-022-00530-6 | PubMed

39. **Kreider-Letterman G,** Castillo A, Mahlandt EK, Goedhart J, Rabino A, Goicoechea S, et al. (2023) ARHGAP17 regulates the spatiotemporal activity of Cdc42 at invadopodia. *Journal of Cell Biology* **222** https://doi.org/10.1083/jcb.202207020 | PubMed

40. **Baldanzi G,** Graziani A (2015) Physiological Signaling and Structure of the HGF Receptor MET. *Biomedicines* **3**:1-31 https://doi.org/10.3390/biomedicines3010001 | PubMed

41. **Cho KW,** Park JH, Park CW, Lee D, Lee E, Kim DJ, et al. (2013) Identification of a pivotal endocytosis motif in c-Met and selective modulation of HGF-dependent aggressiveness of cancer using the 16-mer endocytic peptide. *Oncogene* **32**:1018-29 https://doi.org/10.1038/onc.2012.122 | PubMed

42. **Bhuin T,** Roy JK (2014) Rab proteins: The key regulators of intracellular vesicle transport. *Exp Cell Res* **328**:1-19 https://doi.org/10.1016/j.yexcr.2014.07.027 | PubMed

43. **Parachoniak CA,** Luo Y, Abella JV, Keen JH, Park M (2011) GGA3 Functions as a Switch to Promote Met Receptor Recycling, Essential for Sustained ERK and Cell Migration. *Dev Cell* **20**:751-63 https://doi.org/10.1016/j.devcel.2011.05.007 | PubMed

44. **Chamberland JP,** Ritter B (2017) Retromer revisited: Evolving roles for retromer in endosomal sorting. *Journal of Cell Biology* **216**:3433-6 https://doi.org/10.1083/jcb.201708111 | PubMed

45. **Linford A,** Yoshimura S ichiro, Bastos RN, Langemeyer L, Gerondopoulos A, Rigden DJ, et al. (2012) Rab14 and Its Exchange Factor FAM116 Link Endocytic Recycling and Adherens Junction Stability in Migrating Cells. *Dev Cell* **22**:952-66 https://doi.org/10.1016/j.devcel.2012.04.010 | PubMed

46. **Wang J,** Xiong J, Zhang S, Li D, Chu Q, Chang W, et al. (2024) Biogenesis of Rab14-positive endosome buds at Golgi–endosome contacts by the RhoBTB3–SHIP164–Vps26B complex. *Cell Discov* **10**:38 https://doi.org/10.1038/s41421-024-00651-6 | PubMed

47. **Muller PAJ,** Trinidad AG, Timpson P, Morton JP, Zanivan S, van den Berghe PVE, et al. (2013) Mutant p53 enhances MET trafficking and signalling to drive cell scattering and invasion. *Oncogene* **32**:1252-65 https://doi.org/10.1038/onc.2012.148 | PubMed

48. **Gundry C,** Marco S, Rainero E, Miller B, Dornier E, Mitchell L, et al. (2017) Phosphorylation of Rab-coupling protein by LMTK3 controls Rab14-dependent EphA2 trafficking to promote cell:cell repulsion. *Nat Commun* **8**:14646 https://doi.org/10.1038/ncomms14646 | PubMed

49. **Zhang J,** Liu X, Datta A, Govindarajan K, Tam WL, Han J, et al. (2009) RCP is a human breast cancer–promoting gene with Ras-activating function. *Journal of Clinical Investigation* https://doi.org/10.1172/JCI37622 | PubMed

50. **Dai Y,** Liu Y, Huang D, Yu C, Cai G, Pi L, et al. (2012) Increased expression of Rab coupling protein in squamous cell carcinoma of the head and neck and its clinical significance. *Oncol Lett* **3**:1231-6 https://doi.org/10.3892/ol.2012.652 | PubMed

51. **Ueno H,** Huang X, Tanaka Y, Hirokawa N (2011) KIF16B/Rab14 Molecular Motor Complex Is Critical for Early Embryonic Development by Transporting FGF Receptor. *Dev Cell* **20**:60-71 https://doi.org/10.1016/j.devcel.2010.11.008 | PubMed

52. **Skjeldal FM,** Strunze S, Bergeland T, Walseng E, FGregers T, Bakke O (2012) The fusion of early endosomes induces molecular motor-driven tubule formation and fission. *J Cell Sci.* https://doi.org/10.1242/jcs.092569 | PubMed

53. **Nagasato AI,** Yamashita H, Matsuo M, Ueda K, Kioka N (2017) The distribution of vinculin to lipid rafts plays an important role in sensing stiffness of extracellular matrix. *Biosci Biotechnol Biochem.* **81**:1136-47 https://doi.org/10.1080/09168451.2017.1289074 | PubMed

54. **Sounni NE,** Noel A (2005) Membrane type-matrix metalloproteinases and tumor progression. *Biochimie* **87**:329-42 https://doi.org/10.1016/j.biochi.2004.07.012 | PubMed

55. **Parveen S,** Khamari A, Raju J, Coppolino MG, Datta S (2022) Syntaxin 7 contributes to breast cancer cell invasion by promoting invadopodia formation. *J Cell Sci* **135** https://doi.org/10.1242/jcs.259576 | PubMed

56. **Nabeshima K,** Inoue T, Shimao Y, Okada Y, Itoh Y, Seiki M, et al. (2000) Front-cell-specific expression of membrane-type 1 matrix metalloproteinase and gelatinase A during cohort migration of colon carcinoma cells induced by hepatocyte growth factor/scatter factor. *Cancer Res* **60**:3364-9 PubMed

57. **Murakami Y,** Mizuguchi K (2014) Homology-based prediction of interactions between proteins using Averaged One-Dependence Estimators. *BMC Bioinformatics* **15**:213 https://doi.org/10.1186/1471-2105-15-213 | PubMed

58. **Deryugina EI,** Ratnikov B, Monosov E, Postnova TI, DiScipio R, Smith JW, et al. (2001) MT1-MMP initiates activation of pro-MMP-2 and integrin alphavbeta3 promotes maturation of MMP-2 in breast carcinoma cells. *Exp Cell Res* **263**:209-23 https://doi.org/10.1006/excr.2000.5118 | PubMed

59. **Xia XD,** Alabi A, Wang M, Gu HM, Yang RZ, Wang GQ, et al. (2021) Membrane-type I matrix metalloproteinase (MT1-MMP), lipid metabolism, and therapeutic implications. *J Mol Cell Biol* **13**:513-26 https://doi.org/10.1093/jmcb/mjab048 | PubMed

60. **Alabi A,** Xia XD, Gu HM, Wang F, Deng SJ, Yang N, et al. (2021) Membrane type 1 matrix metalloproteinase promotes LDL receptor shedding and accelerates the development of atherosclerosis. *Nat Commun* **12**:1889 https://doi.org/10.1038/s41467-021-22167-3 | PubMed

61. **Itoh Y** (2015) Membrane-type matrix metalloproteinases: Their functions and regulations. *Matrix Biology* **44–46**:207-23 https://doi.org/10.1016/j.matbio.2015.03.004 | PubMed

62. **Ferrari R,** Martin G, Tagit O, Guichard A, Cambi A, Voituriez R, et al. (2019) MT1-MMP directs force-producing proteolytic contacts that drive tumor cell invasion. *Nat Commun* **10**:4886 https://doi.org/10.1038/s41467-019-12930-y | PubMed

63. **Hoshino D,** Branch KM, Weaver AM (2013) Signaling inputs to invadopodia and podosomes. *J Cell Sci* **126**:2979-89 https://doi.org/10.1242/jcs.079475 | PubMed

64. **Zagryazhskaya-Masson A,** Monteiro P, Macé AS, Castagnino A, Ferrari R, Infante E, et al. (2020) Intersection of TKS5 and FGD1/CDC42 signaling cascades directs the formation of invadopodia. *Journal of Cell Biology* **219** https://doi.org/10.1083/jcb.201910132 | PubMed

65. **Petrelli A,** Gilestro GF, Lanzardo S, Comoglio PM, Migone N, Giordano S (2002) The endophilin–CIN85–Cbl complex mediates ligand-dependent downregulation of c-Met. *Nature* **416**:187-90 https://doi.org/10.1038/416187a | PubMed

66. **Barrow-McGee R,** Kermorgant S (2014) Met endosomal signalling: In the right place, at the right time. *Int J Biochem Cell Biol* **49**:69-74 https://doi.org/10.1016/j.biocel.2014.01.009 | PubMed

67. **Ménard L,** Parker PJ, Kermorgant S (2014) Receptor tyrosine kinase c-Met controls the cytoskeleton from different endosomes via different pathways. *Nat Commun* **5**:3907 https://doi.org/10.1038/ncomms4907 | PubMed

68. **Hey S,** Wiesner C, Barcelona B, Linder S (2023) KIF16B drives MT1-MMP recycling in macrophages and promotes co-invasion of cancer cells. *Life Sci Alliance* **6**:e202302158 https://doi.org/10.26508/lsa.202302158 | PubMed

69. **Castro-Castro A,** Marchesin V, Monteiro P, Lodillinsky C, Rossé C, Chavrier P (2016) Cellular and Molecular Mechanisms of MT1-MMP-Dependent Cancer Cell Invasion. *Annual Review of Cell and Developmental Biology* 555-76 https://doi.org/10.1146/annurev-cellbio-111315-125227 | PubMed

70. **Tanaka N,** Sakamoto T (2023) MT1-MMP as a Key Regulator of Metastasis. *Cells* **12**:2187 https://doi.org/10.3390/cells12172187 | PubMed

71. **Bukhari M,** Patel N, Fontana R, Santiago-Medina M, Jiang Y, Li D, et al. (2023) Fibroblast activation protein drives tumor metastasis via a protease-independent role in invadopodia stabilization. *Cell Rep* **42**:113302 https://doi.org/10.1016/j.celrep.2023.113302 | PubMed

72. **Machesky LM** (2019) Rab11FIP proteins link endocytic recycling vesicles for cytoskeletal transport and tethering. *Biosci Rep* **39** https://doi.org/10.1042/BSR20182219 | PubMed

73. **Peden AA,** Schonteich E, Chun J, Junutula JR, Scheller RH, Prekeris R (2004) The RCP–Rab11 Complex Regulates Endocytic Protein Sorting. *Mol Biol Cell* **15**:3530-41 https://doi.org/10.1091/mbc.e03-12-0918 | PubMed

74. **Lall P,** Lindsay AJ, Hanscom S, Kecman T, Taglauer ES, McVeigh UM, et al. (2015) Structure-Function Analyses of the Interactions between Rab11 and Rab14 Small GTPases with Their Shared Effector Rab Coupling Protein (RCP). *Journal of Biological Chemistry* **290**:18817-32 https://doi.org/10.1074/jbc.M114.612366 | PubMed

75. **Norris A,** Grant BD (2020) Endosomal microdomains: Formation and function. *Curr Opin Cell Biol* **65**:86-95 https://doi.org/10.1016/j.ceb.2020.02.018 | PubMed

76. **Delevoye C,** Miserey-Lenkei S, Montagnac G, Gilles-Marsens F, Paul-Gilloteaux P, Giordano F, et al. (2014) Recycling Endosome Tubule Morphogenesis from Sorting Endosomes Requires the Kinesin Motor KIF13A. *Cell Rep* **6**:445-54 https://doi.org/10.1016/j.celrep.2014.01.002 | PubMed

77. **Goto-Silva L,** McShane MP, Salinas S, Kalaidzidis Y, Schiavo G, Zerial M (2019) Retrograde transport of Akt by a neuronal Rab5-APPL1 endosome. *Sci Rep* **9**:2433 https://doi.org/10.1038/s41598-019-38637-0 | PubMed

78. **Kalaidzidis Y,** Morales-Navarrete H, Kalaidzidis I, Zerial M (2019) Intracellular Background Estimation for Quantitative Fluorescence Microscopy. In: The 39th International Workshop on Bayesian Inference and Maximum Entropy Methods in Science and Engineering. Basel Switzerland: MDPI. pp. 22 https://doi.org/10.3390/proceedings2019033022

79. **Rink J,** Ghigo E, Kalaidzidis Y, Zerial M (2005) Rab Conversion as a Mechanism of Progression from Early to Late Endosomes. *Cell* **122**:735-49 https://doi.org/10.1016/j.cell.2005.06.043 | PubMed

80. **Nazari SS** (2020) Generation of 3D Tumor Spheroids with Encapsulating Basement Membranes for Invasion Studies. *Curr Protoc Cell Biol* **87** https://doi.org/10.1002/cpcb.105 | PubMed

81. **Lord SJ,** Velle KB, Mullins RD, Fritz-Laylin LK (2020) SuperPlots: Communicating reproducibility and variability in cell biology. *Journal of Cell Biology* **219** https://doi.org/10.1083/jcb.202001064 | PubMed

Peer reviews

Reviewer #1 (Public review):

Summary:

This study identifies a mechanism responsible for the accumulation of the MET receptor in invadopodia, following stimulation of Triple-negative breast cancer (TNBC) cells with HGF. HGF-driven accumulation and activation of MET in invadopodia causes the degradation of the extracellular matrix promoting cancer cell invasion, a process here investigated using gelatine-degradation and spheroid invasion assays.

Mechanistically, HGF stimulates the recycling of MET from RAB14-positive endodomes to invadopodia, increasing their formation. At invadopodia, MET induces matrix degradation via direct binding with the metallo protease MT1-MMP.

The delivery of MET from the recycling compartment to invadopodia is mediated by RCP which facilitates the colocalization of MET to RAB14 endosomes. On this compartment, HGF induces the recruitment of the motor protein KIF16B promoting the tubulation of the RAB14-MET recycling endosomes to the cell surface.

This pathway is critical for the HGF-driven invasive properties of TNBC cells as it is impaired upon silencing of RAB14.

Strengths:

The study is well organized and executed using state of the art technology. The effects of MET recycling in the formation of functional invadopodia are carefully studied taking advantage of mutant forms of the receptor that are degradation-resistant or endocytosis-defective.

Data analyses are rigorous and appropriate controls are used in most of the assays to assess the specificity of the scored effects. Overall, the quality of the research is high.

The conclusions are well supported by the results and the data and methodology are of interest for a wide audience of cell biologists.

Previous Weaknesses:

The role of the MET receptor in invadopodia formation and cancer cell dissemination has been intensively studied in many settings including Triple Negative breast cancer cells. The novelty of the present study mostly consists in the detailed molecular description of the underlying mechanism based on HGF-driven MET recycling. The question of whether the identified pathway is specific for TNBC cells or represents a general mechanism of HGF-mediated invasion detectable in other cancer cells is not addressed or at least discussed.

Comments on revised version:

The authors have partially replied to my previous concerns.

https://doi.org/10.7554/eLife.109472.2.sa2

Reviewer #2 (Public review):

Summary:

In this manuscript, Khamari and colleagues investigate how HGF-MET signaling and the intracellular trafficking of the MET receptor tyrosine kinase influence invadopodia formation and invasion in triple-negative breast cancer (TNBC) cells. They show that HGF stimulation enhances both the number of invadopodia and their proteolytic activity. Mechanistically, the authors demonstrate that HGF-induced, RAB4- and RCP-RAB14-KIF16B-dependent recycling routes deliver MET to the cell surface specifically at sites where invadopodia form. Moreover, they report that MET physically interacts with MT1-MMP - a key transmembrane metalloproteinase required for invadopodia function- and that these two proteins co-traffic to invadopodia upon HGF stimulation.

Although the HGF-MET axis has previously been implicated in invadopodia regulation (e.g., by Rajadurai et al., Journal of Cell Science 2012), studies directly linking ligand-induced MET trafficking with the spatial regulation of MT1-MMP localization and activity have been lacking.

Overall, the manuscript addresses a relevant and timely topic and provides several novel insights.

Comments on revised version:

I appreciate the authors' efforts to revise the manuscript and address the reviewers' comments. While the revised version includes additional experiments and several improvements in data presentation, the major methodological and conceptual concerns raised in the initial review remain largely unresolved. In my opinion, these issues critically undermine the central mechanistic conclusions of the study.

(1) Inappropriate experimental design for studying MET trafficking

A major concern remains the use of prolonged HGF stimulation times (2-6 hours) to study MET endocytosis and recycling. This is not an appropriate experimental design for investigating receptor tyrosine kinase trafficking dynamics. Ligand-induced internalization of MET occurs within minutes, with maximal endosomal accumulation typically observed within 5-15 minutes, whereas recycling occurs over approximately 15-60 minutes.

Importantly, the authors have not included short stimulation time points or any kinetic analysis that would allow a proper assessment of MET internalization or recycling. The additional surface biotinylation experiment does not address this issue, as it still does not provide temporal information regarding receptor trafficking.

Therefore, the current data do not support the conclusions regarding MET endocytosis or recycling, and this major methodological concern has not been adequately addressed in the revised manuscript.

(2) Insufficient validation of antibody specificity in immunofluorescence

The validation of antibody specificity for MET, phospho-MET, and MT1-MMP in immunofluorescence experiments remains insufficient. While the authors demonstrate knockdown efficiency by immunoblotting and show some reduction in fluorescence signal, they do not provide rigorous evidence that the immunofluorescence signal is specifically abolished upon gene silencing under identical imaging conditions. Such validation is essential, particularly because the manuscript relies heavily on imaging-based localization and colocalization analyses. Without these controls, it cannot be excluded that the observed signal represents non-specific staining.

Importantly, the authors attempt to justify antibody specificity primarily by citing previous publications that used the same antibodies. However, this is not an adequate substitute for experimental validation within the current study. Previous reports do not guarantee

specificity under the present experimental conditions, particularly in immunofluorescence, where staining patterns can be strongly influenced by fixation procedures, antibody concentrations, imaging settings, and cell type. Moreover, those studies may themselves lack sufficiently rigorous validation of antibody specificity. Therefore, antibody specificity should be demonstrated directly in the experimental system used in this manuscript, especially given that the principal conclusions rely extensively on the subcellular localization of MET, phospho-MET, and MT1-MMP.

(3) Questionable MET localization in TIRF microscopy

The presence of punctate MET signal in TIRF microscopy under unstimulated conditions raises additional concerns. Under basal conditions, MET is generally expected to exhibit a predominantly diffuse distribution at the plasma membrane, whereas prominent punctate structures are typically associated with ligand-induced clustering, endocytosis, or trafficking events.

The observation of numerous MET-positive puncta in unstimulated cells, together with the insufficient validation of antibody specificity, raises the possibility that at least part of the observed signal represents non-specific staining or imaging artefacts rather than bona fide MET localization. This concern is further compounded by the lack of rigorous immunofluorescence antibody validation discussed above and significantly undermines the interpretation of all TIRF-based trafficking analyses presented in the manuscript.

(4) The evidence supporting a MET-specific role in invadopodia remains unconvincing

The authors argue that the role of MET in invadopodia formation is validated using three independent approaches: shRNA-mediated knockdown, SMARTpool siRNA-mediated knockdown, and pharmacological inhibition with PHA665752. However, I do not agree that these constitute three independent orthogonal validations of MET function.

First, the shRNA-mediated knockdown presented in this study achieves only modest depletion of MET protein. The authors themselves acknowledge this limitation and therefore selected cells with visibly reduced MET staining for imaging. Consequently, the shRNA experiments cannot be considered a robust or independent validation of MET function.

Second, although pooled SMARTpool siRNAs are widely used to improve knockdown efficiency, they cannot exclude off-target effects, as each individual guide RNA contributes its own potential off-target profile. Therefore, pooled siRNAs cannot by themselves establish that an observed phenotype is specifically attributable to depletion of the intended target and do not replace validation using independent individual siRNAs or rescue experiments.

Third, the pharmacological data should also be interpreted with caution. Throughout the manuscript, PHA665752 is presented as a MET inhibitor supporting the specificity of the observed phenotype. However, there is essentially no such thing as a truly selective receptor tyrosine kinase inhibitor. PHA665752 inhibits multiple kinases in addition to MET, particularly at concentrations commonly used in cell-based assays. Consequently, the inhibitor cannot be considered an independent validation of MET-specific function.

Importantly, the newly added siRNA experiments do not resolve my original concern regarding the role of MET in invadopodia formation. Although siRNA-mediated MET depletion is substantially more efficient than the shRNA-mediated knockdown presented in the original manuscript, this marked difference in MET depletion is not accompanied by a correspondingly stronger inhibition of invadopodia formation or ECM degradation. If MET were indeed the principal driver of the observed phenotype, one would expect the magnitude of the biological effect to correlate with the efficiency of MET depletion. This inconsistency raises the possibility that the observed phenotype is not solely attributable to MET depletion and calls into question the specificity of the proposed mechanism.

Taken together, the three perturbation approaches used by the authors cannot be regarded as independent orthogonal validation of MET function. One approach provides only modest target depletion, another relies on pooled RNAi reagents that cannot exclude off-target effects, and the third employs a multi-kinase inhibitor rather than a MET-specific compound. Collectively, these limitations substantially weaken the conclusion that the reduction in invadopodia formation is specifically attributable to loss of MET. A convincing demonstration of MET-specific function would require rescue experiments or another truly orthogonal validation strategy.

(5) Weak evidence for MET-MT1-MMP interaction

The evidence supporting a physical interaction between MET and MT1-MMP remains unconvincing. The newly added co-immunoprecipitation experiment does not reveal a convincing MET-MT1-MMP interaction, and I am unable to appreciate a specific co-immunoprecipitated MT1-MMP signal in the presented blot. As presented, these data do not convincingly demonstrate a specific or functionally relevant interaction. Given that this interaction constitutes a central component of the proposed mechanistic model, this remains a major weakness of the study.

(6) Overinterpretation of the data

Taken together, the study proposes a mechanistic model linking MET trafficking to MT1-MMP localization and invadopodia function. However, the experimental evidence largely supports correlative observations rather than demonstrating a direct mechanistic relationship.

Specifically, MET endocytosis and recycling are not properly demonstrated because of the inappropriate temporal resolution of the trafficking experiments; the localization data remain uncertain owing to insufficient validation of the immunofluorescence reagents; and the proposed interaction between MET and MT1-MMP is not convincingly demonstrated. Consequently, the manuscript establishes correlation rather than causality, and the central mechanistic conclusions appear to be substantially overstated relative to the presented data.

Conclusion:

While the manuscript addresses an interesting and biologically relevant question, the current experimental evidence does not adequately support the proposed mechanistic model. The combination of inappropriate experimental design for trafficking studies, insufficient validation of key imaging reagents, questionable interpretation of the localization data, lack of convincing evidence for the proposed MET-MT1-MMP interaction, and the absence of a clear relationship between the degree of MET depletion and the biological phenotype substantially limits the reliability of the conclusions.

In my opinion, these issues cannot be addressed by further revision of the current manuscript, as they require substantial additional experimentation, including appropriately designed trafficking assays with short kinetic time points, rigorous validation of antibody specificity for immunofluorescence, and stronger mechanistic evidence linking MET trafficking to MT1-MMP-dependent invadopodia function.

https://doi.org/10.7554/eLife.109472.2.sa1

Author response:

The following is the authors' response to the current reviews.

We thank the editor and the reviewers for their comments on the revised manuscript. Based on the comments, we decided to go for a minor revision which will address all the comments of reviewer 1.

Towards the comments of the reviewer 2, we would like to state that we already provided the results from the new experiments and the reasons why we did not perform some of the suggested ones. Interestingly, we have not deviated from standard practices in the field in our approaches. Yet, the reviewer is not convinced and raised concern about the robustness of our observations. We therefore decided to carry out a few more control experiments which in our opinion are redundant as they already were carried out multiple times by us as well as by the other field experts under identical conditions and using the identical cell lines.

> ***Reviewer #1 (Public review):***
>
> *Summary:*
>
> *This study identifies a mechanism responsible for the accumulation of the MET receptor in invadopodia, following stimulation of Triple-negative breast cancer (TNBC) cells with HGF. HGF-driven accumulation and activation of MET in invadopodia causes the degradation of the extracellular matrix promoting cancer cell invasion, a process here investigated using gelatine-degradation and spheroid invasion assays.*
>
> *Mechanistically, HGF stimulates the recycling of MET from RAB14-positive endodomes to invadopodia, increasing their formation. At invadopodia, MET induces matrix degradation via direct binding with the metallo protease MT1-MMP.*
>
> *The delivery of MET from the recycling compartment to invadopodia is mediated by RCP which facilitates the colocalization of MET to RAB14 endosomes. On this compartment, HGF induces the recruitment of the motor protein KIF16B promoting the tubulation of the RAB14-MET recycling endosomes to the cell surface.*
>
> *This pathway is critical for the HGF-driven invasive properties of TNBC cells as it is impaired upon silencing of RAB14.*
>
> *Strengths:*
>
> *The study is well organized and executed using state of the art technology. The effects of MET recycling in the formation of functional invadopodia are carefully studied taking advantage of mutant forms of the receptor that are degradation-resistant or endocytosisdefective.*
>
> *Data analyses are rigorous and appropriate controls are used in most of the assays to assess the specificity of the scored effects. Overall, the quality of the research is high.*
>
> *The conclusions are well supported by the results and the data and methodology are of interest for a wide audience of cell biologists.*
>
> *Previous Weaknesses:*
>
> *The role of the MET receptor in invadopodia formation and cancer cell dissemination has been intensively studied in many settings including Triple Negative breast cancer cells. The novelty of the present study mostly consists in the detailed molecular description of the underlying mechanism based on HGF-driven MET recycling. The question of whether the identified pathway is specific for TNBC cells or represents a general mechanism of HGFmediated invasion detectable in other cancer cells is not addressed or at least discussed.*
>
> *Comments on revised version:*
>
> *The authors have partially replied to my previous concerns.*

We sincerely thank the reviewer for careful evaluation of our manuscript and recognizing the strength of our study. We are grateful for the positive assessment about the well-executed methods, rigorous data analysis, usage of appropriate controls, and for acknowledging that we have addressed, at least in part, the concerns raised in the previous round of review. We appreciate the reviewer's constructive comments, which have helped us further clarify the scope and significance of our findings.

> ***Reviewer #1 (Recommendations for the authors):***
>
> *The authors have partially replied to my previous concerns. The following points still have to be addressed.*
>
> *(1) Despite many TNBC tumours present high expression of the EGFR, trials with EGFR inhibitors have been very disappointing (please read PMID: 41651315). EGFR inhibition has been extensively attempted with negative outcome, and this is well known.*
>
> *In the clinical practise, Triple Negative breast cancer patients are commonly treated with chemotherapy, not with EGFR or MET inhibitors.*
>
> *Line 31-38 are misleading at best and should be removed and the incipit of the study modified. The biology of this study is sound there is no need to push the clinical relevance with instances that are notoriously not applicable.*

We are thankful to the reviewer for bringing up this point. We will modify the manuscript as per the reviewer's suggestion.

> *(2) In reply to point 4, the authors claim that they checked MMP2 and the experiment is shown in FigS5I, which is not.....*

We sincerely apologise for uploading an incorrect file. The correct file will be uploaded.

> *(3) I noticed that, in the previous version of the manuscript in Fig. S4A the panel showing the mutation frequency was erroneously indicated in the legend as referring to MET.*
>
> *The authors replied that they fixed this but actually the legend is still wrong...*

We thank the reviewer for bringing this error into our attention. We will attentively correct the legend in the revised version of the manuscript.

> ***Reviewer #2 (Public review):***
>
> *Summary:*
>
> *In this manuscript, Khamari and colleagues investigate how HGF-MET signaling and the intracellular trafficking of the MET receptor tyrosine kinase influence invadopodia formation and invasion in triple-negative breast cancer (TNBC) cells. They show that HGF stimulation enhances both the number of invadopodia and their proteolytic activity. Mechanistically, the authors demonstrate that HGF-induced, RAB4- and RCP-RAB14KIF16B-dependent recycling routes deliver MET to the cell surface specifically at sites where invadopodia form. Moreover, they report that MET physically interacts with MT1MMP - a key transmembrane metalloproteinase required for invadopodia function- and that these two proteins co-traffic to invadopodia upon HGF stimulation.*
>
> *Although the HGF-MET axis has previously been implicated in invadopodia regulation (e.g., by Rajadurai et al., Journal of Cell Science 2012), studies directly linking ligandinduced MET trafficking with the spatial regulation of MT1-MMP localization and activity have been lacking.*

> *Overall, the manuscript addresses a relevant and timely topic and provides several novel insights.*
>
> *Comments on revised version:*
>
> *I appreciate the authors' efforts to revise the manuscript and address the reviewers' comments. While the revised version includes additional experiments and several improvements in data presentation, the major methodological and conceptual concerns raised in the initial review remain largely unresolved. In my opinion, these issues critically undermine the central mechanistic conclusions of the study.*

We thank the reviewer for critically re-evaluating our manuscript and acknowledging the novel insights and relevance of our study.

We thank the reviewer for pointing out the study by Rajadurai et al., Journal of Cell Science, 2012, which provided crucial evidence about the role of MET signaling in invadopodia formation [1]. However, the experimental system largely used by Rajadurai et al. is fundamentally different from the receptor trafficking mechanism investigated in the present study. The group have mostly used overexpression of Tpr-MET, which is a cytosolic MET mutant, that does not undergo the canonical ligand-induced RTK endocytosis and subsequent degradation or recycling. Our study did not only establish another link between MET signaling and invadopodia formation; rather, we identified a trafficking-dependent mechanism whereby HGF stimulation regulates the spatial redistribution and recycling of full-length MET to invadopodia, thus providing more physiologically relevant insights.

We also respectfully disagree that the methodological concerns raised critically undermine our mechanistic conclusions. Although other approaches as suggested by the reviewer could provide complementary information, we believe that the methods used in our study are appropriate for assessing invasive behaviour of the TNBC cells. These methods have been used by us and other research groups in the filed as reflected from the existing literature [2–6].

In this context, we would also like to add that the study referred by the reviewer above, has used a more off target prone approach (SiGenome Smartpool) compared to ONTARGETplus (chemically modified SiRNA pool for minimizing off target effect) in addition to the same small molecule inhibitor used in our study. Additionally, we also used a shRNA-based silencing to verify the phenotype. Since the silencing was not as pronounced as the siRNA-mediated knockdown, the reviewer has expressed concern.

We would like to point out that the antibody we used in IF for MT1-MMP (MMP14) have been published in multiple peer-reviewed journals by various research groups using the identical cell lines (MDA-MB-231, ATCC- HTB-26) [6–8]. MET antibodies used in the study (CST, D1C2 XP & L6E7) has been validated in MDA-MB-231 and MET-depleted cells [9-12]. Since these antibodies have been utilized for IF since a long time across various research groups under identical laboratory/experimental conditions, the exercise of validation suggested by the reviewer is surprising.

> *(1) Inappropriate experimental design for studying MET trafficking*
>
> *A major concern remains the use of prolonged HGF stimulation times (2-6 hours) to study MET endocytosis and recycling. This is not an appropriate experimental design for investigating receptor tyrosine kinase trafficking dynamics. Ligand-induced internalization of MET occurs within minutes, with maximal endosomal accumulation typically observed within 5-15 minutes, whereas recycling occurs over approximately 15-60 minutes.*

> *Importantly, the authors have not included short stimulation time points or any kinetic analysis that would allow a proper assessment of MET internalization or recycling. The additional surface biotinylation experiment does not address this issue, as it still does not provide temporal information regarding receptor trafficking.*
>
> *Therefore, the current data do not support the conclusions regarding MET endocytosis or recycling, and this major methodological concern has not been adequately addressed in the revised manuscript.*

We want to clarify that, our prime objective is to determine how MET trafficking is regulated at the time points at which we observe the functional effects of HGF on invadopodia formation and matrix degradation. Since our functional assays were performed following 2-3 h of HGF stimulation, we specifically examined MET localization and trafficking at these same time points.

Though shorter time points could provide information on the kinetics of MET trafficking, but their absence does not invalidate our conclusions regarding the role of MET trafficking in HGF-induced invasive function. In other words, our conclusions are made for the time points for which we have conducted the experiments. It is needless to add that different cargo molecule will show different kinetics.

In summary, we wanted to study the MET trafficking at the late hours in accordance with our functional assays and accordingly designed our experiments. Also, we have supported our results through biochemical methods which is considered to be one of the gold standards in the field.

> *(2) Insufficient validation of antibody specificity in immunofluorescence*
>
> *The validation of antibody specificity for MET, phospho-MET, and MT1-MMP in immunofluorescence experiments remains insufficient. While the authors demonstrate knockdown efficiency by immunoblotting and show some reduction in fluorescence signal, they do not provide rigorous evidence that the immunofluorescence signal is specifically abolished upon gene silencing under identical imaging conditions. Such validation is essential, particularly because the manuscript relies heavily on imaging-based localization and colocalization analyses. Without these controls, it cannot be excluded that the observed signal represents non-specific staining.*
>
> *Importantly, the authors attempt to justify antibody specificity primarily by citing previous publications that used the same antibodies. However, this is not an adequate substitute for experimental validation within the current study. Previous reports do not guarantee specificity under the present experimental conditions, particularly in immunofluorescence, where staining patterns can be strongly influenced by fixation procedures, antibody concentrations, imaging settings, and cell type. Moreover, those studies may themselves lack sufficiently rigorous validation of antibody specificity. Therefore, antibody specificity should be demonstrated directly in the experimental system used in this manuscript, especially given that the principal conclusions rely extensively on the subcellular localization of MET, phospho-MET, and MT1-MMP.*

We understand the reviewer's concern regarding antibody specificity and agree that appropriate validation is important for imaging-based analyses. However, we strongly disagree with the statement that the MT1-MMP, MET antibody were not adequately validated. The specificity of the MT1-MMP antibody was independently validated by both siRNA- and sgRNA-mediated gene silencing, where we observed a substantially diminished MT1-MMP signal by immunoblotting (Fig S5I, M'). Moreover, the antibody has been used for IF in the same cell line by multiple research groups [6–8]. So, in our opinion, this validation is completely redundant.

We have validated the MET staining/ signal using the antibody in gene-silenced cells by immunoblotting and immunofluorescence (Fig S1I, K, L), as also acknowledged by the reviewer in comment-4. In addition, we would also like to clarify that the references cited in support of antibody specificity were not selected simply because they used the same antibodies. They include studies that provide experimental validation of the antibodies by gene silencing.

To further confirm the antibody specificity, we will add immunofluorescence images of MET or MT1-MMP silenced cells stained with respective antibodies. However, we may not want to add these data to the manuscript as they do not carry any additional values to the manuscript.

> *(3) Questionable MET localization in TIRF microscopy*
>
> *The presence of punctate MET signal in TIRF microscopy under unstimulated conditions raises additional concerns. Under basal conditions, MET is generally expected to exhibit a predominantly diffuse distribution at the plasma membrane, whereas prominent punctate structures are typically associated with ligand-induced clustering, endocytosis, or trafficking events.*
>
> *The observation of numerous MET-positive puncta in unstimulated cells, together with the insufficient validation of antibody specificity, raises the possibility that at least part of the observed signal represents non-specific staining or imaging artefacts rather than bona fide MET localization. This concern is further compounded by the lack of rigorous immunofluorescence antibody validation discussed above and significantly undermines the interpretation of all TIRF-based trafficking analyses presented in the manuscript.*

We would like to highlight the apparent similarities between Fig 2A, B and the unstimulated condition in Fig. 2H. In figure 2A, B, MET is detected using an anti-MET antibody, whereas in Figure 2H, GFP-MET is imaged under live cell condition. We believe the reviewer would agree that imaging GFP-MET in live cells avoids fixation- and antibody-related artifacts. The comparable localization observed using these two independent approaches therefore provides additional support that the MET distribution shown in Fig. 2A, B reflects genuine receptor localization rather than an imaging or staining artefact.

> *(4) The evidence supporting a MET-specific role in invadopodia remains unconvincing*
>
> *The authors argue that the role of MET in invadopodia formation is validated using three independent approaches: shRNA-mediated knockdown, SMARTpool siRNA-mediated knockdown, and pharmacological inhibition with PHA665752. However, I do not agree that these constitute three independent orthogonal validations of MET function.*
>
> *First, the shRNA-mediated knockdown presented in this study achieves only modest depletion of MET protein. The authors themselves acknowledge this limitation and therefore selected cells with visibly reduced MET staining for imaging. Consequently, the shRNA experiments cannot be considered a robust or independent validation of MET function.*
>
> *Second, although pooled SMARTpool siRNAs are widely used to improve knockdown efficiency, they cannot exclude off-target effects, as each individual guide RNA contributes its own potential off-target profile. Therefore, pooled siRNAs cannot by themselves establish that an observed phenotype is specifically attributable to depletion of the intended target and do not replace validation using independent individual siRNAs or rescue experiments.*

> *Third, the pharmacological data should also be interpreted with caution. Throughout the manuscript, PHA665752 is presented as a MET inhibitor supporting the specificity of the observed phenotype. However, there is essentially no such thing as a truly selective receptor tyrosine kinase inhibitor. PHA665752 inhibits multiple kinases in addition to MET, particularly at concentrations commonly used in cell-based assays. Consequently, the inhibitor cannot be considered an independent validation of MET-specific function.*
>
> *Importantly, the newly added siRNA experiments do not resolve my original concern regarding the role of MET in invadopodia formation. Although siRNA-mediated MET depletion is substantially more efficient than the shRNA-mediated knockdown presented in the original manuscript, this marked difference in MET depletion is not accompanied by a correspondingly stronger inhibition of invadopodia formation or ECM degradation. If MET were indeed the principal driver of the observed phenotype, one would expect the magnitude of the biological effect to correlate with the efficiency of MET depletion. This inconsistency raises the possibility that the observed phenotype is not solely attributable to MET depletion and calls into question the specificity of the proposed mechanism.*
>
> *Taken together, the three perturbation approaches used by the authors cannot be regarded as independent orthogonal validation of MET function. One approach provides only modest target depletion, another relies on pooled RNAi reagents that cannot exclude off-target effects, and the third employs a multi-kinase inhibitor rather than a MET-specific compound. Collectively, these limitations substantially weaken the conclusion that the reduction in invadopodia formation is specifically attributable to loss of MET. A convincing demonstration of MET-specific function would require rescue experiments or another truly orthogonal validation strategy.*

We had adopted three independent approaches to validate the phenotype. All three approaches are well practiced in the field. The small molecule inhibitor has been used in the study by Rajadurai et al, J Cell Science, 2012 and it is very much accepted in studying cellular kinases [1].

We agree that even though the smart pool has always chance of off-target effects, the OnTargetPlus Smart pool has the minimum chance of off-target effects because of the patented chemical modifications, compared to the individual oligos and SiGenome SMARTpool, which was used by Rajadurai, et. al. in their study [1].

The shRNA mediated silencing resulted in less reduction in the MET level (~50-60%) but is it scientifically not acceptable, particularly when it showed similar phenotype over n=3 sets of experiments?

The arguments made by the reviewer in this context seems to be harsh. However, we decided to carry out MET silencing using two independent oligos from the SMART pool.

> *(5) Weak evidence for MET-MT1-MMP interaction*
>
> *The evidence supporting a physical interaction between MET and MT1-MMP remains unconvincing. The newly added co-immunoprecipitation experiment does not reveal a convincing MET-MT1-MMP interaction, and I am unable to appreciate a specific coimmunoprecipitated MT1-MMP signal in the presented blot. As presented, these data do not convincingly demonstrate a specific or functionally relevant interaction. Given that this interaction constitutes a central component of the proposed mechanistic model, this remains a major weakness of the study.*

We have detected the interaction in both GFP pulldown assay in 4 different cell lines and the corresponding reverse His-Ni-NTA pulldown assay, providing complementary evidence for their physical association (Fig 6E, S5F, G). We have also clearly stated in the manuscript that

this interaction is weak in nature and have not claimed it to be a strong interaction. While we acknowledge that the signal is modest, disregarding reproducible positive results would not be an appropriate interpretation of the pulldown assays. We believe the reproducibility of these findings supports a genuine MET and MT1-MMP association, and we have reported it accordingly.

> *(6) Overinterpretation of the data*
>
> *Taken together, the study proposes a mechanistic model linking MET trafficking to MT1MMP localization and invadopodia function. However, the experimental evidence largely supports correlative observations rather than demonstrating a direct mechanistic relationship.*
>
> *Specifically, MET endocytosis and recycling are not properly demonstrated because of the inappropriate temporal resolution of the trafficking experiments; the localization data remain uncertain owing to insufficient validation of the immunofluorescence reagents; and the proposed interaction between MET and MT1-MMP is not convincingly demonstrated. Consequently, the manuscript establishes correlation rather than causality, and the central mechanistic conclusions appear to be substantially overstated relative to the presented data.*

We agree that there is scope for further investigation of MET and MT1-MMP cotrafficking, however, we have provided preliminary evidence demonstrating the cotrafficking of MET and MT1-MMP at the cell surface (Fig 6F). Importantly, MET and MT1-MMP co-trafficking represents only one component of the manuscript and not a central mechanistic conclusion. As the title of the study indicates, the major component of the study is focused on MET trafficking and its implication in invadopodia-associated TNBC invasion, for which we have provided direct experimental evidence. Therefore, we believe that describing the overall study as primarily overstated and correlative underestimates the extent of the experimental evidence supporting our mechanistic conclusions.

> *Conclusion:*
>
> *While the manuscript addresses an interesting and biologically relevant question, the current experimental evidence does not adequately support the proposed mechanistic model. The combination of inappropriate experimental design for trafficking studies, insufficient validation of key imaging reagents, questionable interpretation of the localization data, lack of convincing evidence for the proposed MET-MT1-MMP interaction, and the absence of a clear relationship between the degree of MET depletion and the biological phenotype substantially limits the reliability of the conclusions.*
>
> *In my opinion, these issues cannot be addressed by further revision of the current manuscript, as they require substantial additional experimentation, including appropriately designed trafficking assays with short kinetic time points, rigorous validation of antibody specificity for immunofluorescence, and stronger mechanistic evidence linking MET trafficking to MT1-MMP-dependent invadopodia function.*

We thank the reviewer for outlining the remaining concerns. We will address the points raised by performing additional antibody validation and independent oligo-mediated MET silencing experiment, providing further support for the specificity and robustness of our findings.

However, we respectfully disagree, that the conclusions require the extensive additional experimentation suggested by the reviewer. As clarified above, our trafficking experiments were designed around the time points at which the functional invasive phenotype is observed, rather than to define the kinetics of MET internalization.

In conclusion, we would expect that the views of the reviewer 2 towards the manuscript should change and the reliability of our manuscript to the public should improve.

References:

(1) Rajadurai CV, Havrylov S, Zaoui K, Vaillancourt R, Stuible M, Naujokas M, Zuo D, Tremblay ML, Park M. Met receptor tyrosine kinase signals through a cortactinGab1 scaffold complex, to mediate invadopodia. J Cell Sci. 2012 Jun 15;125(Pt 12):2940-53. doi: 10.1242/jcs.100834. Epub 2012 Feb 24. PMID: 22366451; PMCID: PMC3434810.

(2) Sharma P, Parveen S, Vinod Shah L, Mukherjee M, Kalaidzidis Y, Joseph Kozielski A, et al. Title: SNX27-retromer assembly directs MT1-MMP trafficking to invadopodia and promotes breast cancer metastasis.

(3) Mader CC, Oser M, Magalhaes MAO, Bravo-Cordero JJ, Condeelis J, Koleske AJ, et al. Molecular and Cellular Pathobiology An EGFR-Src-Arg-Cortactin Pathway Mediates Functional Maturation of Invadopodia and Breast Cancer Cell Invasion [Internet]. doi:10.1158/0008-5472.CAN-10-1432

(4) Parveen S, Khamari A, Raju J, Coppolino MG, Datta S. Syntaxin 7 contributes to breast cancer cell invasion by promoting invadopodia formation. J Cell Sci. 2022 Jun 15;135(12). doi:10.1242/jcs.259576 PubMed PMID: 35762511.

(5) Joffre C, Barrow R, Ménard L, Calleja V, Hart IR, Kermorgant S. A direct role for Met endocytosis in tumorigenesis. Nat Cell Biol. 2011 Jun 5;13(7):827–37. doi:10.1038/ncb2257 PubMed PMID: 21642981.

(6) Monteiro P, Rossé C, Castro-Castro A, Irondelle M, Lagoutte E, Paul-Gilloteaux P, et al. Endosomal WASH and exocyst complexes control exocytosis of MT1-MMP at invadopodia. J Cell Biol. 2013 Dec 23;203(6):1063–79. doi:10.1083/jcb.201306162 PubMed PMID: 24344185.

(7) Wenzel EM, Pedersen NM, Elfmark LA, Wang L, Kjos I, Stang E, et al. Intercellular transfer of cancer cell invasiveness via endosome-mediated protease shedding. Nat Commun. 2024 Feb 10;15(1):1277. doi:10.1038/s41467-024-45558-8

(8) Pedersen NM, Wenzel EM, Wang L, Antoine S, Chavrier P, Stenmark H, Raiborg C. Protrudin-mediated ER-endosome contact sites promote MT1-MMP exocytosis and cell invasion. J Cell Biol. 2020 Aug 3;219(8):e202003063. doi: 10.1083/jcb.202003063. PMID: 32479595; PMCID: PMC7401796.

(9) Duan Q, Jia HR, Chen W, Qin C, Zhang K, Jia F, Fu T, Wei Y, Fan M, Wu Q, Tan W. Multivalent Aptamer-Based Lysosome-Targeting Chimeras (LYTACs) Platform for Mono- or Dual-Targeted Proteins Degradation on Cell Surface. Adv Sci (Weinh). 2024 May;11(17):e2308924. doi: 10.1002/advs.202308924. Epub 2024 Feb 29. PMID: 38425146; PMCID: PMC11077639.

(10) Wei J, Wang J, Guan W, Li J, Pu T, Corey E, Lin TP, Gao AC, Wu BJ. PlexinD1 is a driver and a therapeutic target in advanced prostate cancer. EMBO Mol Med. 2025 Feb;17(2):336-364. doi: 10.1038/s44321-024-00186-z. Epub 2025 Jan 2. PMID: 39748059; PMCID: PMC11822115.

(11) Yamasaki A, Miyake R, Hara Y, Okuno H, Imaida T, Okita K, Okazaki S, Akiyama Y, Hirotani K, Endo Y, Masuko K, Masuko T, Tomioka Y. Dual-targeting therapy against HER3/MET in human colorectal cancers. Cancer Med. 2023 Apr;12(8):9684-9696. doi: 10.1002/cam4.5673. Epub 2023 Feb 7. PMID: 36751113; PMCID: PMC10166911.

(12) Soonnarong R, Putra ID, Sriratanasak N, Sritularak B, Chanvorachote P. Artonin F Induces the Ubiquitin-Proteasomal Degradation of c-Met and Decreases AktmTOR Signaling.

Pharmaceuticals (Basel). 2022 May 21;15(5):633. doi: 10.3390/ph15050633. PMID: 35631459; PMCID: PMC9145792.

The following is the authors' response to the original reviews.

We sincerely thank the editor and reviewers for thoroughly evaluating the manuscript. Following the comments from the reviewers we caried out four major sets of experiments and added the results and the conclusions derived from them in the revised manuscript. We also modified the abstract and the introduction. As suggested by the reviewers, we have rewritten the discussion. All the mislabelling and typing errors have been corrected, and representative graphs has been replaced as suggested. The list of the newly carried out experiments are -

(i) In the original submission, we carried out a microscopy-based study to investigate the recycling of MET. We now added surface biotinylation approach to show the RCP or KIF16B-mediated surface delivery of MET (Fig. 5J).

(ii) To demonstrate the functional effect of KIF16B silencing on TNBC invasion we have performed ECM degradation assay with depleted KIF16B cells (Fig. S4K-L). Further, the MET degradation in KIF16B-silenced cells has also been investigated using immunoblotting (Fig. S4H).

(iii) To rule out the off-target effect of the siRNA used in this study, we have validated the invadopodia-associated function using 2 individual siRNAs for RAB14 and RCP (Fig. S4K-L).

(iv) We have now introduced MMP2 as a positive control as a substrate of MT1-MMP to show the effect of silencing of the protease on its cleavage (Fig. S5I).

We also incorporated following changes, largely additions of new plots, data in the revised manuscript.

(i) RAB4 and RAB14 colocalization with MET in BT-549 cell line has also been added in Fig. 4 (A, B, C).

(ii) Data showing MET silencing using siRNA and its effect on invadopodia has been added to Fig 1D.

(iii) Graph showing percentage of cells forming invadopodia has added to Fig. S1G.

(iv) Line intensity plots of MET-containing invadopodia has been added in Fig. 2G'.

(v) We have added quantification of all the blots to the figures.

(vi) A graph representing MET degradation kinetics with HGF over 3 experiments has been added to Fig S2F.

(vii) The full field of view of Fig 1F has been added in the Fig S1L. A quantification of the gelatin degradation has been added to Fig 1F.

(viii) The blot for loading control of Fig S1K has been changed from Actin to Vinculin.

(ix) The blot showing expression of MT1-MMP in the SCR and knockout cells has been added to Fig S5M'.

(x) The survival plot for patients with altered or unaltered MET and RCP has been removed. The graph showing frequency alteration of MET has also been removed.

(xi) Additional immunoblots associated with all the figures are now provided in a newly added supplementary figure (Fig S6).

> ***Reviewer #1 (Public review):***
>
> *Summary:*
>
> *This study identifies a mechanism responsible for the accumulation of the MET receptor in invadopodia, following stimulation of Triple-negative breast cancer (TNBC) cells with HGF. HGF-driven accumulation and activation of MET in invadopodia causes the degradation of the extracellular matrix, promoting cancer cell invasion, a process here investigated using gelatin-degradation and spheroid invasion assays.*
>
> *Mechanistically, HGF stimulates the recycling of MET from RAB14-positive endosomes to invadopodia, increasing their formation. At invadopodia, MET induces matrix degradation via direct binding with the metalloprotease MT1-MMP. The delivery of MET from the recycling compartment to invadopodia is mediated by RCP, which facilitates the colocalization of MET to RAB14 endosomes. In this compartment, HGF induces the recruitment of the motor protein KIF16B, promoting the tubulation of the RAB14-MET recycling endosomes to the cell surface. This pathway is critical for the HGF-driven invasive properties of TNBC cells, as it is impaired upon silencing of RAB14.*
>
> *Strengths:*
>
> *The study is well-organized and executed using state-of-the-art technology. The effects of MET recycling in the formation of functional invadopodia are carefully studied, taking advantage of mutant forms of the receptor that are degradation-resistant or endocytosis-defective.*
>
> *Data analyses are rigorous, and appropriate controls are used in most of the assays to assess the specificity of the scored effects. Overall, the quality of the research is high.*
>
> *The conclusions are well-supported by the results, and the data and methodology are of interest for a wide audience of cell biologists.*

We sincerely thank the reviewer for the positive feedback and for considering our study to be well executed and rigorous. The valuable suggestions and comments certainly improved the understanding of the role of the RAB14-RCP-KIF16B axis in MET trafficking and breast cancer invasion.

> *Weakness*
>
> *The role of the MET receptor in invadopodia formation and cancer cell dissemination has been intensively studied in many settings, including triple-negative breast cancer cells. The novelty of the present study mostly consists of the detailed molecular description of the underlying mechanism based on HGF-driven MET recycling. The question of whether the identified pathway is specific for TNBC cells or represents a general mechanism of HGF-mediated invasion detectable in other cancer cells is not addressed or at least discussed*

We thank the reviewer for raising this point. We would like to clarify that in TNBCs, the overexpression of EGFR and MET in the null background of the hormonal receptors; progesterone receptor, estrogen receptor, and HER2 is considered to be very crucial in terms of prognosis and treatment (PMID: 27655711, 25368674). Hence study of MET signalling and trafficking is more relevant for TNBCs compared to other cancer cells. In the current study, we therefore focused on two TNBC cell lines. We have added this in the first paragraph of introduction. Line no: 31-38.

> ***Reviewer #1 (Recommendations for the authors):***

> *Major points*
>
> *(1) My major concern refers to the clinical data presented in this study. Different from the mechanistic findings, the quality of these analyses is too low, the description in the figure legends is scant, and is absent in the Method section. The results concerning the prognostic value of RCP are the most problematic. What is shown in the Kaplan Meier? Is it the correlation between the RCP mRNA levels and the patient's survival? More importantly, to study the correlation between genetic alteration and prognostic outcome, multivariable analyses should be performed comparing the genetic alteration with known prognostic factors (sex, age, tumor size, node status, ER/PrR, HER2, Ki67 if available, tumor grade). This is because breast cancer prognosis depends on multiple interrelated factors, and only multivariate models can adjust for confounding and identify which variables independently predict outcome-providing far more accurate and clinically useful prognostic information than univariate analysis. Furthermore, overexpression of RTKs has been extensively reported and studied in TNBCs. Similarly, the relevance of MET in cancer cell invasion has been firmly established. Therefore, the data presented here, whose quality does not match the mechanistic part of the study, can be considered unnecessary. I would, therefore, recommend removing the "clinical" data. The introduction should be modified accordingly.*

We thank the reviewer for this insightful comment. To generate the graphs, we selected studies available in the publicly accessible database cBioportal (*cbioportal.org/*). The graphs generated by the database, representing the genetic alterations of genes has added in the Fig. S4A. However, as suggested by the reviewer, we have removed the survival plots for MET and RCP, the gene alteration frequency of MET and modified the text accordingly.

> *(2) Overexpression of KIF16B has been shown to inhibit the degradative pathway, stimulating the recycling one. In agreement, silencing of KIF16B accelerates EGFR degradation (PMID: 15882625). Does this also apply to the MET receptor? In the present setting, does the overexpression of KIF16B result in prolonged MET expression?*

We thank the reviewer for raising this question. Although we did not analyze the expression level of MET in the KIF16B overexpressed cells, we have analyzed the total MET levels in the control and the KIF16B silenced cells using immunoblotting and did not observe any significant changes in the MET protein levels (Fig S4H). Line no: 390-391. This led us to believe that the depletion or overexpression of KIF16B may not have any direct effect on MET expression.

> *(3) The contribution of MMP2 and MMP9 to the degradative properties of HGFstimulated TNBC cells should be investigated and compared to MT1-MMP.*

We believe that this is a relevant note from the reviewer. However, MT1-MMP is one of the most well-established metalloproteases, known till date for its role in invadopodia-associated activities in breast cancer (PMID: 35008569, 27501444). Moreover, it is the best-known candidate protease, which is a transmembrane metalloprotease could be the model in studying membrane recycling to invadopodia (PMID: 20605060, 19692588). However, as pointed out by the reviewer, we completely agree that MMP2 and MMP9 also contribute significantly to invadopodia-associated functions in TNBCs (PMID: 23902685, 25699257). HGF is also known to promote the expression and activity of MMP2 and MMP9 (PMID: 23320110, 26259977). Interestingly, the cellular machineries involved in their enhanced activity due to HGF stimulation may be distinct from what was observed in the current study and may require a distinct, elaborated study, which is beyond the scope of the current one.

> *(4) The authors appropriately tested the possible shedding effect of MT1-MMP on MET. They should repeat the experiments, adding a positive control of shedding. Furthermore,*

> *the legends referring to these experiments, shown in Supplementary Figure S6, seem to be wrong (or mislabeled).*

We thank the reviewer for the suggestion. MT1-MMP is known to proteolytically cleave and initiate the activation of MMP2 (PMID: 11161720, 15095267). We now carried out the experiment with MMP2 as a control (Fig S5I). We observe an increase in the unprocessed MMP2 level in the MT1-MMP silenced cells, whereas the MET levels are unaltered. Line no: 467-468.

We sincerely apologize for the oversight in the mislabelling. We have now corrected it in the revised manuscript.

> *(5) Does altered expression of RAB14 and/or KIF16B affect MT1-MMP delivery to invadopodia in the TNBC cell lines? Does KIF16B silencing affect invasion?*

The role of RAB14 and KIF16B in MT1-MMP delivery to podosomes, a structure similar to invadopodia in macrophages has been studied by Hey S. et al. (PMID: 37696580). The study suggests that KIF16B silencing reduces the invasion of macrophages. However, the effect is not known for TNBCs. Thus, we have conducted the ECM degradation assay in TNBC cell lines to show the effect of KIF16B gene silencing on breast cancer invasion to the revised manuscript (Fig S4K-L). In both MDA-MB-231 and BT-549 cells we observed reduced ECM degradation activity upon KIF16B depletion, corroborating the observation from Hey S. et al. Line no: 392-400.

> *Minor points*
>
> *(1) I recommend authenticating cell lines and stable populations by STR profiling.*

All the cell lines used in the study have been purchased from ATCC, and STR is a standard practice followed by ATCC. Further, to avoid any alteration, cells were discontinued after 20 passages. We have added this statement to the methods section in the revised manuscript. Line no: 643-644.

> *(2) In the legend to Supplementary Figure S4A, the panel is described as the frequency of alterations of MET, while, if I correctly interpret it, the bar graph refers to RCP. As mentioned above, these data could be removed.*

We thank the reviewer for pointing out the mistake. We have rectified this in the revised version.

> *(3) Check for typos. Sometimes invadopodia is written with the capital: "Invadopodia", in other instances it is not. The authors should be consistent throughout the manuscript. English language editing would help.*

We sincerely apologize for the inconsistency in the writing. We have removed the unnecessary capitalization of invadopodia in the revised manuscript. Line no: 142, 159, 280, 436.

> ***Reviewer #2 (Public review):***
>
> *Summary:*
>
> *In this manuscript, Khamari and colleagues investigate how HGF-MET signaling and the intracellular trafficking of the MET receptor tyrosine kinase influence invadopodia formation and invasion in triple-negative breast cancer (TNBC) cells. They show that HGF stimulation enhances both the number of invadopodia and their proteolytic activity. Mechanistically, the authors demonstrate that HGF-induced, RAB4- and RCP-RAB14-KIF16B-dependent recycling routes deliver MET to the cell surface specifically at sites*

> *where invadopodia form. Moreover, they report that MET physically interacts with MT1-MMP - a key transmembrane metalloproteinase required for invadopodia function- and that these two proteins co-traffic to invadopodia upon HGF stimulation.*
>
> *Although the HGF-MET axis has previously been implicated in invadopodia regulation (e.g., by Rajadurai et al., Journal of Cell Science 2012), studies directly linking ligand-induced MET trafficking with the spatial regulation of MT1-MMP localization and activity have been lacking.*
>
> *Overall, the manuscript addresses a relevant and timely topic and provides several novel insights. However, some sections require clearer and more concise writing (details below). In addition, the quality, reliability, and robustness of several data sets need to be improved.*
>
> *Strengths:*
>
> *A key strength of the study is the novel demonstration that HGF-mediated, RAB4- and RAB14-dependent recycling of MET delivers this receptor, together with MT1MMP, to invadopodia -highlighting a previously unrecognized mechanism, regulating the formation and proteolytic function of these invasive structures. Another strong point is the breadth of experimental approaches used and the substantial amount of supporting data. The authors also include an appropriate number of biological replicates and analyze a sufficiently large number of cells in their imaging experiments, as clearly described in the figure legends.*

We greatly appreciate the positive assessment from the reviewer, who also acknowledged the novelty and relevance of our study. Below, we have carefully addressed the comments/concerns raised regarding this study and that have strengthened the reliability and robustness by revisiting the data, providing additional analyses where required, and clarifying methodological details.

> *Weakness*
>
> *(1) Inappropriate stimulation times for endocytosis and recycling assays. The experiments examining MET endocytosis and recycling following HGF stimulation appear to use inappropriate incubation times. After ligand binding, RTKs typically undergo endocytosis within minutes and reach maximal endosomal accumulation within 5-15 minutes. Although continuous stimulation allows repeated rounds of internalization, the temporal dynamics of MET trafficking should be examined across shorter time points, ideally up to 1 hour (e.g., 15, 30, and 60 minutes). The authors used 2-, 3-, or 6-hour HGF stimulation, which, in my opinion, is far too long to study ligandinduced RTK trafficking.*

We understand the reviewer's concern regarding the HGF stimulation time point for endocytosis and recycling. We want to highlight that to study the recycling/surface delivery of MET in response to HGF, we performed TIRF microscopy-based imaging, where images were taken within 1h of HGF addition (Fig. 2I). Additionally, we have incorporated surface biotinylation to show the recycling of MET as suggested in comment-7 (Fig. 5J). For this experiment we have used 30 min of HGF stimulation. Line no: 382-391.

Moreover, we have observed the functional effect of HGF on ECM (gelatin) degradation and invadopodia formation after 3 h of HGF stimulation. We were curious to know where does the MET localises with prolonged ligand stimulation. Hence, to study the localization of MET to invadopodia or the endocytic markers, the cells were stimulated with HGF for 2-3 hours.

> *(2) Low efficiency of MET silencing in Figure S1I. The very low MET knockdown efficiency shown in Figure S1I raises concerns. Given the potential off-target effects of a single shRNA and the insufficient silencing level, it is difficult to conclude whether the reduction*

> *in invadopodia number in Figure 1F is genuinely MET-dependent. The authors later used siRNA-mediated silencing (Figure S5C), which was more effective. Why was this siRNA not used to generate the data in Figure 1F? Why did the authors rely on the inefficient shRNA C#3?*

We understand the concern raised by the reviewer. We want to emphasize that we have employed three different approaches to investigate the effect of MET silencing/inhibition on invadopodia formation. (i) A MET kinase inhibitor, PHA665752, which shows reduced invadopodia formation (Fig. 1E, E'). (PMID: 21973114, 41009793) (ii) Silencing with shRNA: Since the level of silencing of MET with the shRNA was not sufficient, cells were stained with MET as a readout for MET silencing, and images of the cells with reduced MET expression were captured. ECM degradation activity and invadopodia numbers were found to be reduced in the MET-depleted cells (Fig. 1F). (iii) We have now added the data showing the effect of siRNA-mediated MET depletion on invadopodia formation to the revised figure 1D. Line no: 123-125. To draw a robust conclusion regarding the role of MET on invadopodia-associated TNBC invasion, we have integrated all three complementary approaches.

> *(3) Missing information on incubation times and inconsistencies in MET protein levels. The figure legends do not indicate how long the cells were incubated with HGF or the MET inhibitor PHA665752 before immunoblotting. This information is crucial, particularly because both HGF and PHA665752 cause a substantial decrease in the total MET protein level. Notably, such a decrease is absent in MDA-MB-231 cells treated with HGF in the presence of cycloheximide (Figure S2F). The authors should comment on these inconsistencies. Additionally, the MET bands in Figure S1J appear different from those in Figure S1C, and MET phosphorylation seems already high under basal conditions, with no further increase upon stimulation (Figure S1J). The authors should address these issues.*

We apologise for the unintentional omission of experimental detailing about HGF or drug incubation time, which we have incorporated into the figure legend appropriately. Regarding the decreased MET level in the drug-treated condition: literature suggests that the MET inhibitor PHA665752 also promotes MET degradation, corroborating our result shown in Fig. S1J (PMID: 15788682, 18327775). Further in Fig. S1J, the relative phosphorylation of MET when compared to the total MET level in the HGF-treated condition is higher (~2-fold). Quantification of the blot has been added now.

Further, addition of HGF for 3 h leads to 40±15% reduction in the MET protein levels as seen in the Author response image 1 representing quantification of different immunoblot. The degradation of MET in the Fig S1J is 65% which nearly fall in the range for HGF-mediated MET degradation.

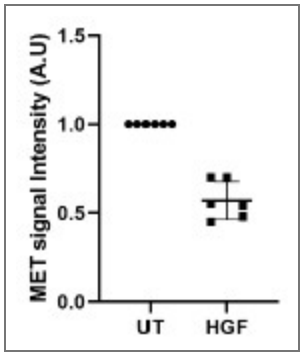

Author response image 1. Quantification of immunoblots showing MET signal intensity in the presence or absence of HGF normalized with the loading control. N=6.

Next, in the fig. S1A, K the rabbit anti-MET (CST, D1C2 XP) antibody has been used, which binds to a C-terminal motif of MET and identifies both the 170kDa as well as 140kDa protein representing the uncleaved and cleaved form of MET. In Fig. S1J, the mouse antiMET (CST, L6E7) antibody has been used, which binds to an N-terminal motif of MET and recognizes only the 140kDa protein.

> *(4) Insufficient representation and randomization of microscopic data. For microscopy, only single representative cells are shown, rather than full fields containing multiple cells. This is particularly problematic for invadopodia analysis, as only a subset of cells forms these structures. The authors should explain how they ensured that image acquisition and quantification were randomized and unbiased. The graphs should also include the percentage of cells forming invadopodia, a standard metric in the field. Furthermore, some images include altered cells - for example, multinucleated cells - which do not accurately represent the general cell population.*

We thank the reviewer for raising this point. The single-cell images are shown for clarity and to visualize the subcellular features; however, the conclusions are made based on the quantitative analysis of multiple cells collected from multiple fields of view (Frames). At least 30 such frames per condition having 4-7 cells/ frame has been acquired and analysed for the quantification throughout this manuscript. We would like to highlight that the image acquisition has been done over random fields on a coverslip. In the revised manuscript, for a better representation of the population of cell-forming invadopodia, a graph showing the percentage of cells forming invadopodia have been added (Fig S1G). Line no: 118-119. The percentage of cells forming invadopodia increased upon HGF stimulation in MDAMB-231.

> *(5) Use of a single siRNA/shRNA per target. As noted earlier, using only one siRNA or shRNA carries the risk of off-target effects. For every experiment involving gene silencing (MET, RAB4, RAB14, RCP, MT1-MMP), at least two independent siRNAs/shRNAs should be used to validate the phenotype.*

We would like to clarify that we are using SMARTPool siRNA, which contains 4 individual siRNAs for the target gene. Literature suggests that using a pool of siRNA has reduced off-target effects compared to using single oligos for gene silencing (PMID: 14681580, 33584737, 24875475).

While SMARTpool siRNA minimizes the off-target effect, it does not eliminate the possibility of it. To confirm that the observed phenotypes are specifically attributable to the genes investigated in this study, we now performed functional experiments using two independent siRNAs targeting RCP and RAB14. The results have been added to figure S4K-L. Silencing of RCP or RAB14 using single oligos resulted in decrease in the degradation index comparable to SMARTpool siRNA, thus phenocopied the SMARTpool siRNA. Line no: 392-400.

Further, RAB4 is well established to be associated with MET trafficking and it served as a positive control in our study (PMID: 21664574, 30537020). Additionally, a recent study by Hey et al. have used individual oligos for KIF16B to demonstrate the effect of KIF16B silencing on gelatin degradation, which corroborate with our observation from the KIF16B silencing using the SMARTpool siRNA (PMID: 37696580).

For MET, we used siRNA, shRNA and an inhibitor to show the effect of MET inhibition/perturbation in the invadopodia-associated activity, which validates the observations of siRNA-mediated gene silencing (detailed in point 2).

We did not perform any experiments using single oligos targeting MT1-MMP, since in our MT1-MMP siRNA-based study, now we have taken an appropriate positive control to validate the efficacy of MT1-MMP silencing (Fig. S1I). In addition, we have shown the effect of MT1-MMP depletion on invadopodia formation using a CRISPR-based gene knock-out study, and

another study from our group has shown a similar effect using siRNA (PMID: 31820782), which supports our MT1-MMP KO cell observation.

> *(6) Insufficient controls for antibody specificity. The specificity of MET, p-MET, and MT1-MMP staining should be demonstrated in cells with effective gene silencing. This is an essential control for immunofluorescence assays.*

The anti-MET antibody (CST, D1C2 XP) has been used in several studied (PMID: 41166312, 41152910, 39748059). The CST L6E7 anti-MET antibody has been used in studied by Radke et al, Wang et el., Kong et al. (PMID: 36435874, 38262412, 32214092). In our study, immunoblots demonstrating depletion of MET in the siRNA or shRNA-treated cells has been provided in Fig. S1I, K respectively. Further, we have demonstrated MET silencing using immunofluorescence. We also have now added the entire field of view in Fig S1L of showing cells treated with control or shRNA against MET. In the shRNA-treated condition, the cell at the centre shows low MET fluorescence intensity indicating depletion of the RTK, while the surrounding cells have MET staining similar to control.

Tyr 1234/35 are present in the active site of MET kinase domain and upon binding of the ligand promotes their autophosphorylation (PMID: 17667909). Earlier studies have established the specificity of the phosphor-MET antibody by immunoblotting and immunofluorescence using MET inhibitors (PMID: 21973114, 41009793). In our study we have shown that the inhibition of MET kinase activity using PHA665752 abolished the MET phosphorylation at the Tyr 1234/35, as shown in Fig S1J which revalidates the specificity of the antibody.

Additionally, in a previous study Joffre et al. have shown that an oncogenic mutant form of MET, M1250T is highly phosphorylated at the Tyr 1234/1235 (PMID: 21642981). Using the phospho-MET antibody, we have shown in Fig 3C, S2I the increased Tyr phosphorylation of M1250T MET mutant as reported by Joffre et al.

The anti-MT1-MMP antibody is also a very well-established antibody reported in multiple studies (PMID:32479595, 31820782, 35762511). In our study, we have shown the specificity of the antibody using immunoblot analysis. Immunoblots showing significant depletion of MT1-MMP protein level following the SMARTpool siRNA and sgRNA-mediated gene silencing has been provided in Fig. S5I, M′, respectively. Further MT1MMP silencing has been also validated by immunofluorescence in the following studies. PMID: 22291036, 21571860, 20505159.

> *(7) Inadequate demonstration of MET recycling. MET recycling should be directly demonstrated using the same approaches applied to study MT1-MMP recycling. The current analysis - based solely on vesicles near the plasma membrane - is insufficient to conclude that MET is recycled back to the cell surface.*

We appreciate the reviewer's suggestion for an alternative approach to show MET trafficking. We have demonstrated MET trafficking using surface biotinylation, where we have shown that the RCP and KIF16B depletion affect the surface delivery of MET (Fig 5J). Line no: 382-391.

In addition, to study the surface delivery of cargo, TIRF is a widely used reliable approach and it is highly sensitive technique for detection of surface delivery events (PMID: 24344185, 20971701). We have also tried to investigate the trafficking of MET using antibody uptake approach; however, it could not be established as the binding of the antibody hindered the ligand binding and vice versa.

> *(8) Insufficient evidence for MET-MT1-MMP interaction. The interaction between MET and MT1-MMP should be validated by immunoprecipitation of endogenous proteins, particularly since both are endogenously expressed in the studied cell lines.*

We thank the reviewer for pointing out the insufficient evidence for MET-MT1-MMP interaction at the endogenous level. We now carried out the immunoprecipitation of endogenous MET to validate the interaction with MT1-MMP (Fig S5H). A light (low intensity) band corresponding to MT1-MMP was detected in the anti-MT1-MMP immunoblot for the immunoprecipitated sample. We believe that the interaction between MT1-MMP and MET may be weak in nature, resulting in limited co-immunoprecipitation of the endogenous MT1-MMP by MET. The immunoblot is now added to the revised manuscript. Line no: 460-461.

> *(9) Inconsistent use of cell lines and lack of justification. The authors use two TNBC cell lines: MDA-MB-231 and BT-549, without providing a rationale for this choice. Some assays are performed in MDA-MB-231 and shown in the main figures, whereas others use BT-549, creating unnecessary inconsistency. A clearer, more coherent strategy is needed (e.g., present all main findings in MDA-MB-231 and confirm key results in BT549 in supplementary figures).*

MDA-MB-231 and BT-549 are two well-characterized TNBC cell lines that readily form invadopodia. These cell lines have been extensively used to study invadopodia-associated breast cancer cell invasion (PMID: 32697977, 35915226, 31533971). These two cell lines also show overexpression of MET, making them suitable model cell lines for our study (PMID: 36139568, 20687930, 27502396).

Overall, most of the conclusions reported in this manuscript are derived from multiple experimental approaches using two TNBC cell lines for generalization.

We agree with the reviewer that showing the results from one type of cell line in the main figure would have been better, and wherever possible, we now provided the observations from a single cell line in the main figures and the data from the other cell line in the supplementary figures. However, some of the overexpression studies were performed in BT-549 cells to derive robust statistically meaningful conclusions. Therefore, we could not avoid adding results from both the cell lines in some of the figures. We would like to add that the legends for these figures have been edited to clearly mention the cell lines associated with each of the figure panels to avoid any confusion or inconsistency.

> *(10) Inconsistency in invadopodia numbers under identical conditions. The number of invadopodia formed in Figure 1E is markedly lower than in Figure 1C, despite identical conditions. The authors should explain this discrepancy.*

We sincerely thank the reviewer for pointing out the inconsistency in invadopodia numbers across 2 experiments. Fig. 1C has 2 conditions: UT and the HGF-treated condition. The Untreated condition has the serum-free media without any stimulation. Whereas we have added vehicle (DMSO) in Fig. 1E, E', since the drug is resuspended in DMSO. This difference in the treatment is likely to be responsible for the decreased numbers of invadopodia in Fig. 1E. In different studies it has been shown that DMSO is not biologically inert and can affect invasive properties of cells by perturbing actin dynamics and metalloprotease activity (PMID: 33552397, 22529897, 7188610).

> *(11) Questionable colocalization in some images. In some figures - for example, Figure 2G - the dots indicated by arrows do not convincingly show colocalization. The authors should clarify or reanalyze these data.*

As suggested by the reviewer, we have now re-analyzed the data for figure 2G. The apparent visual lack of colocalization is likely due to the relatively lower fluorescence intensity of MET

at these structures. We have now added the line intensity plots for the indicated puncta to show the intensity of both channels at the 'dots' in the figure 2G' and they show correlation in their intensity distribution.

We would also like to elaborate that to quantify the colocalization of two channels, we have used the automated image analysis software Motiontracking (*motiontracking.mpi-cbg.de*) (PMID: 16143105), which has been detailed in the method section. Briefly, the algorithm works on object-based co-localization. If the fluorescence intensity distributions at a given object corresponding to any two different channels (fluorophores) show 35% or more overlap (Author response image 2), the object is considered as a multi-colour object and the overlapped area value is used to calculate the degree of co-localization. The calculation is carried out over all the objects in a given field of view (frame) and over all the field of views (frames) acquired for a given condition. Also, the apparent colocalization is corrected for random colocalization, which is the random permutation of object colocalization. This makes object-based colocalization more reliable than intensity-based colocalization.

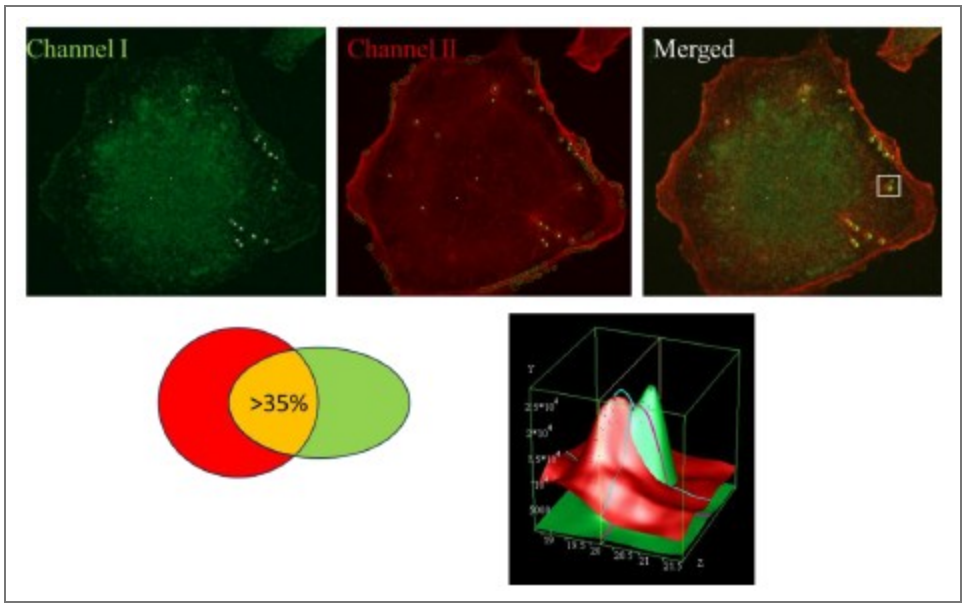

Author response image 2. Image showing the object identification and contour of the multicolour object identified by Motiontracking. The plot shows the intensity distribution of these two objects as analyzed by Motiontracking.

> *(12) Abstract, Introduction, and Discussion require substantial rewriting.*
>
> *(a) The abstract should be accessible to a broader audience and should avoid using abbreviations and protein names without context.*
>
> *(b) The introduction should better describe the cellular processes and proteins investigated in this study.*
>
> *(c) The discussion currently reads more like an extended summary of results. It lacks deeper interpretation, comparison with existing literature, and consideration of the broader implications of the findings.*

We thank the reviewer for this suggestion. We have substantially modified the abstract, and the introduction following the reviewer's suggestion. The introduction has been edited to describe the cellular processes investigated in this study and some of the key associated molecular machineries. In the discussion section, we have avoided redundant descriptions of

the results but retained some of them wherever necessary for interpretation and relevant discussion in the light of existing literature.

> ***Reviewer #2 (Recommendations for the authors):***
>
> *(1) Quality of charts. Several charts (e.g., Figure 1B, 1C, 1F) are of poor visual quality. The authors should provide higher-resolution graphs with clearer axis labels, consistent formatting, and properly scaled data.*

We thank the reviewer for pointing out the insufficient visual quality of some of the charts. We believe the resolution of the charts/graphs have changed while converting to PDF, due to image compression. We will provide the uncompressed charts with much improved visual quality, provided they are not restricted by file size limitation.

> *(2) Full protein names on first mention. Whenever a protein appears for the first time in the manuscript, its full name should be provided, if possible, before using the abbreviation.*

We have incorporated the full name of the protein while reporting for the first time in the manuscript.

> *(3) Correct use of "invadopodium" vs. "invadopodia." Invadopodia is the plural form; the singular is invadopodium. The sentence "Invadopodia, an actin-rich membrane protrusion decorated with proteases, is a tool for ECM and basement membrane degradation during cancer cell invasion" should be corrected accordingly.*

We are thankful to the reviewer for pointing out the grammatical error. We corrected the error in the revised version. Line no: 44.

> *(4) Unclear sentence about resistance and invasion.*
>
> *The sentence "However, often patients develop resistance to EGFR-targeted therapies due to overexpression of MET; yet, the mechanistic understanding of MET-dependent cancer invasion is unclear" is confusing because the shift from drug resistance to invasion is abrupt. The authors should revise this sentence for clarity and logical flow.*

We are thankful to the reviewer for highlighting this sentence. We have rewritten the sentence as follows “Since one of the receptor tyrosine kinases (RTK), EGFR is often amplified in TNBC patients, they are usually targeted for its treatment. However, often patients develop resistance to EGFR-targeted therapies due to overexpression of another RTK MET”. Line no: 35-38.

> *(5) Incorrect figure reference. In the paragraph describing the results related to RAB proteins, there is an incorrect reference to Figure 3 instead of Figure 4. This should be corrected.*

We sincerely apologize to the reviewer for the incorrect figure reference. We have corrected the reference to figures in the revised manuscript. Line no: 251, 261.

> *(6) Ambiguous sentence regarding MET activation. The sentence "MET, upon activation by HGF, triggers the activation of the RTK that induces cancer cell invasion" is unclear and should be rewritten for precision and clarity.*

We are thankful to the reviewer for highlighting the unintentional mistake. We have now added a clearer sentence “MET-HGF signalling axis are reported to promotes invasion in gastric cancer cells and melanoma cells”. Line no: 96-97.

> *(7) Questionable wording of figure legend. The phrase "Immunoblotting of indicated cell lines with MET and Tubulin" is an informal shortcut. The authors should rephrase it.*

We are thankful to the reviewer for highlighting this sentence. We have modified the figure legend with appropriate text. The modified text is as follows: Lysates of MDA-MB-231, BT-549 and MCF10A DCIS were separated by SDS-PAGE and analyzed by Western blot. Membranes were probed with anti-MET and anti-Vinculin antibody.

> *(8) Unnecessary capitalization. Terms such as invadopodia and cortactin should not be capitalized. The authors should correct capitalization throughout the manuscript.*

We are thankful to the reviewer for raising this point. We have modified this accordingly in the revised version. Line no: 142, 159, 280, 436.

https://doi.org/10.7554/eLife.109472.2.sa0